A STUDY OF KINETICS AND MECHANISMS OF IRON ORE REDUCTION IN ORE/COAL COMPOSITES

by

STANLEY SHUYE SUN, M.Eng., B.Eng.

A Thesis

Submitted to the School of Graduate Studies

in Partial Fulfilment of the Requirements

for the Degree

Doctor of Philosophy

McMaster University

June 1997

A STUDY OF KINETICS AND MECHANISMS OF IRON ORE REDUCTION IN ORE/COAL COMPOSITES

DOCTOR OF PHILOSOPHY (1997) McMASTER UNIVERSITY

(Materials Engineering) Hamilton, Ontario

TITLE: A STUDY OF KINETICS AND MECHANISMS OF IRON ORE REDUCTION IN ORE/COAL COMPOSITES

AUTHOR: Stanley Shuye Sun, M.Eng., B.Eng. (University of Science and Technology, Beijing, P. R. China)

SUPERVISOR: Professor W-K. Lu

NUMBER OF PAGES: xii, 198

ABSTRACT

For environmental and economical considerations, it is desirable to use iron ore concentrates directly without agglomeration and coal directly without coking for ironmaking. The present work is a study of the kinetics and mechanisms of iron ore reduction in ore/coal composites. An experimental system has been designed and experiments have been conducted with *in-situ* measurements of temperature and pressure to establish profiles within the ore/coal packing with the furnace temperature maintained at 1200 or 1300 °C. Samples were taken at various locations for chemical analysis in the partially reacted specimens. These experiments lead to a better understanding of this non-isothermal and non-isobaric system. A non-isothermal and non-isobaric mathematical model has been developed and validated by the experimental data. Mechanisms of heat transfer, mass transfer and interfacial reactions were studied using the mathematical model. The contribution of the individual kinetic steps to the rate of overall reaction were compared to evaluate the rate controlling step.

The contribution of the author is the design of the

experimental system which has demonstrated the non-isothermal and non-isobaric nature of the reaction system, and the development of the mathematical model. The present study may be used in new ironmaking processes and carbothermic process, such as FASTMET and cokemaking processes.

ACKNOWLEDGEMENT

The author wishes to express his sincere gratitude to his supervisor, Professor W-K. Lu for his advice and guidance throughout the course of this work and for his countless efforts to provide broad training in both educational and professional aspects. Without his continuous encouragement and criticism, the completion of this work would not have been possible. Similarly, the author extends his gratitude to other members of his Supervisory Committee, Professors G. A. Irons and A. N. Hrymak for their help and guidance.

Financial assistance from Canadian International Development Agency in the form of a scholarship, from the Department of Materials Science and Engineering, McMaster University in the form of a teaching assistantship and a scholarship, and from Natural Science and Engineering Research Council of Canada for a research grant to Professor W-K. Lu are greatly appreciated. Without their support, the present study could not have been carried out.

The author also wishes to express his gratitude to Atlas Specialty Steels and Mr. Paul Uguccioni of the company for their encouragement and help in the form of partial tuition fee and time for preparation of this thesis.

TABLE OF CONTENTS

CHAPTER ONE: INTRODUCTION

The blast furnace ironmaking process is by far the most energy efficient ironmaking process at mass production rates, and thus the most important ironmaking process at the present time. Approximately 534,500,000 tonnes of iron were produced worldwide in 1995; about 516,400,000 tonnes (96.6%) were produced in blast furnaces (ISS, 1996). However, the blast furnace operation demands high quality lumpy raw materials; therefore, ore concentrates must first be agglomerated to sinter or pellets, and coal must be made to coke, prior to being use in the blast furnace.

A modern blast furnace ironmaking plant usually consists of blast furnaces, sinter/pellet plants and coke ovens. The sinter/pellet plants and coke ovens are not only capital intensive, requiring about 60% of total plant capital cost (Smith and Corbett, 1988), but also have high maintenance costs in order to meet environmental standards, which is especially true for the coke ovens. The future of the blast furnace is not clear mainly because of the uncertainty of the availability of coke. These problems have led to a worldwide effort for more economical and environmentally friendly and coke-free ironmaking processes.

Based on the reductant used, coke-free ironmaking processes may be generally classified as (a) natural gas-based processes, such as Midrex and HyL, and (b) coal-based processes, such as SL/RN, FASTMET, COREX, AISI, DIOS, Hismelt and LB process (more detailed review of these processes is available in Chapter 2). Natural gas-based processes (Midrex and HyL) constituted more than 90% of direct reduced iron (DRI) worldwide in 1995. However, coal-based processes have attracted more and more attention for countries with abundant coal resources.

Among the coal-based processes, the only commercial direct reduction process (producing solid sponge iron) is SL/RN process, and the only commercial smelting reduction process (producing liquid iron) is the COREX process. The other processes are either in pilot plant test or in bench scale test.

The FASTMET and LB processes use iron ore concentrate and pulverized coal as raw materials. The gasification of coal and pre-reduction of iron ore proceed in the same reactor. These processes present good kinetic conditions for chemical reactions due to large gas/solid interfacial area and short distances for reactant transport between reacting particles. They have potential advantages of low energy consumption, no high temperature agglomeration of ore, and no coking step. The successful commercialization of these processes will depend on

our knowledge of kinetics and mechanisms in these ore/coal reaction systems.

The objective of the present study is to study the kinetics and mechanisms of reduction of iron ore concentrates in the ore/coal composite; the work includes both experimental and theoretical work.

Experimental work involves the design of a reactor and generation of experimental data under various conditions. It includes *in-situ* measurements of temperature and pressure in the reacting system, determination of profiles of chemical compositions of partially reacted ore/coal mixture, and determination of chemical compositions of exit gas (Chapter Three). Theoretical work includes the development of a non-isothermal, non-isobaric mathematical model to explain experimental results (Chapter Four and Five) and to probe potential advantages of practical applications.

CHAPTER TWO:

LITERATURE REVIEW

The present work is a study of kinetics and mechanisms of the reduction of iron ore concentrate in the presence of coal. It is a fundamental study for the new ironmaking processes, i.e. coke-free ironmaking processes. The literature review is primarily concerned with reduction of solid iron oxides in the presence of solid carbon or coal. The generally accepted mechanism of reduction of iron oxides is by gaseous reductants; therefore, a review of thermodynamics and kinetics of reduction of iron oxides by CO and H_2 is presented. A review of current situation of ironmaking technology is also included.

2.1 Current situation of ironmaking technology

2.1.1 Blast furnace ironmaking technology

The blast furnace is a counter-current packed bed reactor for the reduction of iron ore agglomerate and lump ore to produce liquid iron. Figure 2.1 shows the reaction zones and inner state of a modern blast furnace. The fundamentals of

physical chemistry in blast furnace ironmaking can be found in books by Bodsworth (1963) and Biswas (1981).

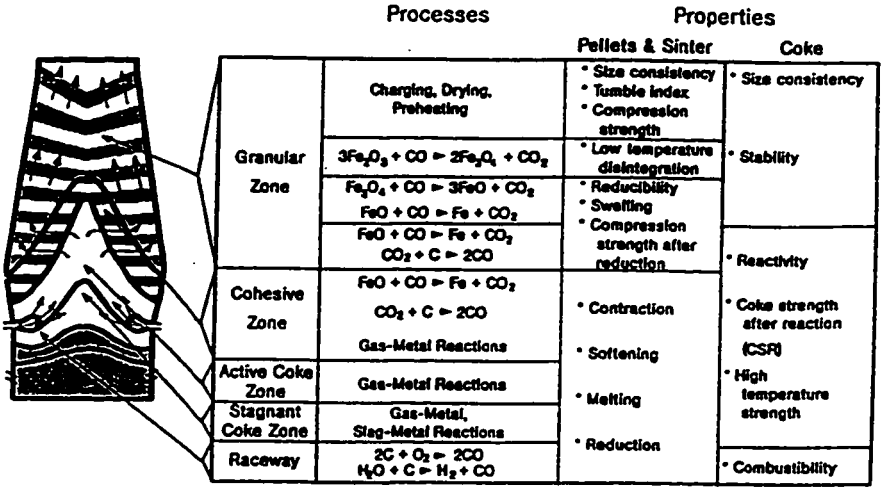

Figure 2.1 Reaction zones and inner state of a blast furnace (Ranade, 1994)

The modern blast furnace operation is based on agglomerates of iron ores, coke and hot blast with the characteristics of countercurrent flows, i.e. the hot reducing gas ascends while solids charged at ambient temperature descend. This countercurrent flow of gas and solid reactants results in the highly efficient use of thermal energy and reducing power of the gas generated in the raceways. The blast furnace ironmaking process is by far the most efficient, and thus the most important ironmaking process at present time. Of the roughly 534,500,000 tonnes of iron produced worldwide in 1995, about 516,400,000 tonnes (96.6%) were produced in blast

furnaces (ISS, 1996).

In the last decade, efforts have been made to improve blast furnace ironmaking technology. These efforts include: fuel injection to lower coke consumption, blast oxygen enrichment to increase productivity, improved raw materials to improve product quality, burden and gas distribution to stabilize operation, sensors and computer control system to better control the operation. With these efforts, remarkable progress in blast furnace ironmaking, in terms of higher productivity, lower coke and fuel consumption and higher quality of product, have been made (Table 2.1).

Table 2.1 Achievement in selected blast furnaces

Item	productivity thm/d/m^{3}WV	Fuel rate kg/thm	Coke rate kg/thm	Coal injection kg/thm	Hot metal silicon, %
Achievement	3.46	439	274	210	0.12
Blast furnace	Rautaruukki, Finland	Rautaruukki, Finland	IJmuiden 6, Netherlands	IJmuiden 6, Netherlands	Nagoya, Japan
Reference	Pisila ,1994	Pisila, 1994	Geerdes,1994	Geerdes,1994	Fukushima,1995

However, the countercurrent movement of gas and solid in a blast furnace demands high quality lumpy raw materials; therefore, ore concentrate must be agglomerated to sinter or pellets, and coal must be converted to coke, prior to its introduction in the blast furnace. A modern blast furnace ironmaking plant usually consists of blast furnaces, sinter/pellet plants and coke ovens. The sinter/pellet plants and coke ovens not only are capital intensive, but also have

high maintenance costs due to requirements to maintain environmental standards, especially for the coke ovens. The future of the blast furnace is not clear mainly because of the uncertainty of the availability of coke. It has led to a worldwide effort to develop more economical, environmentally friendly and coke-free ironmaking processes.

2.1.2 Coke-free ironmaking technology

Coke-free ironmaking processes may be generally classified into groups according to the final product of the process (sponge iron or hot metal), or according to the fuel used (natural gas-based and coal-based). Comprehensive reviews of development of direct reduction processes were published by The Metals Society, London (1979) and Stephenson (1980). Reviews of coal-based ironmaking processes were published by Smith and Corbett (1988). An update review was given by McAloon (1994).

2.1.2.1 Natural gas-based direct reduction

Midrex and HyL processes are natural gas-based direct reduction processes. In 1995, about 91% of direct reduced iron (DRI) worldwide was produced by these two processes (Figure 2.2). Detailed descriptions of these processes can be found in

publication from The Metals Society, London (1979) and Stephenson (1980). Typical examples of the natural gas-based direct reduction processes, both currently existing and under development, are listed in Table 2.2.

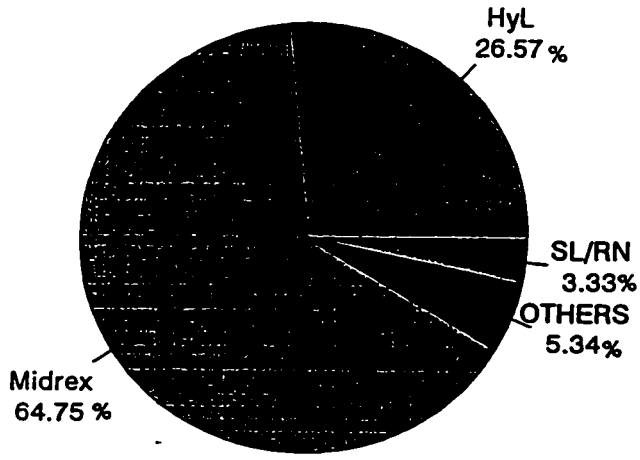

Figure 2.2 DRI production in 1995 by process (Ritt, 1996)

New processes under development include Iron Carbide Process which uses fluidized bed reactor with hydrogen gas and natural gas (without a reformer) as reductants to produce iron carbide. The iron carbide produced was reported to be non-pyrophoric, which is easier for storage and transportation, and finely divided which allows it to be dissolved and melted rapidly in steelmaking furnaces (Geiger and Stephens, 1993).

Table 2.2. Important natural gas-based direct reduction processes (McAloon, 1994)

Process	Midrex	HyL III	HyL I*	Fior	Iron carbide
Status	Industrial	Industrial	Industrial	Industrial	'94 startup
Typical plant cap., t/yr	800,000	1,000,000	400,000	400,000	300,000
Iron ore	lumps/pellets	lumps/pellets	lumps/pellets	fines	fines
Reactor	shaft	shaft	retort	fluidized bed	fluidized bed
Pressure	Atmospheric	5 bars	5 bars	10 bars	-
Energy consumption:					
Natural gas,GJ/t	10	10.9	21	18	13
Power, kWh/t	125	85		200	230
Product:					
Forms	DRI/HBI	DRI	DRI	DRI	Fe_3C
Metallization, %	92	92	86	93	94
Carbon content, %	1.4	2	1.5	1.5	6

* From Dancy (1991)

2.1.2.2 Coal-based direct reduction

Although many coal-based and coke-free direct reduction processes have been reported (The Metals Society, London, 1979 and Stephenson, 1980), SL/RN process is the most successful commercially (Figure 2.2). SL/RN process, Figure 2.3, uses a rotary kiln as reactor. Inside the kiln, hot reducing gas and the ore move counter-currently. Due to the fact that gas and solid moves in different part of the kiln, the gas-solid contact is very poor. It leads to high fuel consumption and low productivity (Table 2.3).

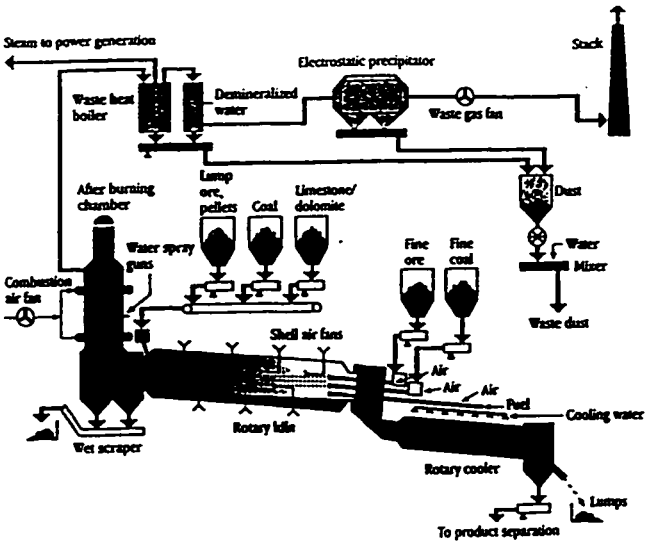

Figure 2.3 Flow sheet for a SL/RN process

(Elsenheimer et al, 1994)

Table 2.3. Important coal based direct reduction processes

PROCESS	Status	Typical plant cap., t/yr	Iron ore	Ore/coal preparation	Reactor	Off gas temp., °C	Coal rate, kg/t	Natural gas used, GJ/t
SL/RN*	industrial	150,000	lumps/pellets	added separately	rotary kiln	900 to 1000	920	
FASTMET**	Demo planned	500,000	fines	green pellets	rotary hearth		380	2.5

* From Elsenheimer et al (1994), ** From McAloon (1994)

FASTMET is a new process being developed by Midrex Direct Reduction Corporation (Lepinski, 1993). In the FASTMET process, shown in Figure 2.4, iron ore fines and pulverized coal are mixed together and pelletized. The dried green pellets are fed to a rotary hearth furnace. As the hearth rotates counter-currently to the flame, the pellets are heated to 1250 to 1350°C and iron oxide is reduced to metallic iron before one revolution is completed. As both iron ore and coal are in small sizes (in form of fine) and well mixed, the

FASTMET process developer claims that it has good kinetic conditions for chemical reactions.

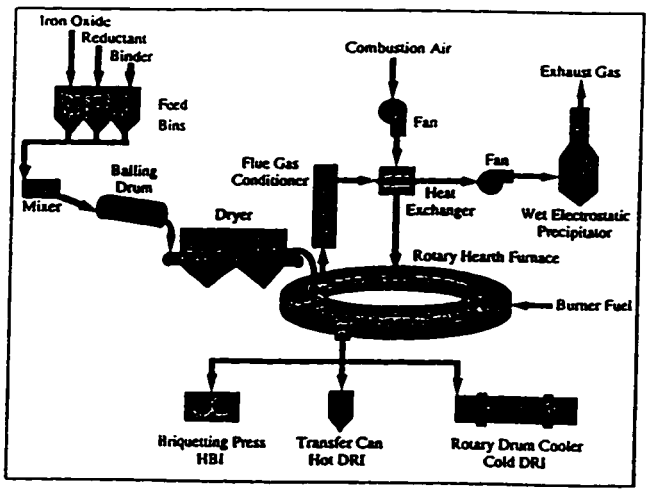

Figure 2.4 FASTMET process

A demonstration plant for the FASTMET process is currently under testing at Kakogawa Works (Hoffman and Myers, 1996), and the first commercial plant will be built in the Southern United States.

2.1.2.3 Coal-based smelting reduction

Coal-based smelting reduction processes usually consist of two reactors for the purpose of better energy efficiency, i.e. one reactor for pre-reduction at lower temperatures, and another high temperature reactor for final reduction and smelting. The exit gas from the smelting reduction reactor, after de-dusting, remains hot enough and have adequate

reducing power to be used as reductant in the pre-reduction reactor. Table 2.4 lists examples of the processes existing and under investigation.

COREX process, Figure 2.5, is the only commercialized smelting reduction process. A COREX unit of 300,000 t/yr capacity has been operating in ISCOR in South Africa and another larger unit is functioning well in Pohang Works, Posco of Korea.

In the COREX process production of high reducing power gas in the melter much exceed the requirement for the shaft furnace. The COREX process operates at a low energy efficiency, at a coal consumption of about 1100 kg/thm. The economics of the process depend on the market value of the excess gas for sale.

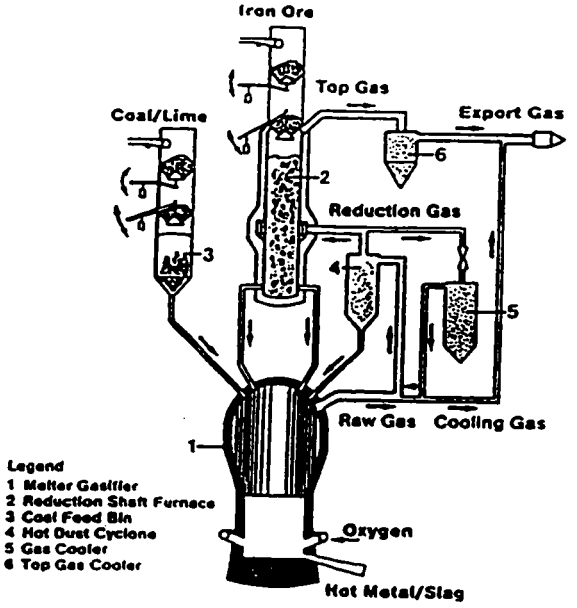

Figure 2.5 COREX process (Smith and Corbett, 1988)

Table 2.4 Selected coal-based iron making process

Process	COREX	AISI	Hismelt	DIOS	LB Furnace
Status	industrial	pilot	pilot	pilot	bench scale
Typical plant capacity	300,000 t/yr	5 t/hr	100,000 t/yr	100 t/day	
Iron ore	lumps/pellets	lumps/pellets	concentrates	fines	concentrates
Pre-reduction reactor	shaft	shaft	fluidized bed	fluidized bed	tube packed with ore/coal mixture
Degree of pre-reduction, %	>90	~30	~22	<30	>90
Final reduction:					
Reactor	fluidized bed	in bath smelter	in bath smelter	in bath smelter	plasma furnace
off gas temperature, °C	1050	1500 to 1650	1690	~1500	750
Post combustion, %	2 to 5	~40	55	~40	>92
Energy consumption					
Coal, kg/thm	1100 to 1250	~1100	630	~1100	~370
Oxygen, Nm^3/thm	600 to 750			500 to 750	
Power, kWh/thm	-				300
References	Delport, 1992	Aukrust, 1992	Wingroveet al, 1994	Ibaraki et al, 1995	Lu et al, 1986

AISI and DIOS processes (Table 2.4) were designed for very high processing rate in a BOF-type vessel at very high temperatures and strong mixing. The smelting reduction vessel was designed to operate at about 30% pre-reduction and metallization is carried out by reducing FeO in slag. However, the high processing rate necessitates high concentration of FeO in slag, high rate of CO generation from reduction and from partial combustion of coal to generate heat for strongly endothermic reactions. It appears to be that the conditions for high productivity, low energy consumption, long refractory lining life and stable operation can not be achieved at the

same time for a period of time of practical importance, at least at present (Nelko, 1994).

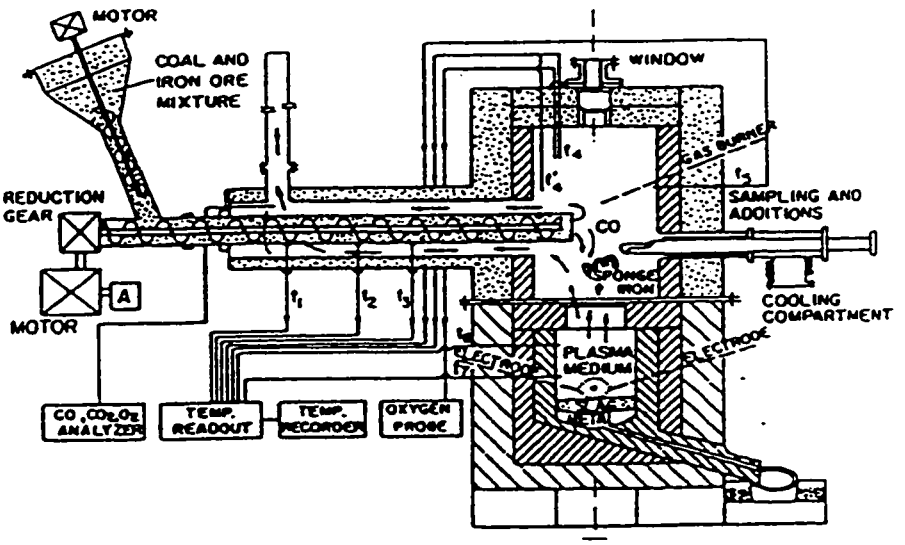

Figure 2.6 LB furnace process (Lu et al, 1986)

LB process at bench scale, Figure 2.6, uses iron ore concentrate and pulverized coal to produce liquid iron in a single furnace. Mixtures of iron ore concentrate and pulverized coal are fed and heated in a tubular reactor for pre-reduction. The chemical heat in the off gas from this reactor is converted into physical heat by combustion in a combustion chamber, and then used to heat the ore/coal mixtures indirectly in the pre-reduction reactor. This configuration gives the LB furnace process a high energy efficiency (Table 2.4). The use of fine raw materials and the

gasification of coal and pre-reduction of iron ore in the same reactor mean that LB furnace process has good kinetic conditions for chemical reactions due to large gas/solid interfacial reaction area and short distances for reactant transportation. The use of fine raw materials also avoids both high temperature iron ore agglomeration and cokemaking. Thus, this process, in comparison with blast furnace ironmaking, has higher energy efficiency and fewer processing steps.

2.2 The thermodynamics of iron oxide reduction

The thermodynamics of iron oxide reduction have been the subject of many books (Bodsworth, 1963; Bogdandy and Engell 1971; Strassburger, 1969; Ross, 1980). This review includes the iron-oxygen system and equilibrium relations between iron oxides, carbon monoxide and hydrogen.

2.2.1 Iron-oxygen system

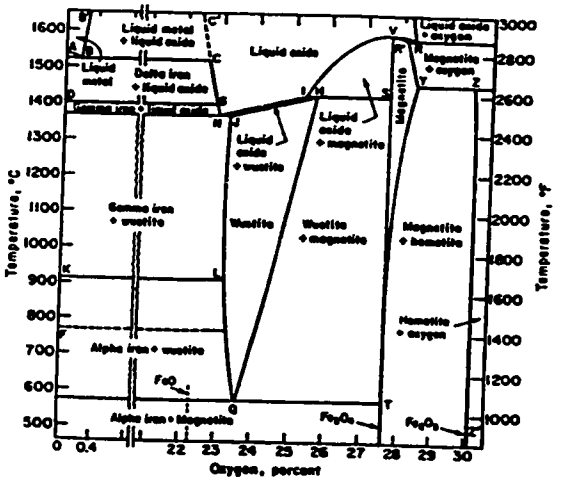

Point	Temperature deg F	Temperature deg C	Oxygen, percent	Point	Temperature deg F	Temperature deg C	Oxygen, percent
A	2795	1535	0	N	2500	1371	22.92
B	2775	1524	0.16	Q	1058	570	23.57
C	2775	1524	22.63	R	2881	1583	28.30
D	2552	1400	0*	R'	2881	1583	28.08
F	1418	770	0*	S	2593	1423	27.64
H	2593	1423	25.60	V	2907	1597	27.64
I	2593	1423	25.26	Y	2651	1455	28.36
J	2500	1371	23.15	Z	2651	1455	30.04
K	1670	910	0*.	Z'			30.06
L	1670	910	23.15				

*The effect of dissolved oxygen on these temperatures is not known but is presumably very small.

Figure 2.7 The binary system of iron-oxygen (Darken and Gurry, 1946)

The system may be best described in the phase diagram by Darken and Gurry (1946) as shown in Figure 2.7.

Iron oxides may exist in three forms, i.e. hematite (Fe_2O_3), magnetite (Fe_3O_4) and wustite (FeO) depending on temperature and oxygen potential of the system. Although the non-stoichiometric wustite is usually written as FeO or Fe_xO, the actual oxygen content in wustite has a wide range from 23.1 to 25.6 wt%. The value of x in Fe_xO is less than unity and close to 0.95 when it co-exist with metallic iron.

2.2.2 The sequence of the reduction of iron oxides by gases

The reduction of hematite to produce iron takes place step-wise, with porous magnetite and wustite (at a temperature above 570°C) as intermediates as shown in Figure 2.8. At temperatures below 570°C wustite will not form.

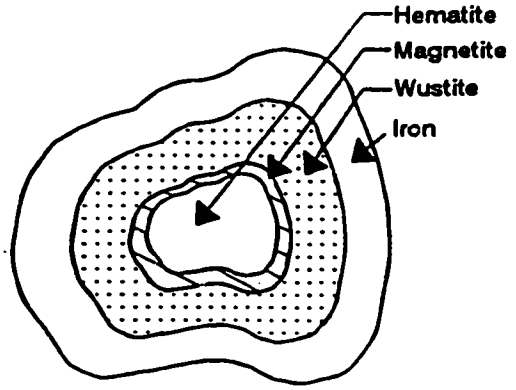

Figure 2.8 Cross-section of a partially reduced dense iron ore particle showing topochemical type of reduction

2.2.3 Equilibrium compositions between iron oxides and reducing gases

Carbon monoxide and hydrogen are the most common reducing agents used in commercial processes. Some thermodynamic data (Bogdandy and Engell, 1971; Ross, 1980) are given below as examples. Heat of reactions for the stoichiometric equations (per gram moles at 25°C) are included.

$$3Fe_2O_3 + CO = 2Fe_3O_4 + CO_2 \qquad \Delta H° = -52,869\ J/g\text{-}mole \qquad (2.1)$$

$$Fe_3O_4 + CO = 3FeO + CO_2 \qquad \Delta H° = 36,250\ J/g\text{-}mole \qquad (2.2)$$

$$FeO + CO = Fe + CO_2 \qquad \Delta H° = -17,305\ J/g\text{-}mole \qquad (2.3)$$

At a temperature below 570°C, magnetite is reduced directly to metallic iron,

$$\frac{1}{4}Fe_3O_4 + CO = \frac{3}{4}Fe + CO_2 \qquad \Delta H° = -3,916\ J/g\text{-}mole \qquad (2.4)$$

The equilibrium constant, K, of reactions listed above can be calculated from the standard free energy change of these reactions as a function of temperature (Elliott and Gleiser, 1960; Bogdandy and Engell, 1971). As an example, for reaction (2.3), the equilibrium constant can be calculated as follows

$$\ln K = \frac{-\Delta G°}{RT}$$

&l1o0o1t016D

$$K = \frac{a_{Fe} \times P_{CO_2}}{a_{FeO} \times P_{CO}} \qquad (2.6)$$

The iron and wustite are assumed to be essentially pure solids, hence, their activities may be considered to be unity, then the equilibrium ratio of partial pressure in the wustite reduction may be calculated from Equation 2.7.

$$K = \frac{P_{CO_2}}{P_{CO}} \qquad (2.7)$$

Similar calculations could be made for the other three reactions. The equilibrium phase diagrams (super-imposed with that for carbon-carbon oxides system) is shown in Figure 2.9.

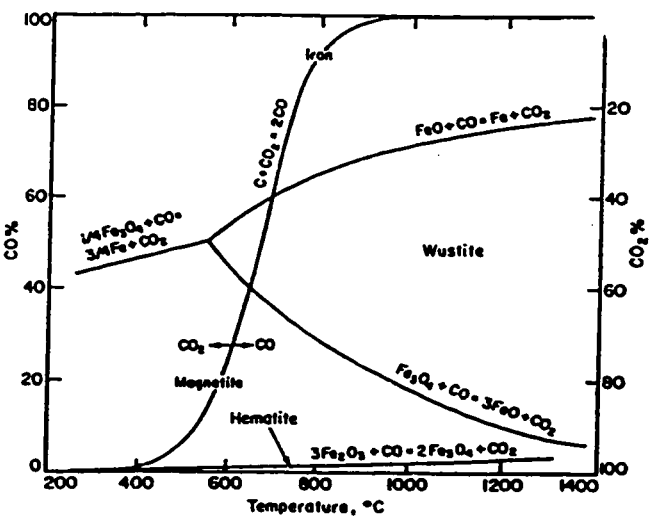

Figure 2.9 Equilibrium gas compositions versus temperature diagram for the iron-carbon-oxygen system (Ross, 1980)

The reduction of iron oxides by hydrogen is endothermic for reactions (2.9) and (2.10). The heat of reactions at 25°C are listed below

$$3Fe_2O_3 + H_2 = 2Fe_3O_4 + H_2O \qquad \Delta H° = -11,715\ J/g\text{-}mole \quad (2.8)$$

$$Fe_3O_4 + H_2 = 3FeO + H_2O \quad (T \geq 570\,°C) \qquad \Delta H° = 77,405\ J/g\text{-}mole \quad (2.9)$$

$$FeO + H_2 = Fe + H_2O \qquad \Delta H° = 23,849\ J/g\text{-}mole \quad (2.10)$$

$$\frac{1}{4}Fe_3O_4 + H_2 = \frac{3}{4}Fe + H_2O \quad (T < 570\,°C) \qquad \Delta H° = 37,238\ J/g\text{-}mole \quad (2.11)$$

The phase diagram of the H-O-Fe system is shown in Figure 2.10.

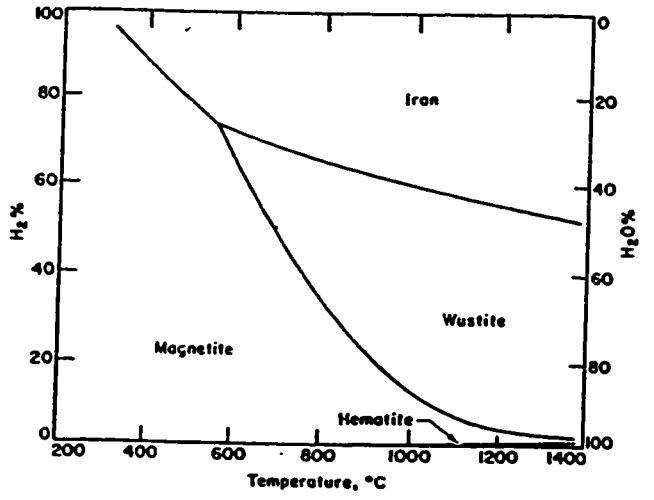

Figure 2.10 Equilibrium gas compositions versus temperature diagram for the iron-hydrogen-oxygen system (Ross, 1980)

2.2.4 Reactions between gases and solid carbon

The equilibrium curve for solid carbon and CO-CO_2 mixture (as shown in Figure 2.9) is highly endothermic

$$CO_2 + C = 2CO \qquad \Delta H^\circ = 172,464 J/g\text{-}mole \qquad (2.12)$$

This reaction is commonly known as Boudouard reaction, or carbon gasification. This reaction is highly endothermic and has a very large activation energy for chemical kinetics; therefore, it proceeds at an appreciable rate only at sufficiently high temperatures for a given reactivity of carbon.

The similar reaction in carbon and H_2-H_2O mixture is given below

$$H_2O + C = CO + H_2 \qquad \Delta H^\circ = 131,294 J/g\text{-}mole \qquad (2.13)$$

In the presence of solid carbon, Reactions (2.12) and (2.13) may restore the reducing power of local gas to sustain the reduction of iron oxides at the expense of heat.

2.3 Kinetics of reduction of iron oxides by CO and H_2

In the kinetic study of the reduction of iron oxides by CO and H_2, a spherical pellet is usually used for mathematical modelling because of its simple geometry and its similarity to commercial products. In this section, the shrinking core model

which was developed in the study of pellet reduction are briefly reviewed. Rate controlling steps and values of rate constants reported in the literature are discussed.

2.3.1 The reduction of a single oxide particle

The monitoring of reduction kinetics of a single oxide particle is usually carried out by suspending a spherical sample from a balance in a flowing-gas stream of known composition and temperature for continuous measurement of weight loss. The pioneer work was done by McKewan (1958) who studied magnetite reduction by hydrogen at temperatures less than 570°C. In order to analysis the weight-loss data, the experiment is usually designed for: (1) isothermal conditions; (2) single solid/solid interface where gas/solid reaction takes place; and (3) dense specimens. A sketch showing the reduction of a dense wustite sphere by CO is given in Figure 2.11.

The system is made of three phases: the gaseous phase, the porous layer of solid product, and the un-reacted pore-free solid reactant. The removal of oxygen from wustite takes place at a sharp iron/wustite interface, which shrinks parallel to the initial outer surface of the pellet, and results in weight-loss. The removal of oxygen proceeds through the following steps occurring successively during the

reaction:

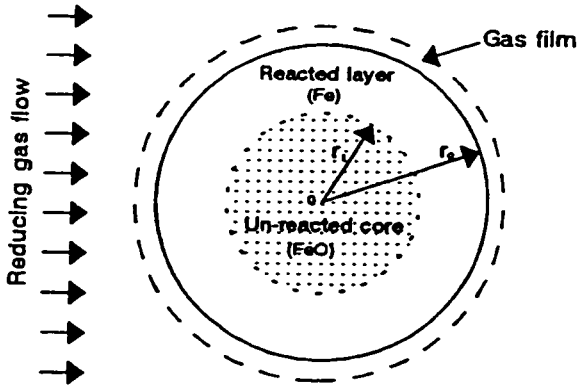

Figure 2.11 Schematic illustration of a partially reduced dense wustite pellet and a shrinking core model

(a) Transport of gaseous reactant (CO) from bulk gas to exterior surface of the particle through a gaseous boundary layer;

(b) Diffusion of gaseous reactant (CO) through the porous iron layer to the iron/wustite interface;

(c) Reduction of wustite by gaseous reactant to form metallic iron and gaseous product (CO_2) at the iron/wustite interface;

(d) Diffusion of gaseous product (CO_2) outward through the porous iron layer; and,

(e) Transport of the gaseous product (CO_2) from the

exterior surface of the particle to the bulk gas through the gaseous boundary layer.

Mathematically, the rate equations of these sequential steps may be expressed in three general classifications as follows (Spitzer et al, 1966):

(i) Mass transfer through a gas film (steps (a) and (e)),

The molar flux of CO from the bulk gas phase to the exterior surface of the sphere is given by:

$$\dot{n}^{m}_{CO} = -h_{CO} 4\pi r_o^2 (C^{b}_{CO} - C^{o}_{CO}) \qquad (2.14)$$

Similarly the molar flux of CO_2 from the exterior surface of the sphere to the bulk gas phase is given by:

$$\dot{n}^{m}_{CO_2} = -h_{CO_2} 4\pi r_o^2 (C^{b}_{CO_2} - C^{o}_{CO_2}) \qquad (2.15)$$

where $\dot{n}^{m}_{CO}$ is molar flow of CO from bulk gas to exterior surface of the pellet, $\dot{n}^{m}_{CO2}$ is molar flow of CO_2 from exterior surface of the pellet to bulk gas, mole/s; h_{CO} and h_{CO2} are mass-transfer coefficients for CO and CO_2, m/s; and C^{b}_{CO}, C^{o}_{CO}, C^{b}_{CO2} and C^{o}_{CO2} are concentrations of CO and CO_2 at bulk gas phase and the exterior surface of the particle, mole/m^3, respectively.

(ii) Diffusion through porous product layer (steps (b) and (d)).

The molar flows of CO and CO_2 ($\dot{n}^{D}_{CO}$ and $\dot{n}^{D}_{CO2}$) by diffusion

through the porous iron layer are given by:

$$\dot{n}_{CO}^{D} = -D_{effCO}\, 4\pi r_i^2 \frac{\partial C_{CO}}{\partial r} \qquad (2.16)$$

and

$$\dot{n}_{CO_2}^{D} = -D_{effCO_2}\, 4\pi r_i^2 \frac{\partial C_{CO_2}}{\partial r} \qquad (2.17)$$

respectively. Where D_{effCO} and D_{effCO2} are effective diffusivities for CO and CO_2, m^2/s, respectively.

(iii) Interfacial chemical reaction (step (c))

Oxygen removal from FeO/Fe interface by reaction (3) is usually considered as a first order, reversible reaction with respect to the concentration of a gaseous composition. Its rate of interfacial reaction is expressed as

$$\dot{r}_o = k\, 4\pi r_i^2 \,(C_{CO} - C_{CO_2}/K_e) \qquad (2.18)$$

where $\dot{r}_o$ is the rate of oxygen removal, mole/s; k is the rate constant, m/s; and K_c is the equilibrium constant.

Each step may contribute resistance to the completion of the overall chemical reaction. The slowest step among these five which are connected in series will provide the largest resistance to the overall reaction. If a step is much slower than all others so that resistances attributed to the other steps become relatively insignificant, this step is called rate-limiting or rate-controlling.

2.3.2 Mathematical modelling of isothermal systems

McKewan (1960) observed the rate of weight loss due to the removal of oxygen at magnetite/iron interface in spherical pellets (0.009 m in diameter) at a temperature lower than 570°C is proportional to the area of the iron/iron oxide interface. He proposed an 'area-controlled model' i.e. the rate of reduction was controlled by gas-solid interfacial reaction (Equation 2.18). He assumed that the un-reacted core of magnetite retains the shape of a sphere but shrinks with increased reaction time. The rate of reduction, in terms of rate of removal of oxygen per unit time, may be expressed as:

$$-\frac{dw_o}{dt} = -\rho_o 4\pi r^2 \frac{dr}{dt} \qquad (2.19)$$

where dw_o/dt is the rate of removal of oxygen in the solid specimen, mole/s; r is radius of the un-reacted core, m; and ρ_o is the oxygen density of the solid reactant, mole/m^3.

By integrating Equations 2.18 and 2.19, McKewan (1960) obtained following equation for the calculation of the degree of reduction or the size of the core as a function of the time of reaction.

$$r_o\rho_o[1-(1-\varphi)^{\frac{1}{3}}] = kt \qquad (2.20)$$

where φ is the fraction of the magnetite reduced and expressed as

$$\varphi = 1-(\frac{r_i}{r_o})^3 \qquad (2.21)$$

This model fits his data very well as shown in Figure 2.12 except at very long reaction times.

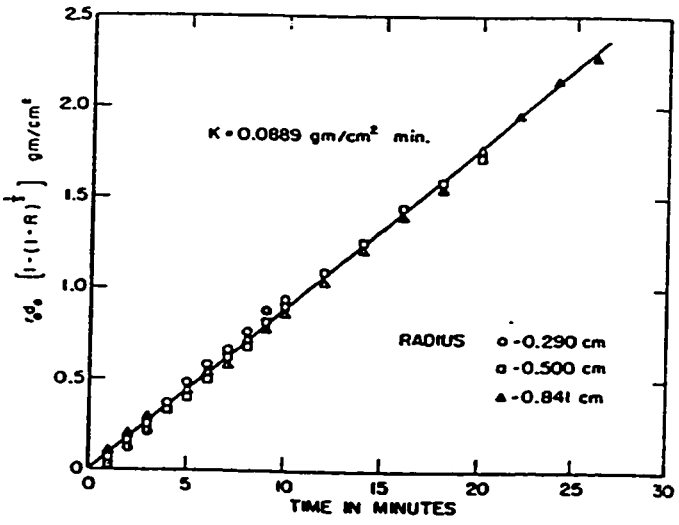

Figure 2.12 Interfacial reaction mechanism, linear relationship between the thickness of reacted layer and time (McKewan, 1960)

Kawasaki et al (1962) used larger artificial pellets with a diameter of 0.015 to 0.044 m and conducted the experiments at temperatures of 870 to 1200°C. They reported that their data can be explained very well by a model which assumed the rate of overall reaction is controlled by gaseous diffusion

through the porous product layer except at the early period of reduction. Their resulting diffusion mechanism equation is the integrated form of Equation 2.14, 2.16 and 2.19,

$$\frac{W_o r_o}{A_o(C_o-C_e)}\left[\frac{3}{2}[1-(1-\varphi)^{\frac{2}{3}}]-\frac{r_o\varphi}{(r_o+y)}\right]=D_{eff}t \qquad (2.22)$$

where W_o is oxygen molar weight loss of the oxide when fully reduced, mole; A_o is outside area of the specimen, m^2; and y is gas film thickness surrounding specimen, m. Their experimental and theoretical results are found in Figure 2.13.

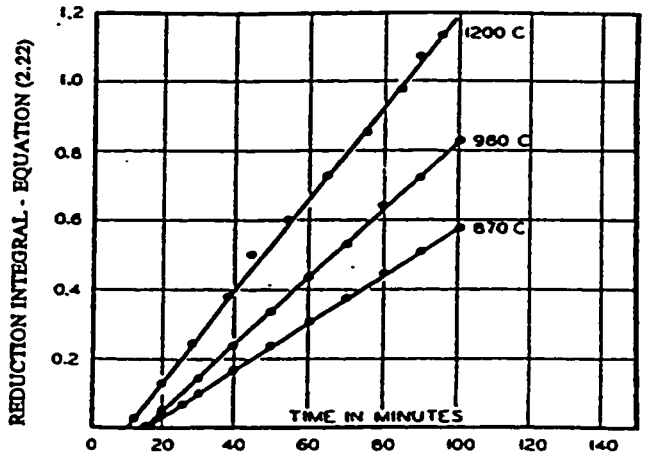

Figure 2.13 Diffusion mechanism for reduction of 0.028 m hematite sphere from wustite to iron by carbon monoxide (Kawasaki et al, 1962)

Lu (1963) recognized that interfacial reaction control and gas diffusion control are two extreme situations in the reduction of a iron oxide. During a reduction reaction, it is

possible that rate control may shift gradually from one mechanism to another. Lu (1963) proposed a mixed control model to include interfacial reaction and diffusion steps. In order to eliminate the unknown concentration of gaseous reductant in the interface, Lu proposed a quasi-steady state model to connect steps (b) and (c) in Section 3.2.1 and derived a general rate equation in the integrated form as follows

$$\frac{r_o D_{eff} k C_o t}{\rho_o} = D_{eff} r_o (r_o - r) + (k/6)(r_o^3 + 2r^3 - 3r_o r^2) \quad (2.23)$$

Experimental data reported by McKewan (1960) and by Kawasaki et al (1962) is explained very well for the whole range of degree of reduction based on Equation 2.23.

Spitzer et al (1966) and Nabi and Lu (1968) extended Lu's model to include all five steps to a system with up to 3 reacting solid/solid interfaces, i.e. Fe_2O_3/Fe_3O_4, Fe_3O_4/FeO and FeO/Fe interfaces. The model is limited for the case that kinetics of all heterogeneous reactions are assumed to be first order with respect to the concentration of gaseous reactants and products, and that diffusion coefficients are independent of gas concentration.

2.3.3 Determination of the value of the rate constant of an interfacial reaction

The rate constant k is a temperature-dependent parameter usually to be determined from kinetic data obtained isothermally according to a mathematical model. The meaning of a rate constant is determined by the rate expression adapted for a heterogeneous reaction. For low temperature reduction of magnetite to metallic iron k is defined as the rate constant, the single kinetic parameter, for forward reaction (McKewan, 1960).

The common approach in determining a value of a rate constant of an interfacial reaction is by careful experimental design to minimize the effect of transport steps, so that a simple mathematical model, such as Equation 2.18, could be used to analyze the data. It should be borne in mind that Equation 2.18 is for a special case, i.e. solid reactant is pore-free and spherical, and gas-solid reaction takes place at a sharp solid-solid interface (topochemical) as depicted in Figure 2.11. However, most specimens used in kinetic studies are multi-grain samples (green pellet) or porous agglomerates; therefore, the gas-solid reaction usually takes place in a reacting zone with a certain thickness as shown in Figure 2.14. Then the rate of reaction should be expressed as

$$\dot{r}_o = A_z k(C_{CO} - C_{CO_2}/K_e) \qquad (2.24)$$

where A_z is the area of reaction surface at time t.

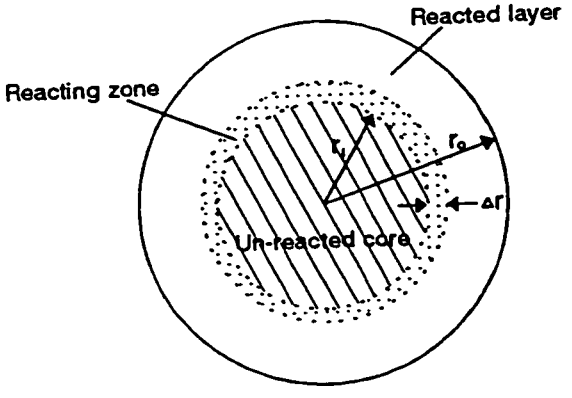

Figure 2.14 Schematic illustration of a partial reduced wustite pellet of high porosity

As the rate of reduction is usually measured by specimen weight loss, the value of gas-solid interfacial area must be provided before the value of rate constant could be determined using equation 2.24.

Another special case is that the solid reactant is small in size and highly porous, so that pores are open and well connected with the external surface. Due to the ease of mass transfer through void space by gaseous diffusion, the whole specimen takes part in the chemical reaction with slightly varying intensity in different regions at the same time. The initial interfacial area for the gas-solid reaction of the specimen at the start of the reaction is the total solid

surface of the specimen, decreases with time

$$A_z = \frac{4}{3}\pi r_o^3 \rho\, a_s \qquad at \quad t = 0 \qquad (2.25)$$

where ρ is the density of the solid reactant, and a_s is specific surface area of the solid reactant. The a_s is usually determined by B.E.T. method.

However, most of the solid reactants used in the experiments represent neither of these two special cases. In general, in the analysis of experimental data, the product $A_z k$ in Equation 2.24 can not be separated without additional information.

Although numerous works have been conducted for the purpose of evaluation of kinetic parameters, there are only a few with the proper experimental design and mathematical modelling so that rate constants could be extracted from data with a defined meaning. Only those papers with some details on experimental conditions and mathematical modelling are selected for review here.

Figure 2.15 shows the plot of rate constant for wustite reduced by CO against the reciprocal temperature, reported by different investigators. The difference in the reported values is substantial. The reported experimental condition are listed in Table 2.5. It is clear that the use of Equation 2.18 would result in an under-estimation in the value of reaction surface area, and thus an over-estimation in the value of the rate

constant, from the value of their product $A_z k$. On the other hand, the use of Equation 2.25 has the opposite effect.

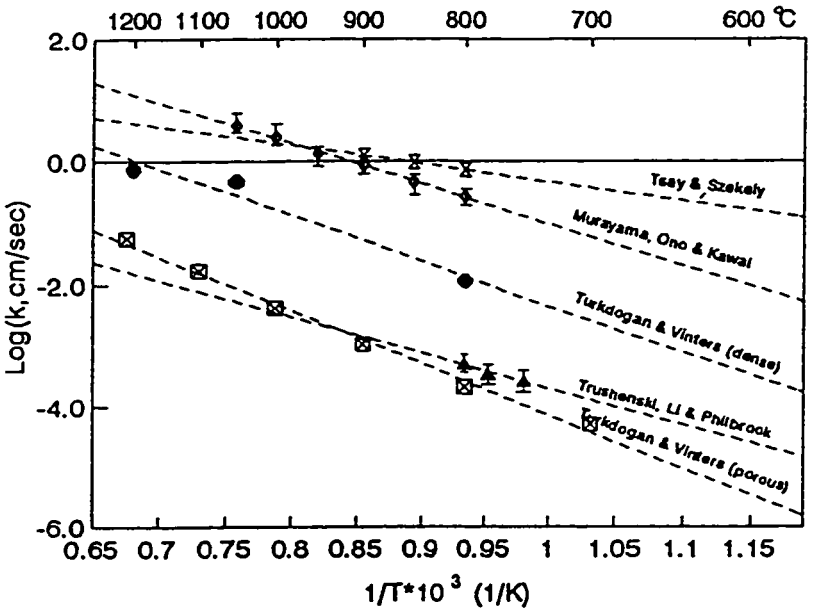

Figure 2.15 Plot of rate constants against the reciprocal temperature for reduction of FeO by CO

Murayama, Ono and Kawai (1978) and Tsay and Szekely (1976) assumed a pore-free specimen and used Equation 2.18. The values of rate constant they obtained may be considered as the upper limit of the true value (Figure 2.15). Trushenski, Li and Philbrook (1974) and Turkdogan and Vinters (1972) assumed porous specimens and used Equation 2.25. The values of rate constant they obtained may be considered the lower limit in Figure 2.15. Turkdogan and Vinters (1972) also estimated the rate constants for reduction of dense wustite plate using similar technique as in Equation 2.18. The rate constants thus

obtained are shown in Figure 2.15 marked as Turkdogan & Vinters (dense). The difference between the limiting values of rate constants extends over three orders of magnitude. However, it is important to note that the values of the product $A_z k$ for the specimen of similar size from different work at 800°C (the third row from bottom in Table 2.5) are of the same order of magnitude. Therefore, the difference in the reported values of the rate constant reflected the difference in the assumed value of A_z. This insight provides a guidance in our search for values of rate constants in the present work.

Table 2.5 Reported experimental condition for rate constant determination for wustite reduction

authors	Murayama et al	Tsay et al	Trushenski et al	Turkdogan	& Vinters
Starting materials	hematite ore	hematite powder	hematite powder	hematite ore	steel strip
Wustite shape	fired pellet	green disk**	green pellet	granule	plate
Size, m	ϕ0.0105 to 0.013	ϕ0.0286×0.11	ϕ0.0135	ϕ0.0004 to 0.0036	0.02×0.05× 0.001
Porosity,%	13	60	45-78	30	very dense
interface area determination	topochemical	topochemical	B.E.T.	B.E.T	topochemical
Specific surface at 800°C, m^2/kg			460	1400	
initial surface per specimen at 800°C, m^2			0.95	0.42	
$4\pi r_o^2$, m^2	4.5×10^{-4}	8.98×10^{-4}			2.0×10^{-3}
Gas velocity, m/s (STP)	2 to 6	15	1	4.7 to 7.8	4.7 to 7.8
Gas composition,	CO	CO	72.38% CO 27.62% CO2	90%CO 10%CO_2	90%CO 10%CO_2
Temperature, °C	800 to 1050	800 to 900	600 to 900	600 to 1200	800 to 1200
Kinetic measurement	weight loss	weight loss	weight loss	weight loss	weight loss
Steps in model	reaction,diffusion, mass transfer	reaction, diffusion	reaction, diffusion	reaction	reaction
Claimed R.C.S.	mixed	mixed	mixed	interfacial reaction	interfacial reaction
Data used	whole range	whole range	whole range	initial rate	initial rate
$A_o k$ at 800°C, m^3/s	4.19×10^{-6}	6.47×10^{-6}	4.67×10^{-6}	0.88×10^{-6}	0.22×10^{-6}
A_o	Equation 2.18	Equation 2.18	Equation 2.25	Equation 2.25	Equation 2.18***
k at 800°C, m/sec	0.0093	0.0072	4.9×10^{-6}	2.1×10^{-6}	0.0011

* R.C.S.: rate controlling steps
** bottom and top side of the sample were ceramic coated.
*** for flat plate

2.4 Reduction of iron oxide in iron oxide/carbon composites

The reduction of iron oxide in iron oxide/carbon composites has been extensively investigated in the last three decades. However, due to the complex nature of this reaction system and limitations of existing experimental techniques, the reduction kinetics and mechanisms in this system are less understood than that of reduction by gaseous reductants. In this section, the experimental techniques used and mathematical models developed, and their limitations are reviewed.

2.4.1 Experimental studies of iron oxide reduction in iron oxide/carbon composites

In experimental studies reported in the literature, hematite was commonly used as the iron oxide, the forms of carbon used included graphite, coke, coal char, coconut char, charcoal, and coal. The particle size of both iron oxide and carbon ranged from -60 to -325 mesh. The specimen of iron oxide/carbon mixture was prepared either in the form of pellets, with a size ranging from 0.006 m to 0.019 m in diameter (Ghosh and Tiwari, 1970; Rao, 1971; Fruehan, 1977; Seaton et al, 1983), or in packed beds (Otsuka and Kunii, 1969; Bryk and Lu, 1986; Haque et al, 1992 and 1993). Table

2.6 lists some examples of these studies; experimental techniques and conditions are also included.

Table 2.6 Reported study of iron oxide reduction in oxide/carbon composite

References		Ghosh & Tiwari	Rao	Fruehan	Srinivasan et al	Seaton et al	Otsuka & Kunii	Bryk & Lu
ore	Form	hematite ore	hematite powder	hematite powder	hematite ore	Fe_3O_4, Fe_2O_3 ore	hematite powder	magnetite
	Size, mesh	-60	-325	-200	-300		-100 to -325	-200
carbon	Form	coke	amorphous carbon	charcoal, char, coke, graphite	graphite	coal char	graphite	coal
	Size, mesh	-60	-48 to -325	-200	-300	-325	-65 to - 325	-16 to -200
specimen	Oxide to C ratio	85/15 to 60/35 by wt-%	1/1.5 to 1/9, by mole	84/16 by wt%	1/3 to 1/8, by mole	~80/20 by wt%	80/20 by wt%	80.7/19.3 to 70/30, wt%
	Form	pellets	pellets	pellets, packed bed	pellets	pellets	packed bed	packed bed
	Size,m	ϕ0.019	ϕ0.008×0.013	ϕ0.006 to 0.014	ϕ0.012	ϕ0.014	ϕ0.016×0.02	ϕ0.019 to 0.043 ×0.09 to 0.132
Temperature,°C		900 to 1100	850 to 1087	900 to 1200	925 to 1060	800 to 1200	1050 to 1150	900 to 1300
Atmosphere			Ar	Ar	N_2	N_2	N_2	air
Weight measurement		weighted B & A[2]	weighted B & A	micro-balance	micro-balance	weight B & A	micro-balance	chemical analysis
Gas analysis		no	no	G.C[3].	G.C.	no	G.C.	no
model			$dW_c/dt=-kW_c$	$dW_c/dt=-kW_c$		$dW_c/dt=-kW_c$		
R.C.S.[1]		FeO reduction	C gasification	C gasification	C gasification FeO reduction	C gasification, heat transfer	C gasification Feo reduction	heat transfer

[1]. R.C.S.: Rate Controlling Steps, suggested by the author;
[2]. weighted B & A: weighted specimen before and after reaction;
[3]. G.C.: Gas chromatography;

(a) **Pellet specimens:** Weight-loss method was commonly used in the kinetic study of pellet specimen. In these types of experiments, the specimen was suspended in a vertical tubular furnace. At the beginning of an experiment, the furnace was quickly heated to the pre-set temperature. The specimen weight-loss was recorded continuously by microbalance (Fruehan, 1977; Srinivasan and Lahiri, 1977; Bandyopadhyay et al, 1993), or by weighing the specimen before and after the reaction (Ghosh and Tiwari, 1970; Rao, 1971; Seaton et al, 1983). Gas chromatography was also used to analyze exit gas composition to get the rate of carbon gasification indirectly by some investigators, including Fruehan (1977), Srinivasan and Lahiri (1977), Bandyopadhyay et al (1993).

These experiments provided a qualitative understanding of these reacting system. The rate of the overall reaction increases with the increase of several experimental parameters such as furnace temperature, carbon/iron oxide ratio, reactivity of carbon, and specific surface of both iron oxide and carbon. However, quantitative information, particularly with respect to the composition changes and temperature variations within the specimen as functions of reaction time, were not available in these investigations.

The weight-loss method measures only the weight-loss of the specimen during reduction, which consists of loss of weight due to gasification of carbon (i.e. Reaction (2.8)), and

removal of oxygen from iron oxides (i.e. Reactions (2.1) to (2.4)). It is impossible to calculate contributions of individual reactions to the measured weight loss in these studies.

(b). **Packed bed:** Different sizes of packed beds were used in the study of iron oxide reduction. Otsuka and Kunii (1969) and Fruehan (1977) packed the iron oxide/carbon mixture in a small crucible, 0.016 and 0.014 m I. D. respectively, and used the same method as that for the pellet specimen experiments, i.e. a weight-loss method and exit gas analysis, with similar shortcomings as discussed above.

In order to obtain kinetic information of the reacting solids within the bed, Bryk and Lu (1986) designed their experiments with a larger crucible. They packed the mixture of magnetite ore/coal in steel crucibles with inside diameters of 0.019, 0.032 and 0.043 m, and heights of 0.09 and 0.132 m. The loaded crucibles were heated in either a muffle furnace or a tubular furnace. Temperatures at the centre of packing were monitored continuously by an embedded thermocouple. After a predetermined time, the crucibles were taken out of the furnace and cooled externally under argon atmosphere. Samples of reacted mixture at various locations along the radial direction were taken for chemical analysis. These experiments were the first to confirm concentration gradients of solid phases along the direction of heat flow within the specimen.

However, only two temperatures were measured, i.e. centre and surface of packing, the temperature distribution within the system was uncertain, and no attempt was made to obtain information of gaseous phase.

2.4.2 Reduction mechanisms

It is generally agreed among authors in this field that the reduction of iron oxide and oxidation of carbon proceed by simultaneous gas/carbon and gas/iron oxide reactions, i.e. Reactions (2.1) to (2.4), and (2.8). The reaction between the two solid phases can only happen at points of direct contact which will be destroyed as soon as solid product forms and carbon is gasified.

Otuska and Kunii (1969) and Fruehan (1977) observed that the rate of weight-loss decreased significantly after a loss of 10% of the initial weight. Assuming the specimen is homogeneous, a mass balance calculation indicates that it corresponds to complete reduction of hematite to wustite. They concluded that in the "first stage" reduction, hematite was reduced to magnetite and then wustite uniformly throughout the specimen, and assumed that no metallic iron was up to that time. Wustite was then reduced to metallic iron in the "second stage" of reduction. Srinivasan and Lahiri (1977) supported this conclusion with their X-ray investigation results of

partially reduced pellets. However, in x-ray analysis of partially reduced specimens of similar size, all of Fe_2O_3, Fe_3O_4, FeO and metallic iron were identified in the single pellet by Ghosh and Tiwari (1970) and Rao (1971). This suggests the reduction of the iron oxide, depending on the size of the specimen and the temperature, may not be uniform in composition and temperature throughout the pellet. This non-uniformity in the reduction of iron oxide within the specimen was confirmed by Bryk and Lu (1986), who observed concentration gradients of iron oxides along the direction of heating in their chemical analysis of partially reduced specimens.

2.4.3 Isothermal mathematical model

In this system with a strongly endothermic reaction, heat is supplied outside of the specimen and consumed in the interior. The existence of a large temperature gradient within the specimen is necessary to maintain a large heat flux to sustain endothermic reactions. It is a non-isothermal system, even though the furnace temperature can be kept constant. For the overall reaction, gases are produced in the interior of the specimen from solid reactants. It would be necessary to include temperature and pressure gradients and flows of heat and gases in the mathematical model to yield better co-

relations and explanations. However, due to lack of information, heat and mass transfer were not included in modelling except Seaton (1983) and Bryk and Lu (1986).

In the modelling of iron oxides and carbon system, Rao (1971), Fruehan (1977) and Seaton et al (1983) assumed that it is an isothermal system and that gasification of carbon was the rate controlling step. The following rate equation for a pseudo-homogeneous reaction of first order with respect to the remaining carbon in the system was used to explain their experimental results.

$$\frac{dW_c}{dt} = -W_c k_c \qquad (2.26)$$

where W_c is the weight of carbon and k_c is a rate constant. Alternatively, its integral form is:

$$\ln(1-f_c) = -k_c t \qquad (2.27)$$

where f_c is the fraction of carbon reacted.

Equation 2.27 was used to fit their experimental data; however, agreement was obtained only for a certain range of reaction times and temperatures. In Rao's (1971) study, the computed results from Equation 2.27 fitted his experimental data only after the process reached a weight-loss of about 15% of the initial weight in temperature ranges from 957 to 1087°C as shown in Figure 2.16, but failed at temperatures of 907 and 947°C as shown in Figures 2.17. It should be noted that at higher temperatures and after 15% of weight loss, carbon is

also participating in the rate-controlling step.

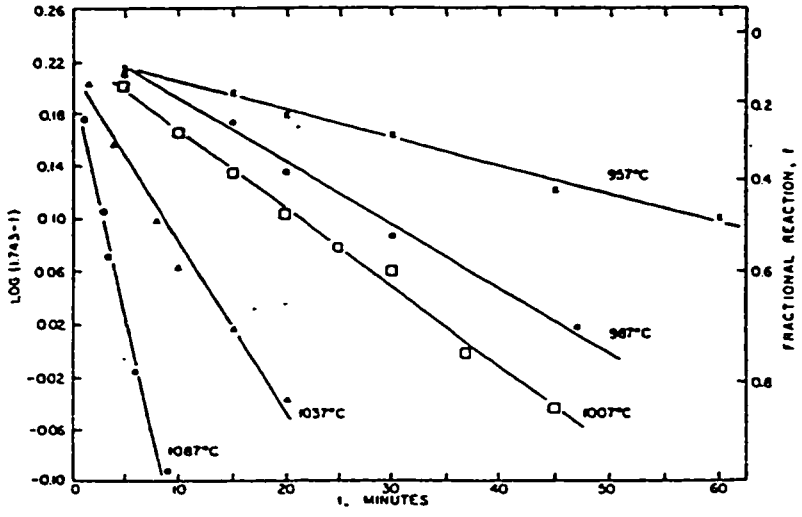

Fig. 2.16. Plot of experimental results according to Equation 2.27, 957 to 1087°C (Rao, 1971)

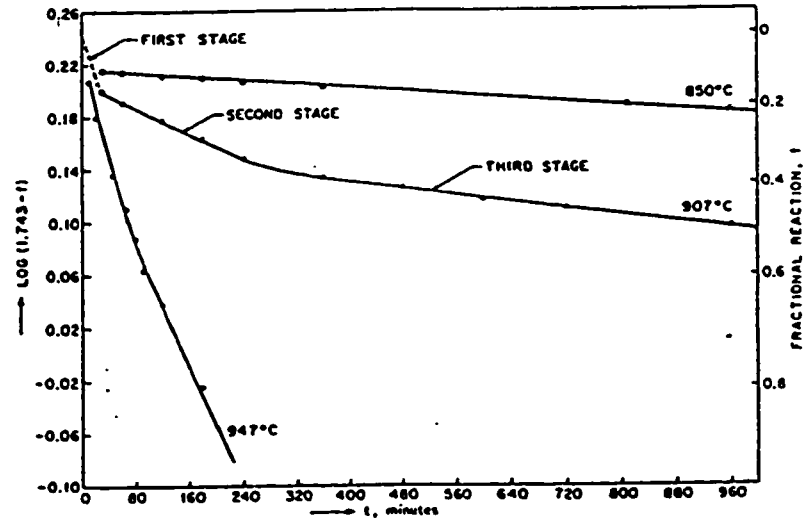

Fig. 2.17. Plot of experimental results according to Equation 2.27, 907 to 947°C (Rao, 1971)

In a study of reduction of very fine hematite (-325 mesh) by graphite, Otsuka and Kunii (1967) plotted the rate of oxygen removal against the reciprocal of temperature at two levels of reduction degree, 20% and 60%. At 20% degree of reduction, the "activation energy" was found to be 230,120 to 313,800 J/mole, and 62,760 to 98,324 J/mole at 60% degree of reduction. By comparing with reported values of "activation energy" for iron oxide reduction and carbon gasification, they claimed that the reduction of fine hematite (-325 mesh) in this system was controlled by carbon gasification at the "first stage" of reduction, and by wustite reduction at the "second stage" of reduction. With the same technique, Srinivasan and Lahiri (1977) reached a similar conclusion about the rate controlling step.

However, in the analysis of off gas from the reaction tube, Fruehan (1977) observed that CO/CO_2 ratio during the entire reduction process was found to be close to the equilibrium value for FeO/Fe under CO/CO_2. He concluded that the carbon gasification reaction is the rate controlling step for the process.

2.4.4 Non-isothermal condition of the system

Recognizing that the highly endothermic carbon gasification would act as a heat sink preventing the reacting system from reaching thermal equilibrium, Seaton et al (1983) considered the reduction of iron oxide in the iron oxide/carbon system might take place under significant temperature gradients, and the process might be controlled by heat transfer. In order to estimate the effect of heat transfer on the reduction process, they measured temperature changes near the surface and at the centre of the pellets by placing thermocouples at these locations with furnace temperature set at 1000, 1100 and 1200°C. The measured results are shown in Figure 2.18.

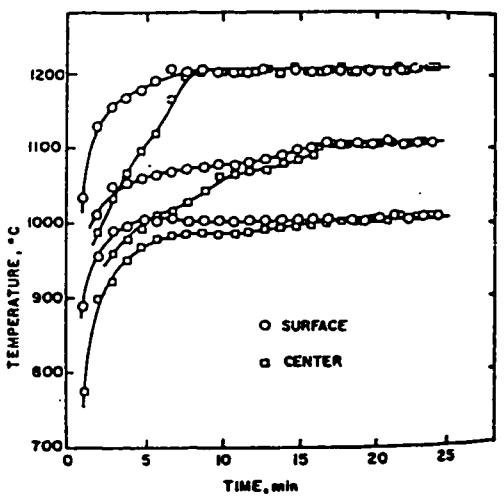

Figure 2.18 Measured temperature at surface and core of magnetite pellet (Seaton et al, 1983)

The results indicated that the reduction process occurs under non-isothermal conditions. They suggested that although the

rate of reduction of iron oxide is controlled by the rate of the carbon gasification reaction, the limiting step could be the rate at which energy is supplied to the interior to maintain a significant rate for the carbon gasification reaction.

Bryk and Lu (1986) observed not only a significant temperature difference between the furnace and at the centre of mixture packed in the steel crucible, as shown in Figure 2.19, but also gradients for the degree of metallization along the radial direction of the packing during the reduction of magnetite concentrate in ore/coal composite, as shown in Figure 2.20. The results suggested that the heat transfer in the mixture is relatively slow and could be the rate controlling step to the overall reaction.

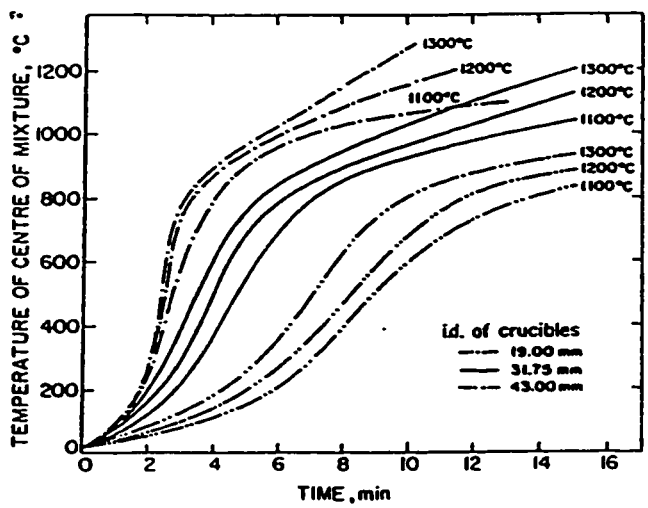

Figure 2.19. Measured temperature at centre of crucible of different size (Bryk & Lu, 1986)

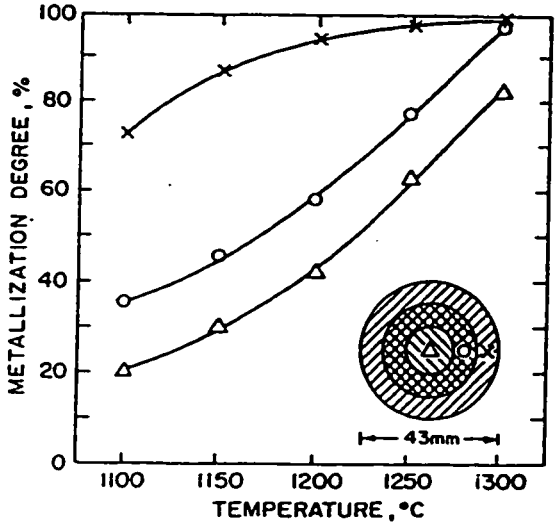

Figure 2.20. Metallization degree at various distances from centre of crucible and temperature (Bryk & Lu, 1986)

2.5 Summary

Blast furnace ironmaking technology, by far the most important ironmaking process, is based on coke and iron ore pellets or sinter to produce liquid iron. However, it faces significant environmental challenges as coke ovens and sintering plants are considered to be serious polluters and extensively regulated. In order to meet regulatory requirements, high capital and operational cost are incurred. Thus, a worldwide effort to search for a more economical and environmentally friendly ironmaking process is under way, which includes a coal-based and coke-free ironmaking process.

Among the other processes under investigation, FASTMET and LB furnace processes use iron ore concentrate and pulverized coal as raw materials. They have the potential advantages of low energy consumption and without high temperature agglomeration of ore, nor the coking step. The successful commercialization of these processes will depend on our knowledge of kinetics and mechanisms in these ore/coal reaction system, which is the subject of the present work.

CHAPTER THREE: EXPERIMENTAL STUDY

The reduction of iron ore concentrate by pulverized coal in a ore/coal mixture is a very complex process. It involves simultaneous heat transfer, mass transfer and heterogeneous chemical reactions (gas/solid reactions). For kinetic and mechanism studies, properties of both solid and gaseous phases in the reacting system as functions of location and reaction time must be determined. The objective of experimental work consists of the design of a reactor and the generation of experimental data under various conditions. It includes *in-situ* measurements of temperature and gaseous pressure in the system, measurement of the profiles of the chemical compositions in the partially reacted ore/coal mixtures, and the chemical compositions of exit gas.

3.1 Experimental design

3.1.1 Experimental set up

A one-dimensional system was designed for its simplicity in both measurements and modelling. It consists of a cylindrical stainless steel crucible (0.105 m in height and

0.058 m i.d.) heated from the bottom with an open ended top, and a sensor locating frame as shown in Figures 3.1 and 3.2. The outer surface of the crucible wall is wrapped with ceramic fibre for thermal insulation. To minimize the wall effect of the crucible, the height of packing is set at 0.028 m, less than the inside radius of the crucible. During an experiment, the crucible, packed with an iron ore/coal mixture, is heated from the bottom surface by a vertical tubular furnace that is kept at a pre-set temperature. The uniformity of heating in the radial direction has been confirmed in the preliminary experiments. The top end of the crucible is open, which allows gases generated to exit and keeps heat and gas flow parallel in the axial direction.

Five thermocouple or pressure sensors are embedded along the height of the packing from bottom to top at every 0.007 m vertical distance as shown in Figure 3.1. The terms "Location 1, 2, 3, 4 and 5" used to display the experimental results signify the location at the same height where the corresponding sensor is embedded. In order to minimize both the disturbance from other sensors and the wall, these sensors are located separately in a central area 0.009 m in radius, where the horizonal distance between the two nearest sensors is 0.009 m. A sixth thermocouple was placed at the outer surface of the crucible bottom to monitor the furnace temperature.

3.1.2 Monitoring Instruments

The thermocouples used are Chromel-Alumel (type K) thermocouples of 0.001 m O.D., calibrated and supplied by the Thermo-Kinetics Company. The recommended temperature range of measurement for this type of thermocouple is 0 to 1250°C with an error of $\pm$0.4%. Thermocouples were connected to a data-logging computer (Zenith data system) and temperatures were monitored and recorded every 12 seconds.

For pressure measurement, stainless steel tubing of 0.0011 m O.D. was used for pressure probes. Each probe was connected to a variable reluctance differential pressure transducer. Pressure signals from the probe were transduced to a DC voltage and recorded by the same data-logger at the same frequency as for temperature measurements. The pressure transducers (Validyne DP15) were supplied by Validyne Engineering Corporation. After preliminary experiments, two pressure ranges of measurement of this transducer (0 to 8800 and 0 to 22500 Pa) were selected. The error of measurement claimed by the manufacturer is $\pm$0.25% of the full scale. The pressure measurement system was calibrated against a water manometer before each experiment with a error of $\pm$1.0% of the full scale reading.

The exit gas was sampled by a syringe (250μl) at about 3 to 0.005 above the top of the packing every 5 minutes, and

analyzed immediately by a gas chromatograph (GC) (Shimadzu GC-9A, supplied by Shimadzu Corporation, Japan). The GC was controlled by a microcomputer (Chrimatopac CR601) which also served as a data processor. The analytical column used was a HayeSep DB (30'×1/8", 100/120 mesh) supplied by Chromatographic Specialties Inc., and was capable of separating H_2, N_2, CO, CO_2, CH_4 and C_2H_4. The sensitivity and linearity of the detector of the GC was 0.01 vol% and $\pm$0.1%, respectively, and these accuracy were confirmed by calibration against standard gases before an experiment.

3.1.3 Raw materials

The raw materials used in the present experiments were magnetite concentrate and high volatile coal. Tables 3.1 and 3.2 show the chemical compositions of the iron ore concentrate and proximate analysis of the coal. The concentrate was from Sherman Mines, Ontario, and the chemical analysis was provided by Dofasco Inc. of Hamilton, Ontario, with an accuracy of $\pm$1.0% of the reported values. The coal was provided by Dofasco Inc. and analyzed by the Energy Research Laboratory of CANMET, Ottawa, Ontario, with a accuracy of $\pm$5.0% of the reported values. The size distribution of the concentrate and pulverized coal were analyzed in our laboratory and are shown in Table 3.3.

Table 3.1. Chemical analysis of iron ore concentrate (wt%)

T.Fe	Fe^{2+}	SiO_2	CaO	MgO	Al_2O_3	MnO	K_2O	S
66.21	9.66	5.27	0.28	0.39	0.58	0.01	0.18	0.01

Table 3.2. Chemical analysis of the coal (wt%)

Proximate analysis				analysis of volatile matter			
Fixed carbon	Volatile matter	Ash	S	Carbon	H	N	O
57.34	34.53	6.90	1.23	21.16	8.50	1.30	4.53

Table 3.3. Particle size distribution of the raw materials (%wt)

Size ×1000, m	+0.300	0.300-0.212	0.212-0.149	0.149-0.088	0.088-0.075	0.075-0.053	0.053-0.044	-0.044
Ore	2.41	1.83	2.77	4.25	7.83	19.91	27.40	33.60
Coal	4.05	4.95	7.55	9.97	15.16	36.26	18.28	3.78

The iron ore concentrate was dried at approximately 110°C for 6 hours, and the coal was dried at approximately 95°C for 8 hours to remove moisture.

3.1.4 Experimental conditions

In most experiments, the dried concentrate and pulverized coal were mixed in an ore/coal ratio of 80/20 by weight %, which is very close to the theoretical requirement of carbon (total carbon in the coal) to remove oxygen in the ore according to the following stoichiometric relationship and preliminary experimental results:

$$Fe_3O_4 + 4C = 3Fe + 4CO \qquad (3.1)$$

The packing density of the mixture was 1900 kg/m^3. Most of the experiments were conducted with the furnace temperature set at 1200° C. The reaction time was 10, 20, 30, 40, 50 and 60 minutes.

In order to investigate the effect of furnace temperature on heat transfer and rate of reaction, a series of experiments were conducted with the furnace temperature at 1300°C and reaction times of 30 and 60 minutes, with the same ore/coal ratio and packing density.

Two sets of experiments were conducted with ore/coal ratio of 82/18 and 85/15 to determine the effect of ore/coal ratio on the rate of reactions, with the packing density of 1900 kg/m^3 and furnace temperature of 1200°C.

3.1.5 Experimental procedure

"Time zero" of an experiment is defined when the steel crucible packed with the ore/coal mixture was placed on the top of the furnace which was already stabilized at the preset temperature. Temperature and pressure data were recorded by the data logging computer in 12 second intervals. Exit gas was sampled by using a syringe (250 μl) and analyzed by gas chromatography every 5 minutes during the experiment. After a predetermined reaction time (i.e. 10, 20, 30, 40, 50 and 60

minutes), the crucible was quickly removed from the furnace, placed in a spot with argon shrouding from above and quenched by running water over the bare wall of the crucible to stop the reactions in the mixture. Samples were taken at each location at the same height as thermocouples and pressure probes by careful removal of the partially reacted mixture, layer by layer, from the top. The amounts of total iron, metallic iron (Fe°) and ferrous iron (Fe^{2+}) were determined by titration, and ferric iron (Fe^{3+}) was by determined the difference. The carbon content were determined by a Leco Carbon Analyzer.

3.2 Experimental results

Experimental results are presented generally as data points in figures. In addition to the experimental work, a mathematical model has been developed (presented in subsequent chapters) for the present study. Computed curves, which are compared with and used to explain these experimental results in Chapters 4 and 5, are included in these figures to avoid duplication.

3.2.1 Temperature profile

Figure 3.3 shows the typical local temperatures as functions of reaction time including the cooling periods after 60 minutes of reaction. The furnace temperature was set at 1200 °C. The reproducibility of the temperature measurements is shown in Figures 3.4 and 3.5, which show the results of three sets of measurements, and the average values and deviations of these measurements, under supposedly the same experimental conditions.

As shown in Figure 3.3, the temperatures at locations 4 and 5 remained at about 100°C for a period of 2 to 4 minutes at the early stage of heating. This may be due to the condensation of water vapour originating from the high temperature locations (1 and 2) followed by re-vaporization.

Temperature profiles over the height of the bed at different times are shown in Figure 3.6. The temperature gradients are steeper near the hot surface, for shorter reaction times. It may be due to the lower effective thermal conductivity of the initial ore/coal mixture and the highly endothermic nature of carbon gasification by CO_2 and H_2O, which are also reactive at higher temperatures. A detailed explanation is presented in the Chapter Five.

3.2.2 Measurement of gaseous pressure

Figures 3.7 and 3.8 show gaseous pressures measured at different locations as functions of reaction time in two duplicate experiments. It is understood that variable values for pressures are expected in the ore/coal reacting system due to the complicated bed structures that are changing during the reaction. However, these results show the same pattern and magnitude of pressure build-up in the system.

Pressure peaks were observed during first 20 minutes of reaction time. The build up of gaseous pressure in the system is determined by the local rate of gas generation, temperature, and temperature gradient and the resistance of the solid bed to gas flow. The pressure peaks are most likely the result of a higher rate of gas generation by coal devolatilization and lower porosity of packing. The mechanisms of pressure built-up are discussed in Chapter 5.

3.2.3 Compositions of partially reacted mixtures

Samples of partially reacted mixtures were chemically analyzed for carbon, total iron, Fe^{2+}, and Fe^{o}. It is common in the literature to use the degree of metallization and degree of reduction to express the extent of metallization and

reduction of iron oxide, and to use the degree of carbon gasification to express that of carbon gasification. The degree of metallization is defined as the percentage of iron in the form of metallic iron (Fe^0) in terms of the total iron initially in iron oxide. The degree of reduction is defined as the percentage of oxygen removed from the iron oxide in terms of the total removable oxygen combined with iron initially in iron oxide. The degree of carbon gasification is defined as the percentage of carbon gasified in terms of the total carbon initially in the coal. These terms will be used in the discussion throughout the following chapters.

3.2.3.1 Degree of iron ore reduction

The degrees of local metallization and reduction of iron oxide as functions of time are shown in Figures 3.9 and 3.10. The profiles with respect to the degree of reduction are shown in Figure 3.11.

Figure 3.12 shows fractions of the element iron in Fe^{2+} as functions of time and location. The iron ore is magnetite, $FeO \cdot Fe_2O_3$. One third of iron in the concentrate initially is in the ferrous state. Ferrous iron is the intermediate state when ferric iron is being reduced to metallic iron. Therefore, it shows as an increase in the earlier stage of reduction and then as a decrease at a higher degree of metallization. Figure

3.13 shows the computed results of the element iron in ferric state (Fe^{3+}) from data shown in Figures 3.9 and 3.12.

3.2.3.2 Degree of carbon gasification

The degree of carbon gasification as a function of reaction time is shown in Figure 3.14. The profiles of the degree of carbon gasification are shown in Figure 3.15.

The profiles of the degree of iron ore reduction and carbon gasification (Figures 3.11 and 3.15) show a similar dependence on time and location as that in Figure 3.6 for temperature profiles. This fact is certainly anticipated because these chemical reactions are faster at a higher temperature with plenty of heat supplied.

3.2.3.3 Errors in chemical analysis

Errors in the measurement of the chemical composition of the partially reacted mixtures may be attributed to every step in the process, i.e. from cooling of reacting mixture, sampling, sample preparation and chemical analysis.

Error due to the continuation of the reaction after the crucible was taken out of the furnace under a given cooling rate should be considered. Locations 1 and 2 (Figure 3.3), which were closer to the crucible wall and contained more

metallic iron, were quickly cooled from above 1000°C to under 600 °C within about one minute. Under 600°C, rates of chemical reactions are not fast enough to cause significant errors, except devolatilization. Locations 3, 4 and 5, materials were cooled to under 600 °C in about 2 to 4 minutes. The upper limit of errors introduced due to the failure to rapidly stop the chemical reaction may be estimated by extrapolation from Figures 3.10 through 3.14 according to the cooling time at different locations. It is estimated that the maximum error due to the cooling of the reacting mixtures is less than 4.0% of the reported values.

Samples taken from the cooled partially reacted mixtures were analyzed to determine the chemical compositions. Total iron, metallic iron and ferrous iron were determined by volumetric method (titration), and carbon was determined by a Leco Carbon Analyzer (Model 577-100). Both methods were calibrated using standard specimens to determined their errors; these errors were found to be less than ±0.5% for the report value by titration, and ±1.0 % by the Carbon Analyzer. However, due to inhomogeneity in a small sample, which is a mixture of different solid particles, the importance of adequate grinding of the sample to minimize variation is paramount. The error in sample preparation must be noted. It is most serious in carbon analysis. The Leco Carbon Analyzer was originally designed to determine the carbon content in

steel. In the present work, carbon content in partially reacted mixtures ranges from 2 to 15 wt %, much higher than those in steel. Thus, a smaller amount of sample (i.e. less than 0.1 gram) must be used. To reduce this error, samples were carefully ground in an agate mortar to the size of under 100 mesh and well blended before part of the sample could be taken for chemical analysis. The errors in sample preparation and chemical analysis were thus controlled within ±2.0% of the reported values for total iron, metallic iron and ferrous iron, and ±4.0 % for carbon.

Combining errors in each step, the total errors in the analysis of partially reacted mixtures are presented as error bars in Figures 3.9 to 3.14.

3.2.4 Exit gas analysis

Figure 3.16 shows a typical printout of the gas analysis by a gas chromatograph at the thirty-fifth minute of reaction time. The chemical species in the exit gas during the reaction are mainly CO, CO_2, H_2, H_2O, CH_4 and N_2. The changes in the composition of exit gas analysis during the reaction are shown in Figure 3.17. It should be borne in mind that all results of gas analysis are reported on dry basis, after the removal of water vapour and tar in the gas sampling process.

CH_4 was formed mainly from the devolatilization of coal at lower temperature (<800 °C), and H_2 was mainly from devolatilization of coal and decarbonization at higher temperature. Carbon monoxides may be from both the devolatilization of coal and gasification of carbon by H_2O or CO_2. The results suggested that most of devolatilization of the coal was completed within 30 minutes of the reaction within this system.

3.2.5 Effect of furnace temperature

A series of experiments with the furnace temperature kept at 1300 °C, instead of 1200 °C, were carried out. Figures 3.18 to 3.24 show the measured temperatures, degrees of iron ore reduction, three states of iron in iron oxides, degrees of carbon gasification and gas pressures as functions of reaction time and locations in the packing, respectively. For convenience in comparison, the measured degrees of iron ore reduction and carbon gasification at a furnace temperature of 1200°C are also included in Figures 3.19 and 3.20. The higher furnace temperature increased the rate of heat transfer, and resulted in a faster temperature increase within the bed (Figures 3.3 and 3.18). The higher temperatures, in turn, increased the rate of iron ore reduction (Figure 3.19) and carbon gasification (Figure 3.23). The increased rate of

reactions and temperature rise resulted in an increase of gas pressure development (Figures 3.7, 3.8 and 3.24).

3.2.6 Effect of ore/coal ratio

In experiments with ore/coal ratios of 82/18 and 85/15, three experiments were conducted for each ore/coal ratio with a reaction time of 60 minutes, i.e. one experiment each for a temperature measurement, a pressure measurement and a chemical analysis of solid composition. The results of experiments are shown in Figures 3.25 to 3.32.

Figures 3.27 and 3.28 show measured degrees of iron ore reduction and carbon gasification when the initial mixture was packed at ore/coal ratios of 82/18 and 85/15, respectively, with other conditions unchanged. The results with a ore/coal ratio of 80/20 are also included for comparison. With a lower ore/coal ratio, a higher degree of reduction is reached at the same location and reaction time (see Figure 3.27). This is due to more reductant being available for reductions. However, lower ore/coal ratio results in a higher residual carbon content in the partially reacted mixture (Figure 3.28).

3.3 Summary of experimental results

Before mathematical analysis, the following qualitative conclusions may be reached.

(a) A one-dimensional reaction system was designed to simplify the experimentation and to facilitate mathematical analysis.

(b) Temperature gradients in the reacting bed have been observed so that the non-isothermal nature of the system must be recognized in mathematical modelling for the study of mechanisms.

(c) Pressure build-up and pressure gradient development in the reacting bed have been observed, so that the non-isobaric nature of the system must be recognized in mathematical modelling for the study of mechanisms.

(d) The variation of the extent of completion of overall reaction over the height of the bed has suggested that the size of the system is one of the important kinetic parameters.

(e) The importance of heat transfer within the bed has been confirmed by the observed temperature gradients, and strong dependence on furnace temperature.

(f) In the binary mixture of iron ore concentrate and pulverized coal, more coal leads to faster reaction rate, a higher residual carbon and a weaker solid product. With 20% of coal addition, there is enough reductant to result in complete metallization of the iron ore in the mixture.

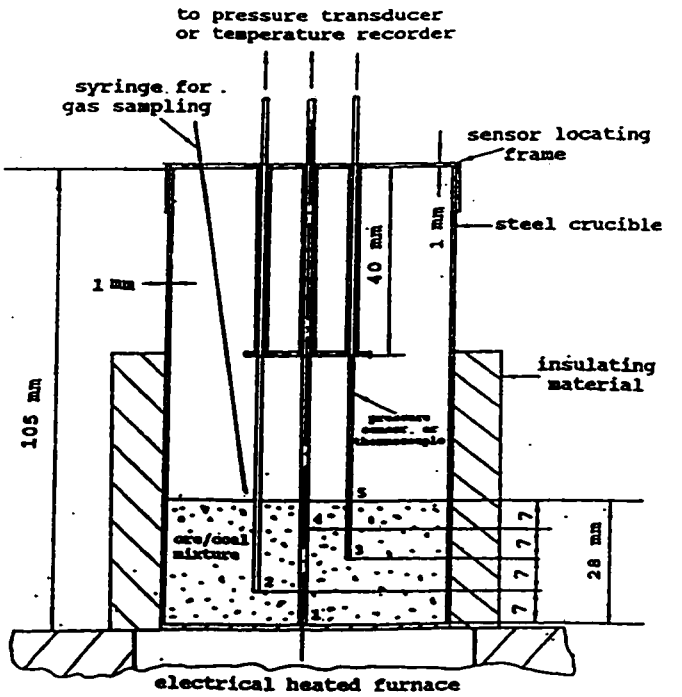

Figure 3.1 Schematic diagram of the experimental apparatus

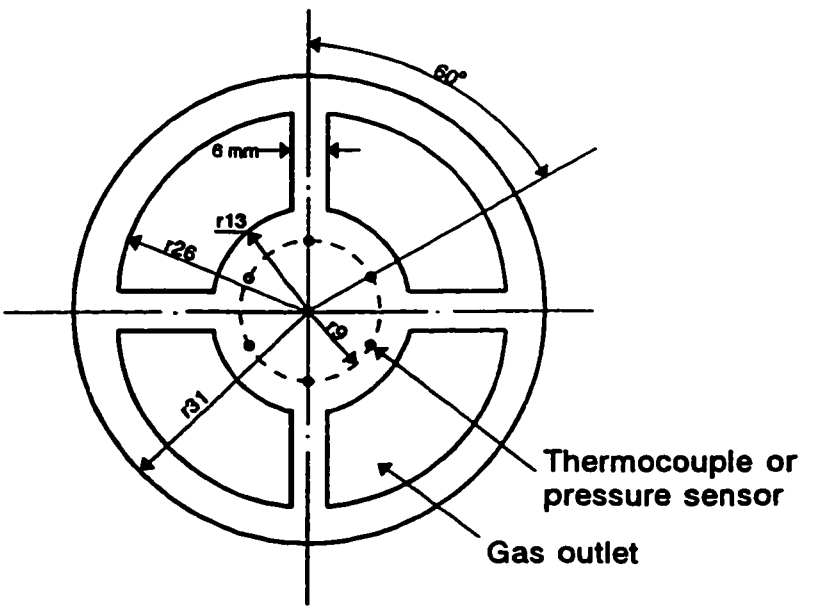

Figure 3.2 Top view of the sensor locating frame

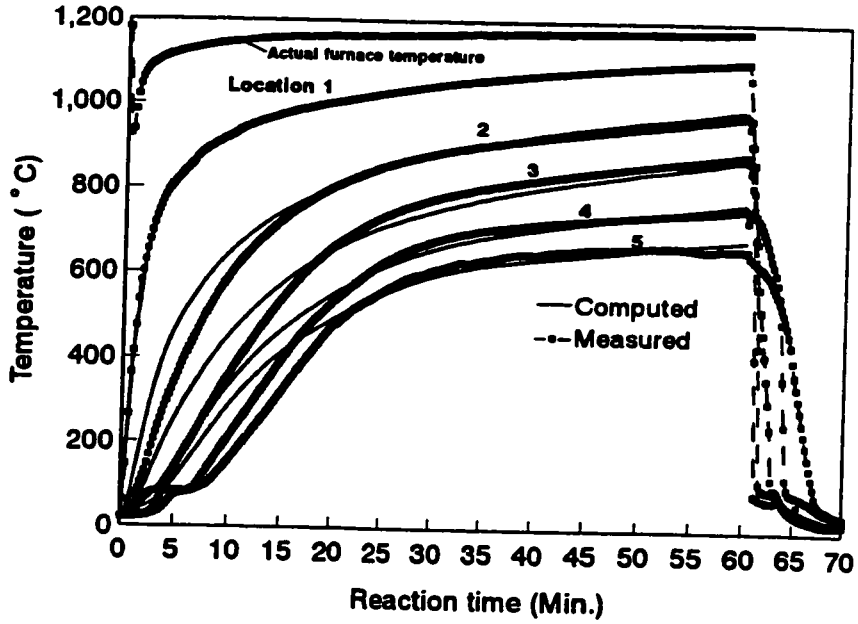

Figure 3.3 Measured and computed temperature as a function of reaction time (Ore/coal=80/20, furnace temperature = 1200°C)

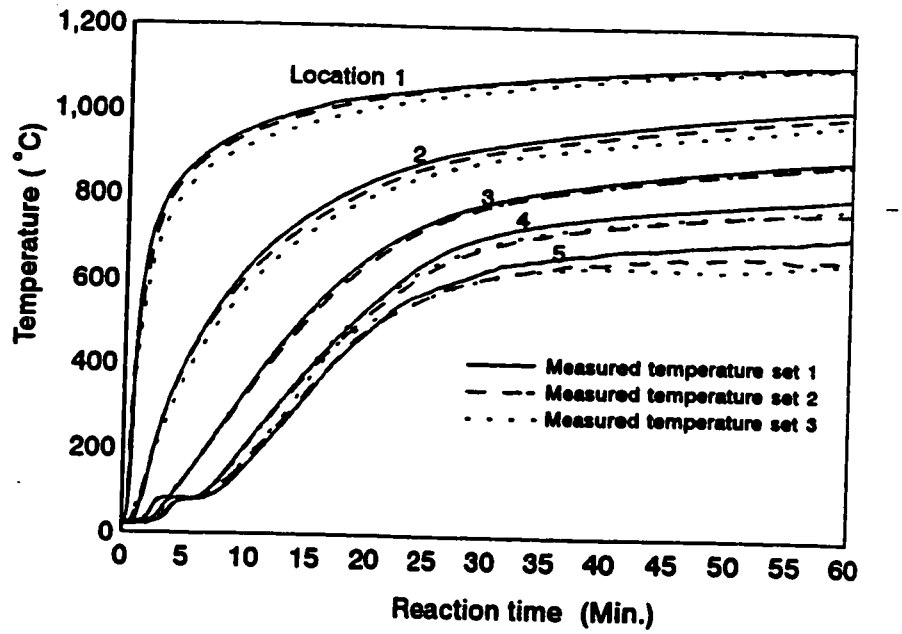

Figure 3.4 Three sets of measured temperatures as a function of reaction time (Ore/coal=80/20, furnace temperature = 1200°C)

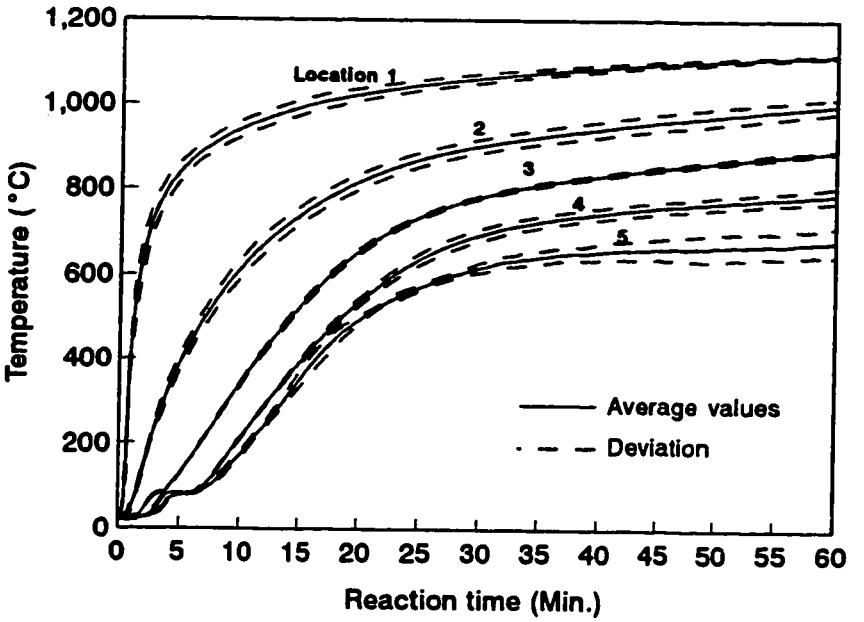

Figure 3.5 Average values of measured temperatures with deviations (Ore/coal=80/20, furnace temperature=1200°C)

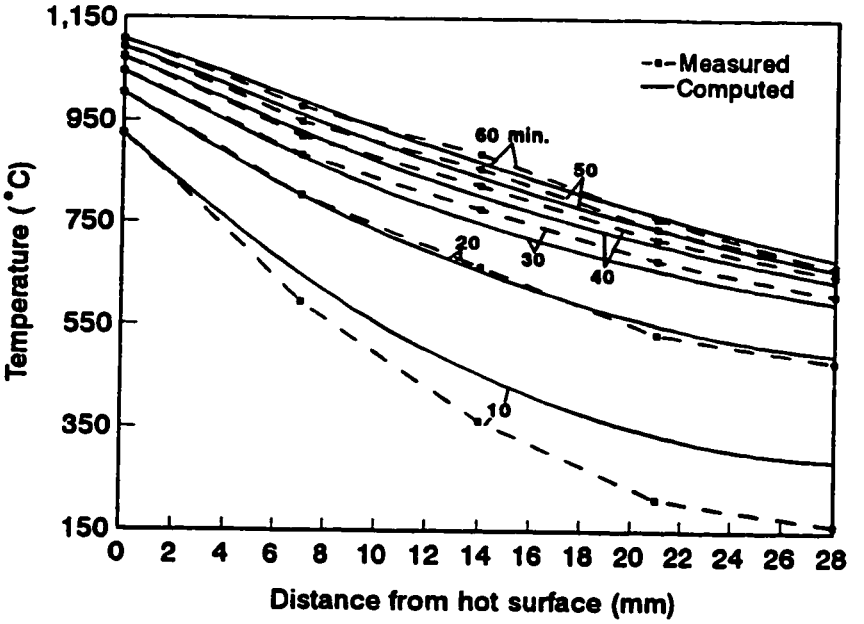

Figure 3.6 Measured and computed temperature profile over the height of the packing (Ore/coal=80/20, furnace temperature=1200°C)

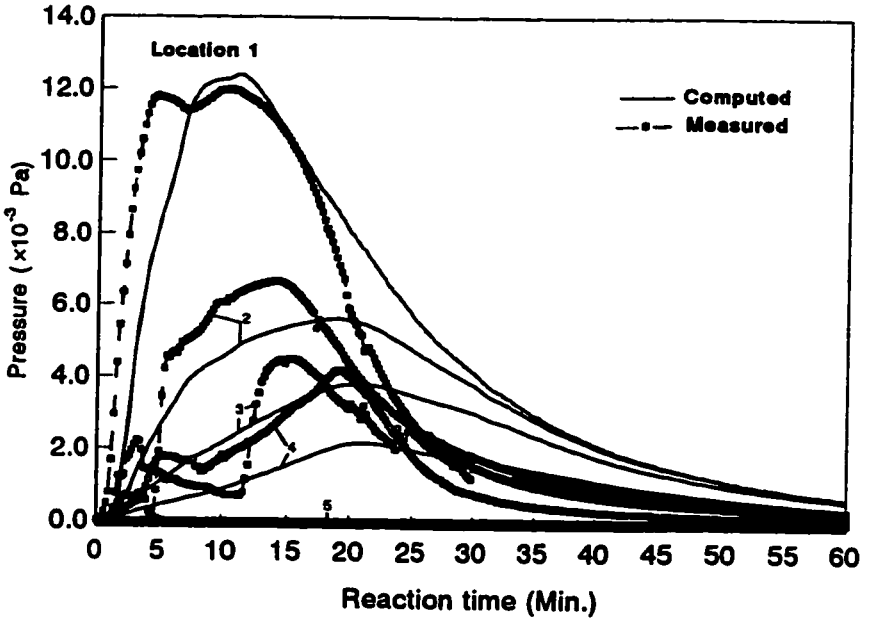

Figure 3.7 Measured and computed local pressure as a function of reaction time (Ore/coal=80/20, furnace temperature = 1200°C)

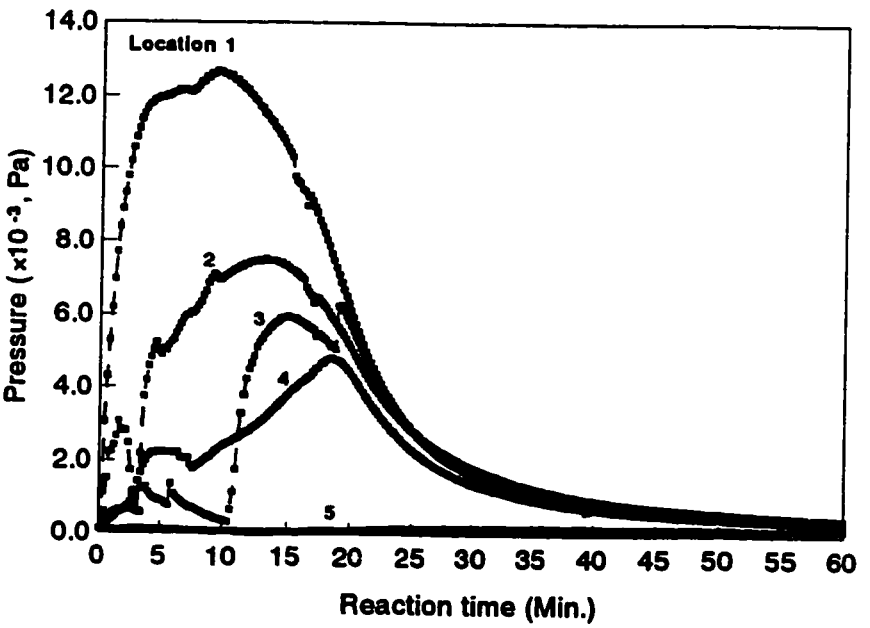

Figure 3.8 Measured local pressure as a function of reaction time (Ore/coal=80/20, furnace temperature = 1200°C, second set)

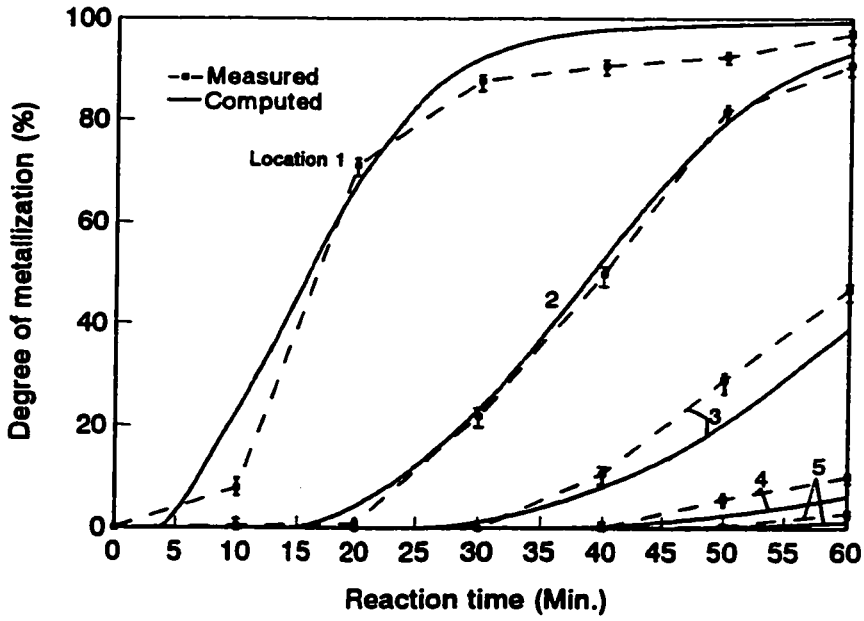

Figure 3.9 Degree of metallization as a function of reaction time (Ore/coal=80/20, furnace temperature=1200°C)

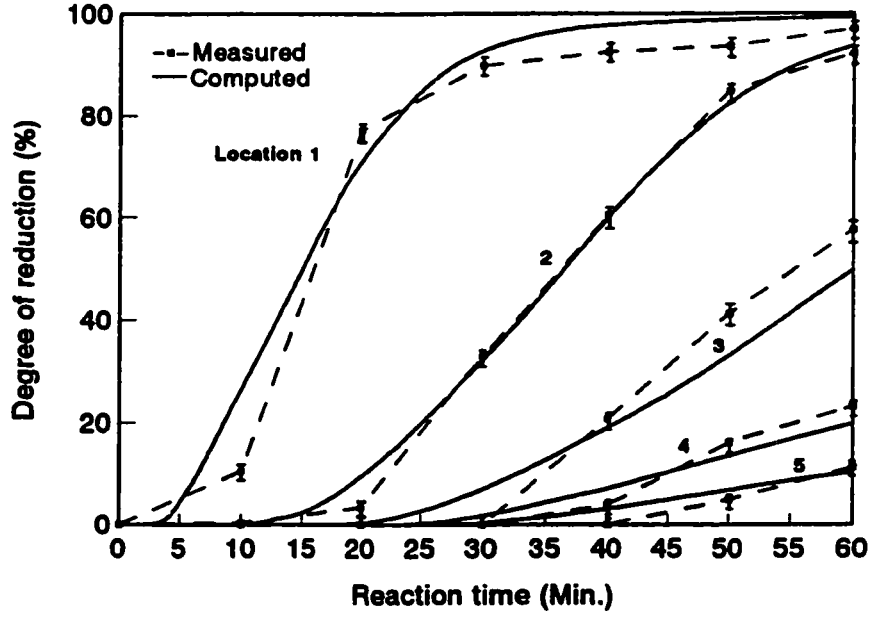

Figure 3.10 Degree of reduction as a function of reaction time (Ore/coal=80/20, furnace temperature = 1200°C)

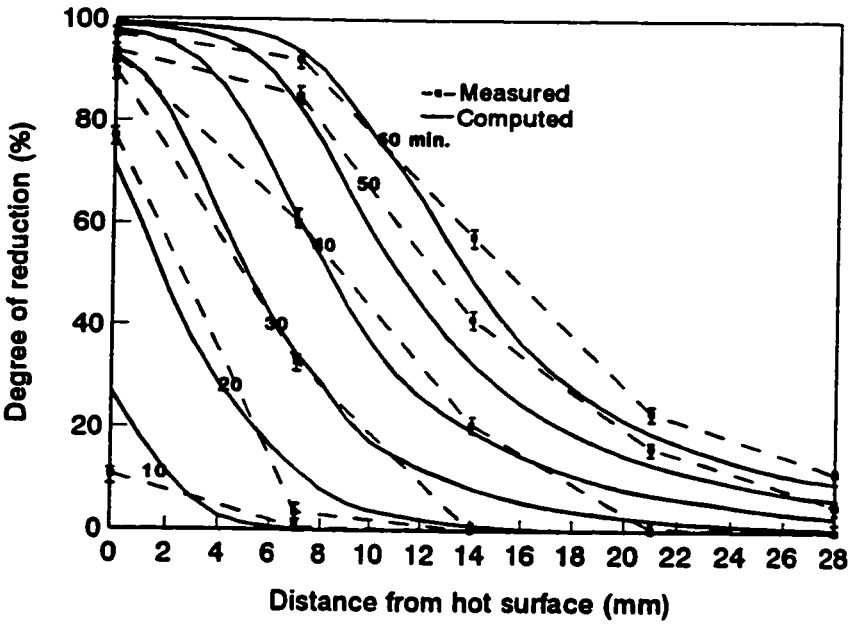

Figure 3.11 Profile of degree of iron ore reduction over the height of the packing (Ore/coal=80/20, furnace temperature = 1200°C)

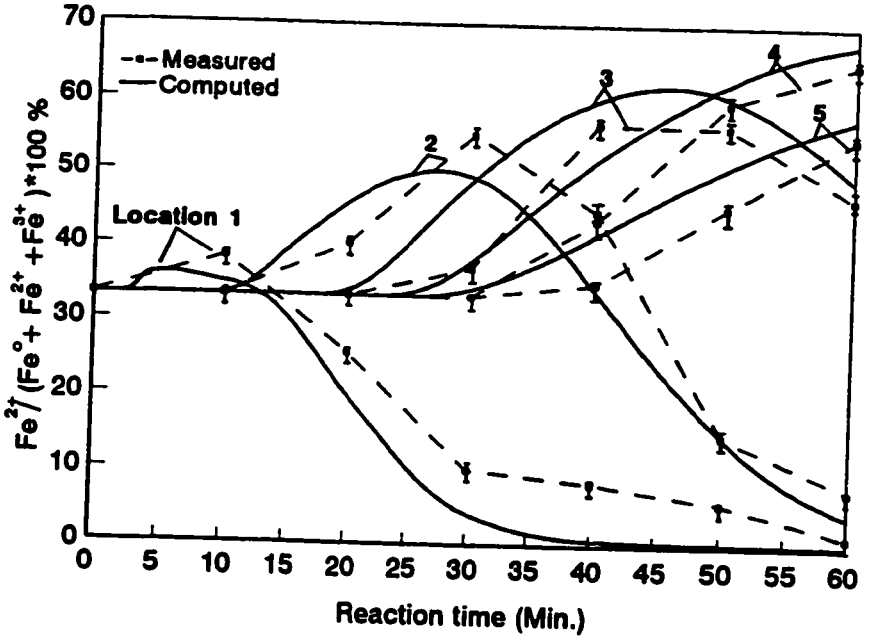

Figure 3.12 Percentage of iron in ferrous state iron oxide as a function of reaction time (Ore/coal=80/20, furnace temperature=1200°C)

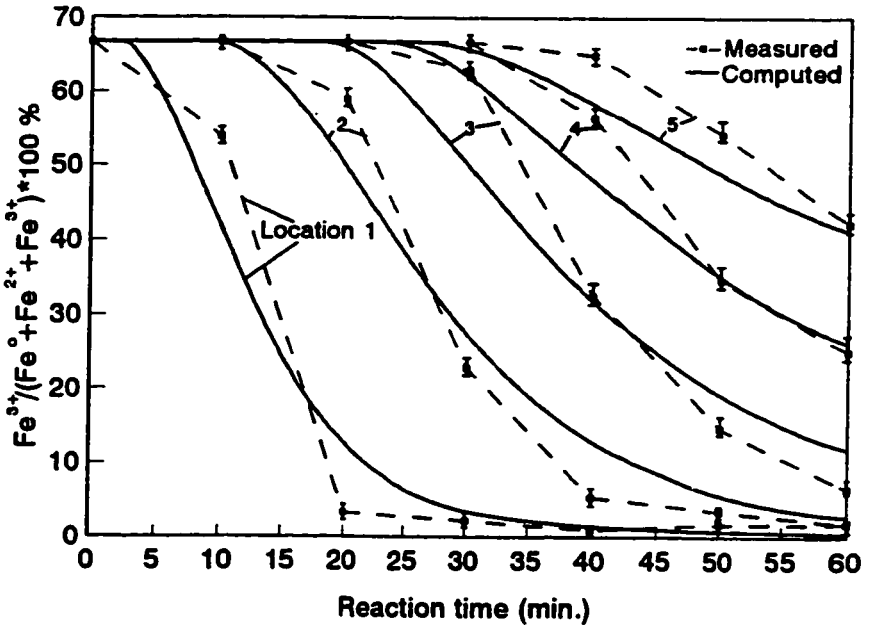

Figure 3.13 Percentage of iron in ferric state iron oxide as a function of reaction time (Ore/coal=80/20, furnace temperature=1200°C)

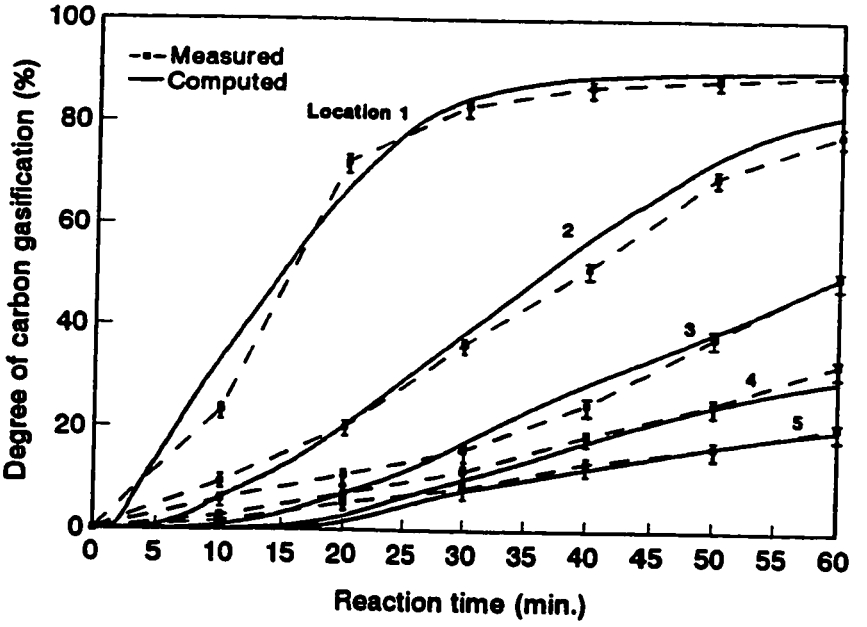

Figure 3.14 Degree of carbon gasification as a function of reaction time (Ore/coal=80/20, furnace temperature = 1200°C)

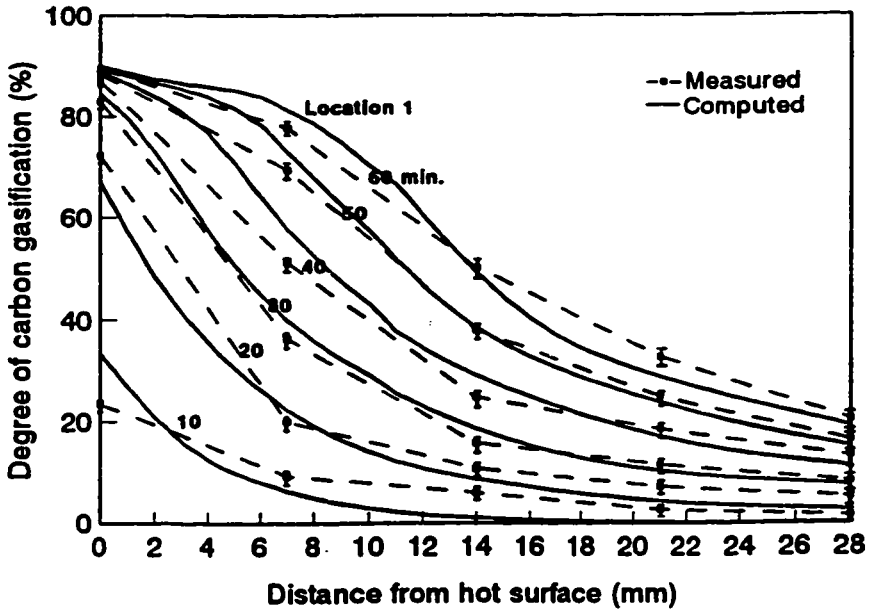

Figure 3.15 Profile of degree of carbon gasification over the height of the packing (Ore/coal=80/20, furnace temperature = 1200°C)

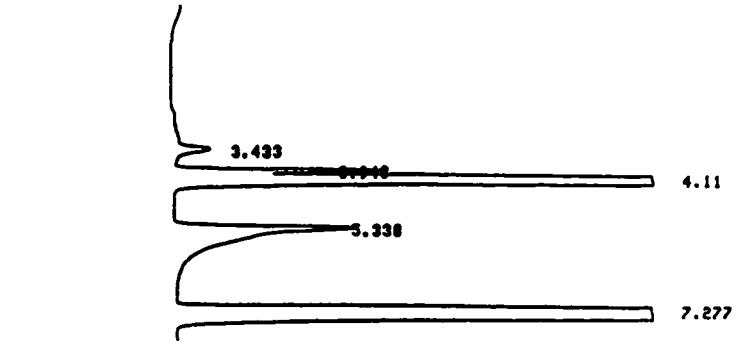

CHROMATOPAC CR601 FILE 0
SAMPLE NO 0 METHOD 44
REPORT NO 401 SAMPLE WT 250

PKNO	TIME	AREA	MK	IDNO	CONC	NAME
1	3.433	520		6	0	H_2
2	3.948	2147		6	0	N_2
3	4.11	60111	V	6	0	CO
4	5.338	5985		6	0	CH_4
5	7.277	58890		6	0	CO_2
	TOTAL	127654			0	

Figure 3.16 Original record of gas analysis from the gas chromatograph

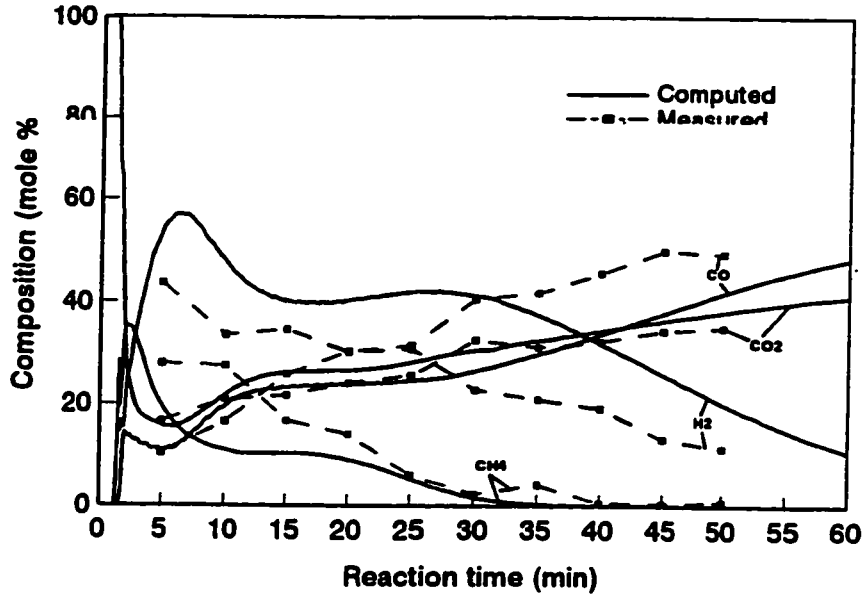

Figure 3.17 Measured and computed compositions of the exit gas (Ore/coal=80/20, furnace temperature = 1200°C)

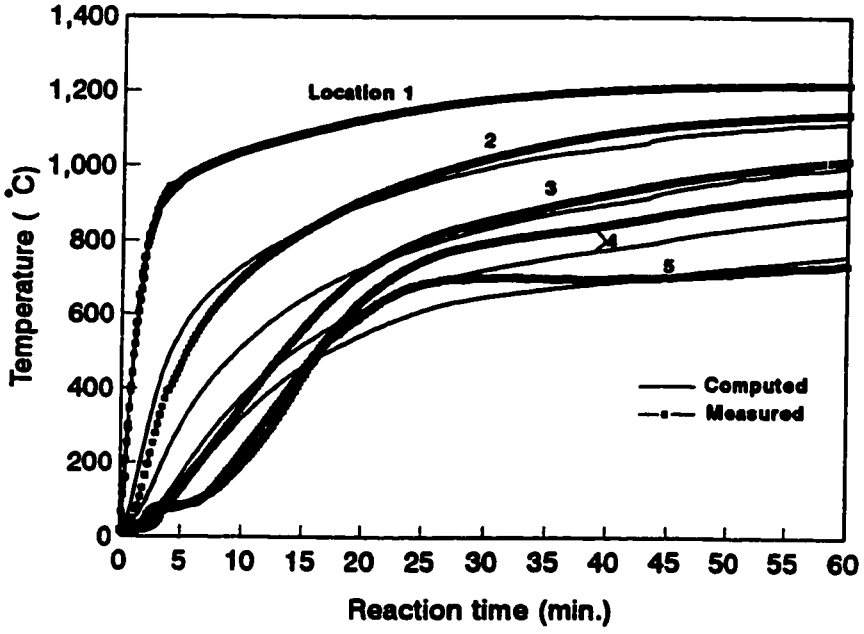

Figure 3.18 Measured and computed local temperature as a function of reaction time (Ore/coal=80/20, furnace temperature = 1300°C)

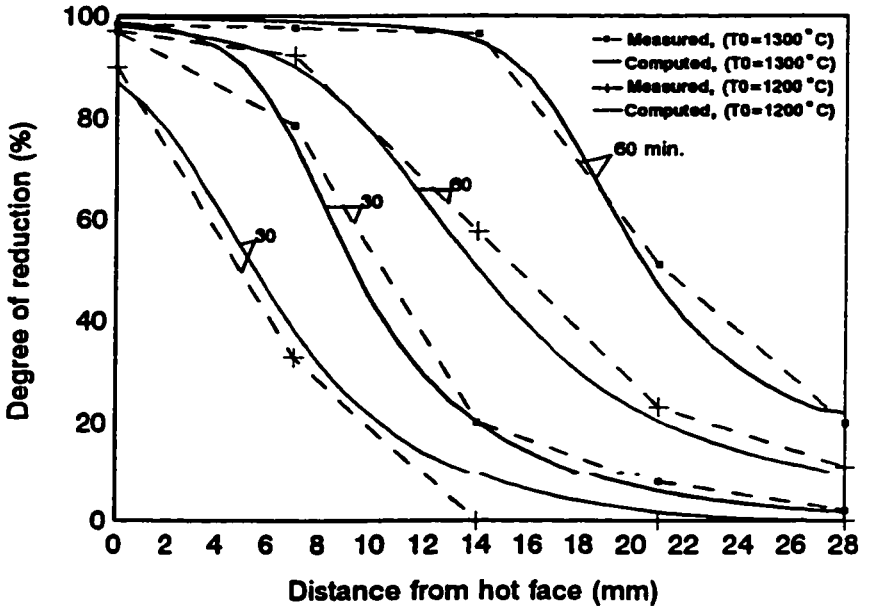

Figure 3.19 Effect of furnace temperature on degree of iron ore reduction (Ore/coal=80/20)

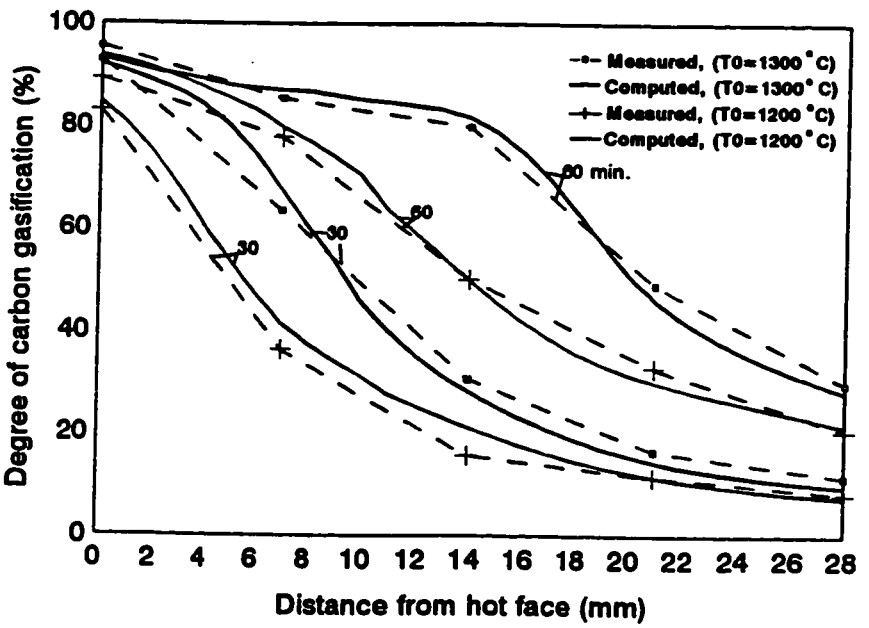

Figure 3.20 Effect of furnace temperature on degree of carbon gasification (Ore/coal=80/20)

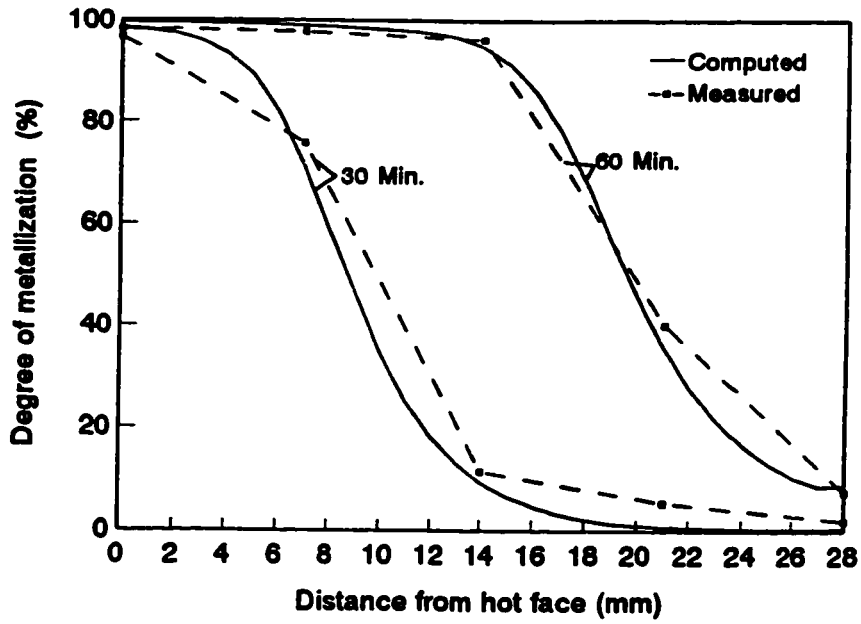

Figure 3.21 Measured and computed profiles of degree of metallization over the height of the packing, (Ore/coal=80/20, furnace temperature=1300°C)

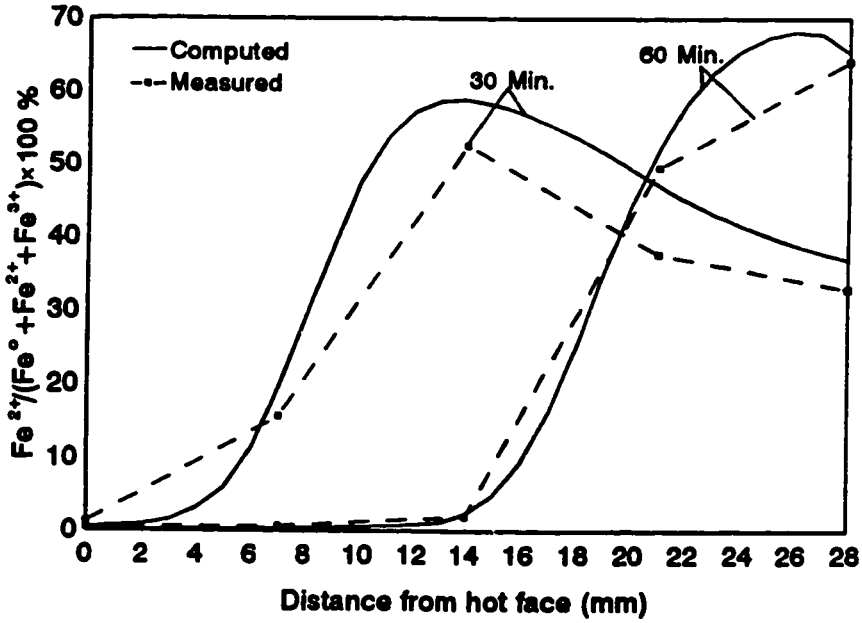

Figure 3.22 Measured and computed profile of iron in ferrous state over the height of the packing (Ore/coal=80/20, furnace temperature=1300°C)

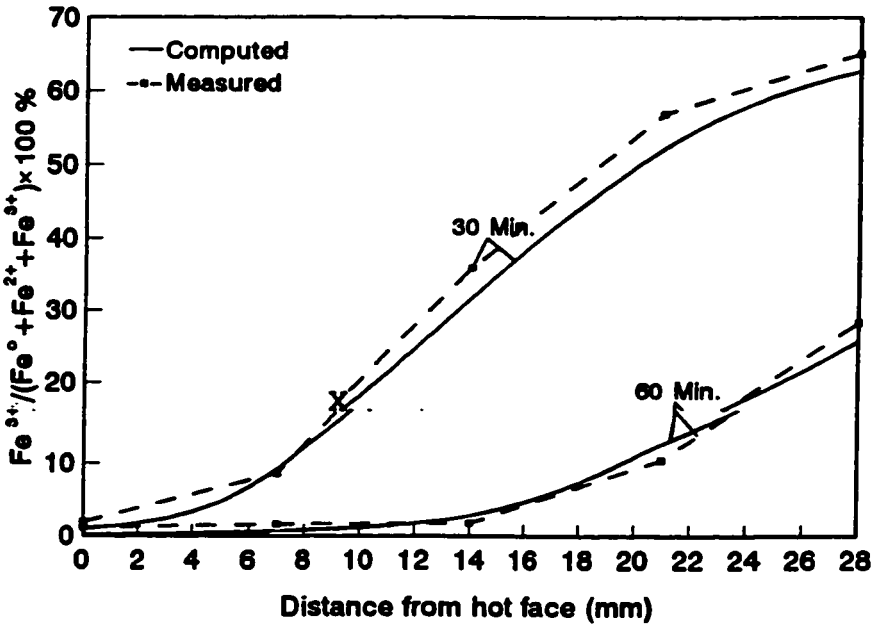

Figure 3.23 Measured and computed profiles of iron in ferric stat iron oxide over the height of the packing, (Ore/coal=80/20, furnace temperature =1300°C)

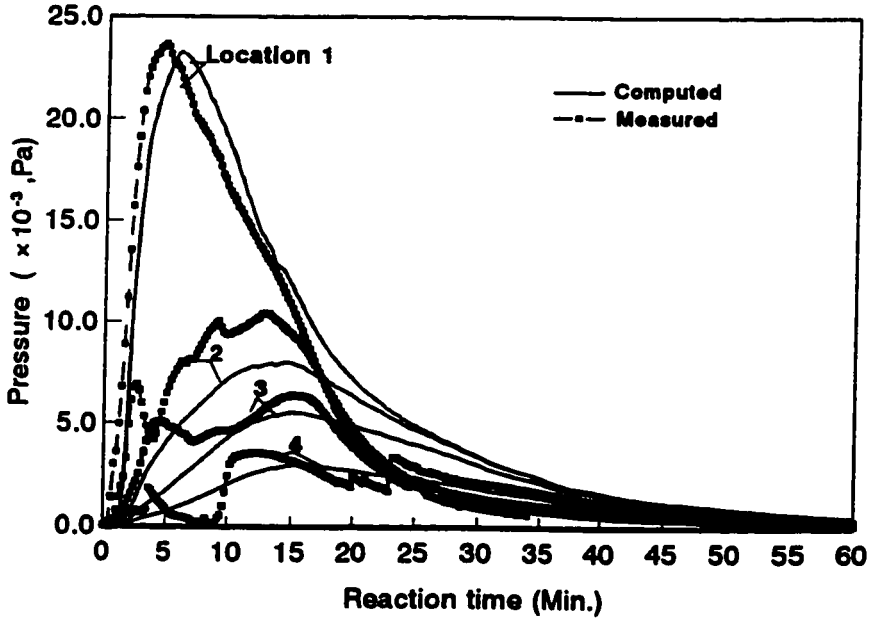

Figure 3.24 Computed and measured local pressure as function of reaction time (Ore/coal=80/20, furnace temperature=1300°C)

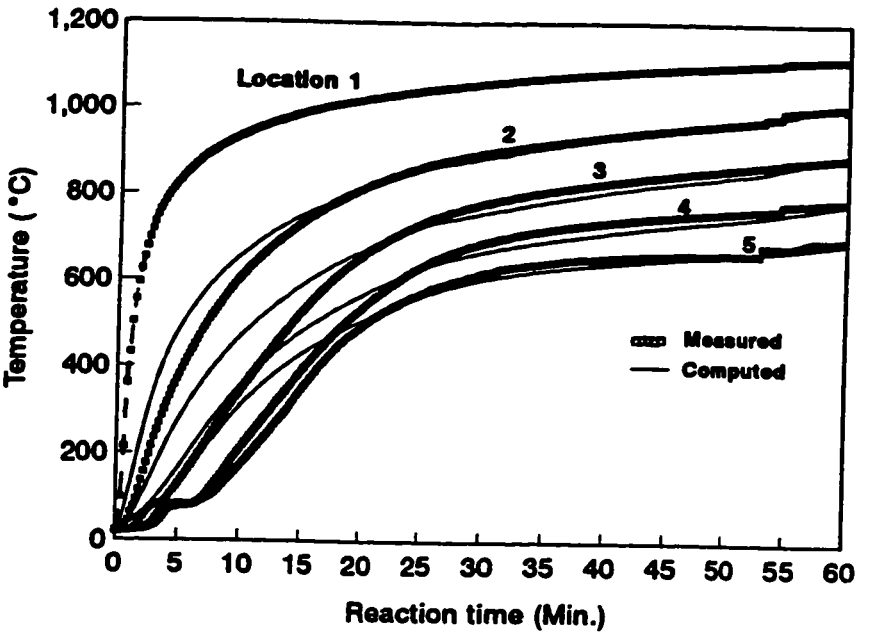

Figure 3.25 Computed and measured local temperature as a function of reaction time (Ore/coal=82/18, furnace temperature = 1200°C)

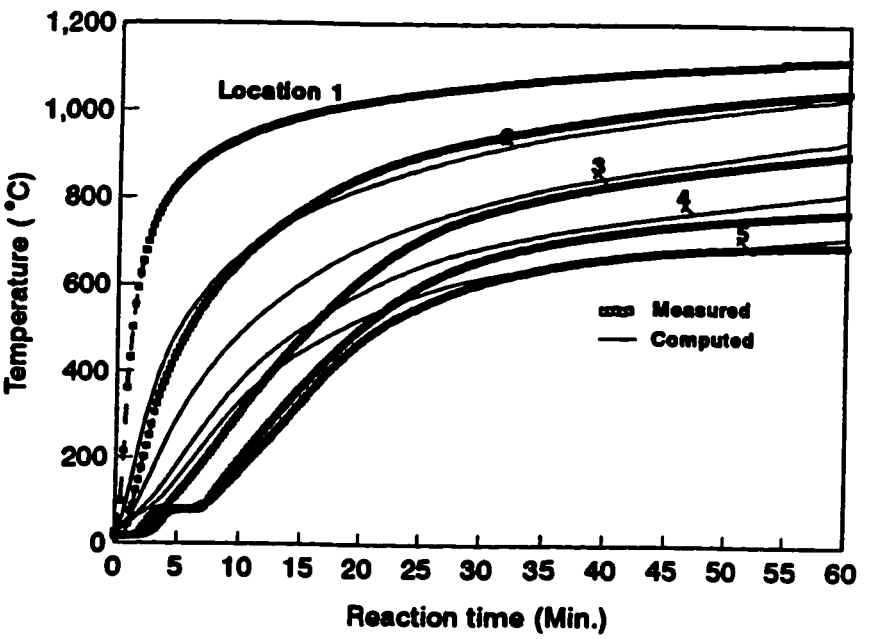

Figure 3.26 Computed and measured local temperatures as a function of reaction time (Ore/coal=85/15, furnace temperature=1200°C)

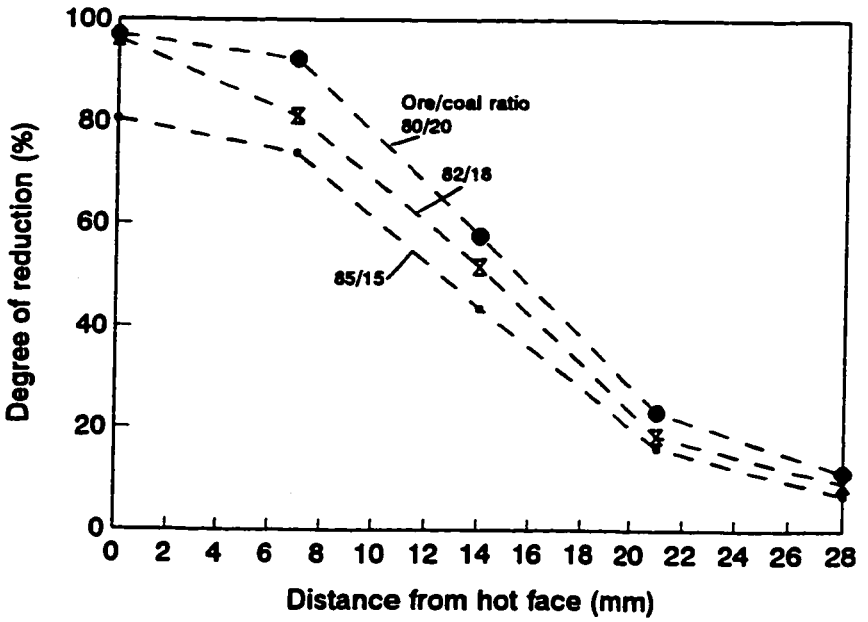

Figure 3.27 Measured profiles of degree of iron ore reduction over the height of the packing (3 ore/coal ratios, furnace temperature=1200°, reaction time=60 Min)

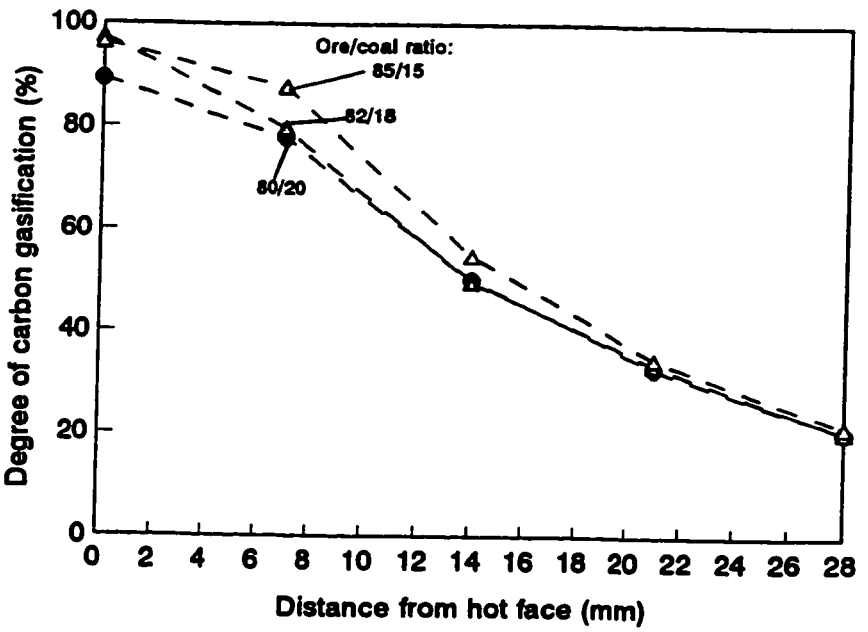

Figure 3.28 Measured profiles of degree of carbon gasification over the height of the packing (3 ore/coal ratios, furnace temperature=1200°, reaction time=60 Min)

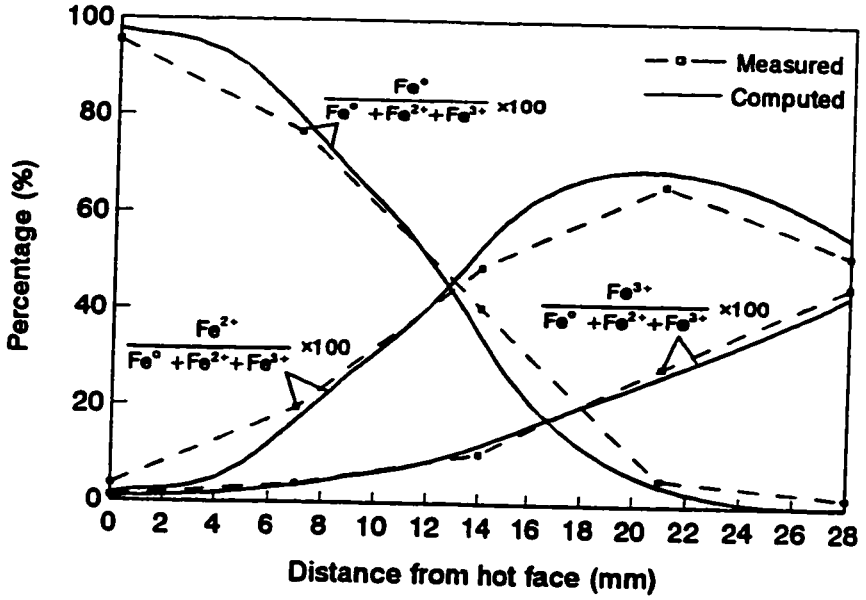

Figure 3.29 Measured and computed values of three states of iron over the height of the packing at 60-th minute of reaction, (Ore/coal=82/18)

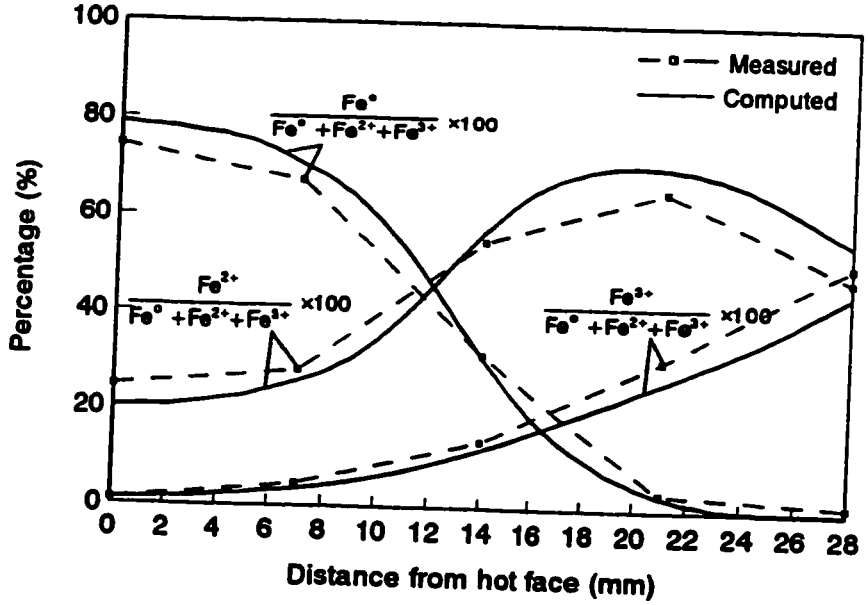

Figure 3.30 Measured and computed values of three states of iron over the height of the packing at 60-th minute of reaction, (Ore/coal=85/15)

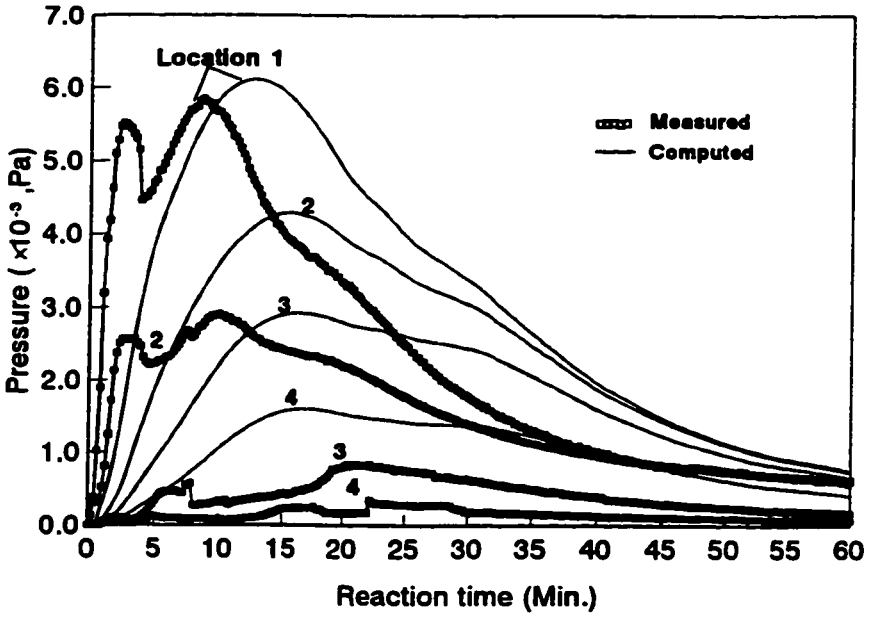

Figure 3.31 Measured and computed local pressure as a function of reaction time (Ore/coal=82/18, furnace temperature=1200°C)

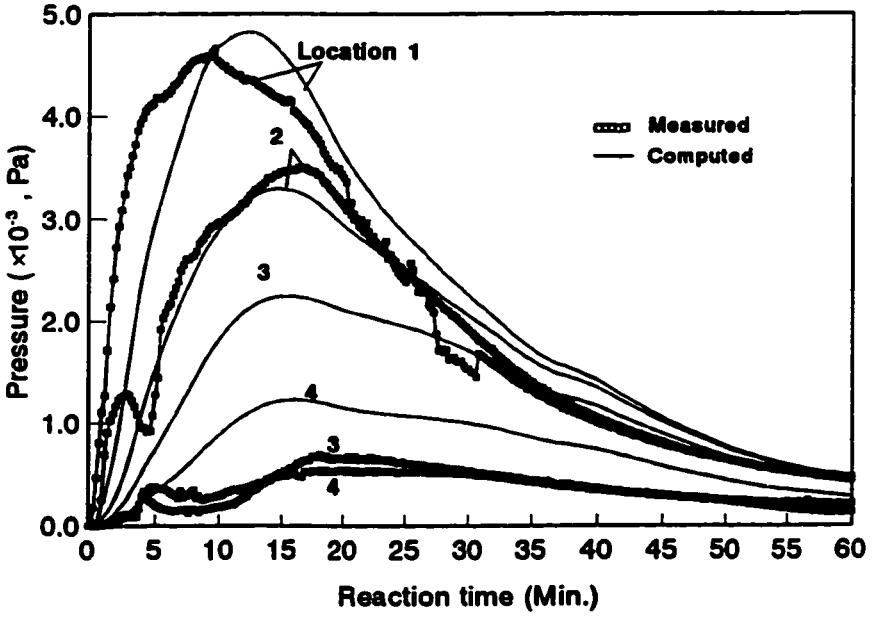

Figure 3.32 Measured and computed local pressure as a function of reaction time (Ore/coal=85/15, furnace temperature=1200°C)

CHAPTER FOUR

MATHEMATICAL MODELLING

The comprehensive experimental investigation, described in Chapter Four, leads to the following summary:

1) Steeper temperature gradients exist at the locations where endothermic reaction (carbon gasification) is more intensive.

2) Gaseous pressures and pressure gradients develop at locations where coal gasification and iron ore reduction are intensive.

In order to explain quantitatively the above observations, a non-isothermal and non-isobaric mathematical model for reactions in this system has been developed.

4.1 The strategy

Physical and chemical processes in this system (eg. heat transfer, gaseous flow and rates of chemical reactions) are all temperature dependent through physical properties and kinetic parameters, i.e. conductivities, viscosities and reaction rate constants, etc. It is clear that all kinetic

expressions must be functions of temperature. The variation of local temperature is determined by all activities involving heat, such as heat of chemical reactions within a locality and the net heat flux due to conduction, convection and radiation. Therefore, the equation of energy balance, which is necessary for temperature determination, must include terms for all chemical reactions and convection due to gas flow through porous medium in addition to conduction and radiation. The equation for gas flow through a porous medium should consist of terms of the local pressure gradient, local void fraction, temperature and rates of chemical reactions. It should be pointed out that the model must consist of a number of simultaneous equations to determine the set of unknown variables as functions of reaction time, distance from the hot face, and initial and boundary conditions.

4.2 The configuration and properties of the system

The system geometry is cylindrical and one-dimensional in the axial direction, as in the experimental set-up. The axis of the cylinder is the X-axis in the modelling. A control volume, with a unit cross-section area, is shown in Figure 4.1.

4.3 Heat Transfer within A Porous Medium

In a porous medium or a packed bed, heat transfer is active not only within each phase (solid and gaseous phases), but also between phases. In the present ore/coal mixture, there exits a very large area of solid surface (about 95,000 m^2/m^3 of bed), which gives an extensive gas-solid contact in the packed bed. Subsequently, the rate of heat transfer between solid and gas phases is relatively high; therefore, the gas temperature is assumed to be equal to that of solid in the same location.

The equations for heat transfer in a porous medium, in principle, should include conductive, radiant and convective terms. The relative importance of these mechanisms varies, which depends on solid properties, pore structure, temperature range and gas flow. The common approach in treating radiant heat transfer in a porous medium is to include it in a conductive heat transfer formulation by using an effective heat conductivity (Geiger and Poirier, 1973; Gabor and Botterill, 1985). Thus the equation for heat transfer is in the form of heat conduction and convection, with heat of chemical reactions as the source and sink terms.

Heat balance in this control volume of one-dimensional system may be expressed as

$$\begin{pmatrix}\text{rate of}\\ \text{heat in by}\\ \text{conduction}\end{pmatrix}+\begin{pmatrix}\text{rate of}\\ \text{heat in by}\\ \text{convection}\end{pmatrix}-\begin{pmatrix}\text{rate of}\\ \text{heat out by}\\ \text{conduction}\end{pmatrix}+\begin{pmatrix}\text{rate of}\\ \text{heat out by}\\ \text{convection}\end{pmatrix}+\begin{pmatrix}\text{rate of}\\ \text{heat consumed}\\ \text{by reactions}\end{pmatrix}+\begin{pmatrix}\text{rate of}\\ \text{change of}\\ \text{enthalpy}\end{pmatrix} \quad (4.1)$$

i.e.

$$q_{cond,\,x}+q_{conv,\,x}=q_{cond,\,x+\Delta x}+q_{conv,\,x+\Delta x}+q_{re}+\frac{\partial H}{\partial t}\Delta x \qquad (4.2)$$

where:

(1) the heat fluxes by conduction are

$$q_{cond,\,x}=-\left(K_{effm}\,\frac{\partial T}{\partial x}\right)_x \qquad (4.3)$$

$$q_{cond,\,x+\Delta x}=-\left(K_{effm}\,\frac{\partial T}{\partial x}\right)_{x+\Delta x} \qquad (4.4)$$

where K_{effm} is the effective thermal conductivity, including radiation, of the local mixture.

(2) heat fluxes by convection are

$$q_{conv,\,x}=(\rho_g V_a C_{Pg} T \phi)_x \qquad (4.5)$$

$$q_{conv,\,x+\Delta x}=(\rho_g V_a C_{Pg} T \phi)_{x+\Delta x} \qquad (4.6)$$

where ρ_g and C_{Pg} are the average density and specific heat of local gas, respectively, V_a is the average velocity of gas flow in the interstices of the bed, and ϕ is the local void fraction of packed bed.

It is often more convenient to use superficial velocity, instead of average velocity, in the formulation of fluid flow in a porous medium. The superficial gas velocity, V_o, is defined as the velocity when the gas flows through the empty

control volume; i.e.

$$V_o = \phi V_a \tag{4.7}$$

Substituting Equation (4.7) into Equation (4.5) and (4.6) yields

$$q_{conv,x} = (\rho_g V_o C_{Pg} T)_x \tag{4.8}$$

$$q_{conv,x+\Delta x} = (\rho_g V_o C_{Pg} T)_{x+\Delta x} \tag{4.9}$$

(3) the rate of heat consumption and generation by chemical reactions is

$$q_{re} = (\sum_i \dot{R}_i \Delta H_i)\ \Delta x \tag{4.10}$$

where $\dot{R}_i$ and ΔH_i are the rate and heat of reaction of chemical reaction i; and i is the index for reactions to be presented later.

(4) the change of enthalpy due to temperature variation

$$\frac{\partial H}{\partial t}\Delta x = \frac{\partial}{\partial t}(\rho_m C_{Pm} T)\ \Delta x \tag{4.11}$$

where ρ_m and C_{Pm} are the average density and specific heat of local mixtures, respectively.

By substituting Equations (4.3), (4.4), and (4.8) - (4.11) into Equation (4.2), and dividing Equation (4.2) by the Δx, in the limit as Δx approaches to zero, the following

differential equation us obtained.

$$\frac{\partial}{\partial t}(\rho_m C_{Pm} T) = \frac{\partial}{\partial x}\left(K_{effm} \frac{\partial T}{\partial x}\right) - \sum_i \dot{R}_i \Delta H_i - \frac{\partial}{\partial x}(\rho_g V_o C_{Pg} T) \qquad (4.12)$$

The effective thermal conductivity of the mixture should include heat conduction through the solid and gaseous phase in pores and radiation across internal pores within each particle and interstices between particles. The relative importance of each mechanism depends on temperature, solid properties and pore structure of the mixture. A numerical evaluation of these two mechanisms shows that under the present experimental conditions, conduction is the dominant heat transfer mechanism, and radiation heat transfer may be neglected without introducing significant error in computation. Details of the evaluation of the effective thermal conductivity and the effective thermal capacity of the mixture are given in Appendix I. The change of density of the ore/coal mixture may be calculated from its initial value and the rate of chemical reactions.

To solve the equation for heat transfer (4.12), other equations are to be established simultaneously, which are given below.

4.4 Rate Equations for Heterogeneous Chemical Reactions

The important chemical reactions in a mixture of magnetite concentrate and coal are:

(a) Iron ore reduction:

$$Fe_3O_4 + 4CO(H_2) = 3Fe + 4CO_2(H_2O) \quad when\ T < 570\,^{\circ}C \quad (4.13)$$

$$Fe_3O_4 + CO(H_2) = 3FeO + CO_2(H_2O) \quad when\ T \geq 570\,^{\circ}C \quad (4.14)$$

$$FeO + CO(H_2) = Fe + CO_2(H_2O) \quad (4.15)$$

(b) Coal devolatilization:

$$Coal \rightarrow C + volatile\ matter \quad (4.16)$$

(c) Carbon gasification:

$$C + CO_2(H_2O) = CO + CO(H_2) \quad (4.17)$$

Considering all possibilities in this system, chemical reactions could include solid-solid reactions (ore reduction directly by char) and gaseous reactions (the water gas reaction and secondary reactions of volatile) as well as the gas-solid reactions listed above. Limited by the requirement of continuing contact between solid reactants in order to complete the reaction, the mechanism of solid-solid reactions are relatively insignificant except at the initial stage. In general, the kinetics of heterogeneous reactions of ironmaking systems are dominated by gas solid reactions as written above. The gaseous reactions are usually intermediate steps in the

overall reactions under investigation. Thus, only these reactions listed in (4.13)-(4.17) are considered to be necessary and sufficient in the present modelling. It is also understood that the rate for the individual reaction listed above is expressed as the rate of disappearance of the solid reactant in the reactions.

For gas-solid reaction of individual particles of iron ore or char, the shrinking core model for reversible reaction is used. The rate of the topochemical reaction is both proportional to gas-solid interfacial area, and a first order reaction with respect to the concentration of gaseous reactants. This model implies that the number of particles of ore and their shape and size do not change during the course of reduction. As the number of particles and average surface area of individual particles per unit volume of the porous medium can be estimated by characterization of raw materials, the units for rate equations can be expressed in moles per unit volume of porous medium per unit time. Since the reacting mixture is made of very fine particles, the movement of gaseous molecules through porous product layers of the particles are over a very short distance. It would be reasonable to assume that mass transfer through the product layers will not contribute significant resistance to the rate of the overall reactions, in comparison to that of the interfacial reactions. With these assumptions, the rate

equations for these reactions may be derived in following sections.

4.4.1 Iron oxide reductions

The iron oxide reduction takes place simultaneously by both CO and H_2 as both reductants are present in the system. The gas-solid reactions of iron oxide reduction by CO and H_2 are independent; therefore; the observed rate of reduction is the sum of these two gaseous reductants as shown below:

$$\dot{R}_i = \dot{R}_i^{CO} + \dot{R}_i^{H_2} \qquad (4.18)$$

where $\dot{R}_i$, $\dot{R}_i^{CO}$ and $\dot{R}_i^{H2}$ are the total rate of reduction, and the rate of reduction by CO and by H_2, respectively, for reactions (4.13), (4.14) and (4.15).

According to the un-reacted core model, the rate of iron oxides reduction by CO (i.e. reactions (4.13), (4.14) and (4.15)), may be expressed as follows:

$$\dot{R}_i^{CO} = S_{fi}\, n_i\, 4\,\pi\, \overline{r}_i^2\, k_i^{CO}\left(C_{CO} - \frac{C_{CO_2}}{K_{Ei}^{CO}}\right) \qquad (4.19)$$

where

$$k_i^{CO} = k_{i0}^{CO} EXP(\frac{-\Delta E_{ico}^*}{RT}) \qquad (4.20)$$

The rate equation for the reduction of the iron oxides by H_2 may be expressed as:

$$\dot{R}_i^{H_2} = S_{fi}\, n_i\, 4\,\pi\, \bar{r}_i^2\, k_i^{H_2}\left(C_{H_2} - \frac{C_{H_2O}}{K_{Ei}^{H_2}}\right) \qquad (4.21)$$

where

$$k_i^{H_2} = k_{i0}^{H_2} EXP(\frac{-\Delta E_{iH_2}^*}{RT}) \qquad (4.22)$$

and S_{fi} is the shape factor of the particle of solid reactant in reaction i; n_i is the number of the particles in reaction i per unit volume of mixture; $\bar{r}_i$ is the average radius of the un-reacted core in iron ore particles; k_i^{CO} and k_i^{H2} are rate constants for reaction i with CO and H_2 as reductant; k_{i0}^{CO} and k_{i0}^{H2} are pre-exponential constants for above rate constant; C_{CO}, C_{CO_2}, C_{H_2} and C_{H_2O} are concentrations of CO, H_2, CO_2 and H_2O; ΔE_{ico}^* and ΔE_{iH2}^* are 'activation energies' for reaction i by CO and H_2; and K_{Ei}^{CO} and K_{Ei}^{H2} equilibrium constant for reaction i, respectively.

The values of pre-exponential constants and 'activation energies' in the above rate equations are obtained by fitting computational results with experimental data through the use of present model. These results are compared with that

reported in the literature.

As the size of iron ore particle is assumed to be constant, $\bar{r}_i$ may be calculated from the extent of completion as shown below:

$$\bar{r}_i = \bar{r}_i^{\circ} (1 - \varphi_i)^{\frac{1}{3}} \qquad (4.23)$$

where $\bar{r}_i^{\circ}$ is initial average radius of iron ore particles, and φ_i is the fraction of completion of the i-th reaction.

4.4.2 Coal devolatilization

During devolatilization, the coal undergoes thermal decomposition to form solid (char), liquids (oils) and gaseous products. As the amount of liquid is relatively small (about 2 wt% of coal), liquid products are usually neglected in the modelling. The gaseous products of coal decomposition are mainly CO, CO_2, H_2, H_2O, hydrocarbons and tar. In the present experimental observations, CH_4 is the dominant species of the hydrocarbons (see Chapter 4); therefore, hydrocarbons higher than methane are considered as 'methane equivalent'. It is also understood that tar is a mixture of many compounds which is a gaseous product at decomposition temperature and becomes a liquid or solid at room temperature (Gavala, 1982). For simplicity in the modelling, it is assumed that tar does not undergoes secondary decomposition and reacts with iron ore

before it leaves the system, and that an average molecular weight and properties of tar may be used in modelling. According to Unger and Suuberg (Unger and Suuberg, 1984), the molecular weight distribution of tar is in the range from 250 to 750 in the temperature range from 600 to 1300K. An average molecular weight of 400 is used in the present work.

Modelling the kinetics of coal devolatilization includes rate of coal decomposition and the distribution of gaseous products. According to Solomon and Colket (1979), the coal is assumed to be a compound made up of fixed carbon and volatile components: CO_2, tightly bound CO, H_2O, loosely bound CO, hydrocarbons, H_2 and tar. They also proposed that during the devolatilization, individual gas evolves from coal independently and simultaneously. The rate of evolution of individual volatile component may be assumed to be proportional to its weight fraction remaining in the char and expressed as follows (Solomon and Colket, 1979);

$$\dot{R}_{vi} = k_{vi0} EXP(\frac{-\Delta E^*_{vi}}{RT}) W_{vi} \qquad (4.24)$$

where $\dot{R}_{vi}$ is the rate of evolution of volatile component i; and W_{vi} is the remaining portion of volatile component i.

Solomon and Colket (Solomon and Colket, 1979) extracted the 'activation energy' for rate constants in the above equation from their experimental results based on 13 coals ranging in rank from a 'high volatile bituminous coal to

lignite. These values are listed in Table 4.1 and used in the present work.

Table 4.1. Values of 'activation energy' for rate of evolution of concerned volatile components (Solomon and Colket, 1979)

Component	Weight fraction	ΔE_i^* (J/mol)
CO_2	0.03	33,472
Loosely bound CO	0.037	86,190
H_2O	0.055	41,421
Tightly bound CO	0.046	100,416
Hydrocarbons (CH_4)	0.034	81,170
H_2	0.04	106,274
Tar	0.12	66,944

4.4.3 Char gasification

Fixed carbon in char is oxidized simultaneously by CO_2 and H_2O in the system. The gas-solid reaction of char oxidation by CO_2 and H_2O are considered to be independent; therefore, the total rate of char gasification is the sum of that by these two gaseous species as follows:

$$\dot{R}_c = \dot{R}_c^{CO_2} + \dot{R}_c^{H_2O} \qquad (4.25)$$

where $\dot{R}_c$, $\dot{R}_c^{CO2}$ and $\dot{R}_c^{H2O}$ are the total rate of gasification of char, and the rates of gasification by CO_2 and by H_2O, respectively. The rate of char gasification by CO_2 and by H_2O may be represented according to the un-reacted core model as follows:

$$\dot{R}_c^{CO_2} = S_c\, n_c\, 4\,\pi\, \overline{r}_c^2\, k_c^{CO_2}\left(C_{CO_2} - \frac{C_{CO}^2}{K_{Ec}^{CO_2}}\right) \qquad (4.26)$$

and

$$\dot{R}_c^{H_2O} = S_c\, n_c\, 4\,\pi\, \overline{r}_c^2\, k_c^{H_2O}\left(C_{H_2O} - \frac{C_{CO}\times C_{H_2O}}{K_{Ec}^{H_2O}}\right) \qquad (4.27)$$

The rate constants in Equations (4.26) and (4.27) are defined in a similar way as that in Equations (4.20) and (4.22). The values of these pre-exponential constants and 'activation energies' in these rate constants are extracted by fitting computational results through the use of the present model with experimental data, and comparing with that reported in the references.

The change in the size of coal particles happens due to the swelling and contraction behaviour of coal. The coal used in present work was a high volatility coking coal. It would undergo softening, swelling and contraction during the heating process. Although only one type of coal was used in the present study, the heating rate and temperature of the coal at different locations in the ore/coal mixture during experiments

were very different. Detail modelling of the swelling and contraction behaviour of the coal during the reaction is not a part of the present work. An empirical approach should be proposed to deal with particle size change due to the swelling and contraction.

The packed bed of the present study may be divided into three regions along the heating direction. For the high swelling and contraction region near the hot face, an empirical equation (Equation 4.28) is proposed. For the low swelling and contraction region near the top of the bed, the change in the size of coal particles due to swelling and contraction may be neglected. For the portion of the bed between the two mentioned regions, the size of coal particles changes linearly between the two regions. The justification for proposing the empirical Equation (4.28) is given below.

According to experimental observations (Loison et al, 1963), coking coal usually swells at temperatures of 350 to 400 °C, begins to contract at around 650 °C and stops at about 1000 °C. The general pattern of coal particle size versus temperature under the investigated heating rate is approximated by a normal distribution curve peaked at 650°C, as expressed by the following equation

$$\overline{r}_c = \overline{r}_c^{\,o}\left(1 + \gamma \times \exp\left(\frac{-(T-650)^2}{2\times 300^2}\right)\right) \qquad (4.28)$$

where γ is a constant, and extracted in present model to be 0.18 by data fitting.

4.5 Mass balance for individual gaseous species

In the present work, direct measurement of local gas composition was attempted but failed. However, in addition to chemical reactions, concentrations of gases as functions of location and time may change due to changes in temperature, pressure and mass transfer through pores.

Gaseous species, which are products of Reaction (4.13) through (4.17) are mainly CO, CO_2, H_2, H_2O, CH_4 and tar, are included in this model.

The change in mass of the j-th (j = CO, CO_2, H_2, H_2O, CH_4 and tar) gaseous species in the control volume results from (a) flow of the species into the control volume due to bulk motion, (b) diffusive flux of the species due to a concentration gradient and, (c) generation/consumption of the species by gas-solid reactions (i.e. by chemical reactions (4.13) to (4.17). It may be expressed as

$$\frac{\partial}{\partial t}(\phi \rho_j) = \frac{\partial}{\partial x}\left(\frac{\phi}{\tau} D_{effj} \frac{\partial \rho_j}{\partial x}\right) - \frac{\partial}{\partial x}(\rho_j v_o) - \sum_i \dot{N}_{ij} M_j \qquad (4.29)$$

where ρ_j and D_{effj} are density and effective diffusivity of species j in the gaseous phase, respectively; τ is tortuosity factor; $\dot{N}_{ij}$ is the net rate consumption/generation of gaseous species j by chemical reaction i; and ϕ is local void fraction of the reacting bed.

The effective diffusivity of a species j in a gaseous mixture, D_{effj}, can be estimated from a knowledge of all of the relevant binary diffusion coefficients D_{ij} by following equation (Rosner, 1986)

$$D_{effj} = (1-y_j)\left[\sum_{\substack{i=1 \\ (i\neq j)}} \frac{y_i}{D_{ij}}\right]^{-1} \qquad (4.30)$$

Where binary diffusion coefficients D_{ij} can be calculated by following equation (Sherwood, Pigford and Wilke, 1975)

$$D_{ij} = \frac{0.00158T^{\frac{3}{2}}\left(\frac{1}{M_i}+\frac{1}{M_j}\right)^{\frac{1}{2}}}{P\sigma_{ij}^2\Omega_D} \qquad (4.31)$$

where Ω collision integral for i-j mixture; and σ_{ij} is collision diameter.

4.6 Continuity and momentum equations and the equation of state in the gaseous phase

In the present system, gases are not only the necessary intermediate reactants to sustain the overall chemical

reactions, but also contribute to convective heat and mass transfer. In this section, continuity and momentum equations, as well as equation of state, are established to calculate gaseous pressure, flow velocity and composition.

4.6.1 Continuity equation

By summing six mass balance equations (Equation 4.29) , the continuity equation may be obtained as follows:

$$\frac{\partial}{\partial t}(\phi \rho_g) = -\sum_j \sum_i \dot{N}_{ij} M_j - \frac{\partial}{\partial x}(\rho_g V_o) \qquad (4.32)$$

where $\dot{N}_{ij}$ may be positive or negative, which can be calculated from rate of chemical reactions; M_j is molecular weight of gaseous species j; and ρ_g is the density of gaseous phase.

As size and shape of ore particles in the mixture are assumed to be constant during the reaction, change in void fraction of the mixture (ϕ) is a result of the disappearance of char by oxidation. Therefore, local void fraction of the mixture was updated by adding the volume of gasified char to its initial void fraction.

4.6.2 Momentum equation

The rate of momentum change of a fluid flowing through the void space of a solid packing is the resultant of all

external forces acting on the fluid, i. e. pressure, gravity and frictional forces. In the present study, gases which are generated within the system flow through a solid packing of 0.028 m high. By comparison, the contribution of gravity may be neglected without introducing significant error in modelling.

Momentum in the x-direction in the control volume may be balanced as

$$\begin{pmatrix}\text{rate of}\\ \text{momentum in}\\ \text{by convection}\end{pmatrix}+\begin{pmatrix}\text{pressure force}\\ \text{acting on}\\ \text{surface } x\end{pmatrix}-\begin{pmatrix}\text{rate of}\\ \text{momentum out}\\ \text{by convection}\end{pmatrix}+\begin{pmatrix}\text{pressure force}\\ \text{acting on}\\ \text{surface } x+\Delta x\end{pmatrix}+\begin{pmatrix}\text{frictional force}\\ \text{acting on}\\ \text{gaseous phase}\end{pmatrix}+\begin{pmatrix}\text{rate of}\\ \text{momentum}\\ \text{accumulation}\end{pmatrix} \tag{4.33}$$

that is,

$$\dot{M}_{conv,\,x}+\dot{F}_{P,\,x}=\dot{M}_{conv,\,x+\Delta x}+F_{P,\,x+\Delta x}+F_{fr}+\frac{\partial M}{\partial t} \tag{4.34}$$

where:

(1) The momentum flux by convection is

$$\dot{M}_{conv,\,x}=\left(\rho_g\frac{V_o^2}{\phi^2}\phi\right)_x \tag{4.35}$$

(2) The pressure forces acting on the cross-sectional area is

$$F_{P,\,x}=(P\phi)_x \tag{4.36}$$

(3) The frictional force acting on the gaseous phase by the packing is

$$F_{fr}=f_r\,\Delta x\,\phi \tag{4.37}$$

where f_r is frictional force acting on the gas in the control volume, and is determined by the solid and fluid properties. These properties are (a) rate of fluid flow; (b) viscosity and density of the fluid; and (c) detailed structure of the passage for gases. Ergun has successfully correlated the frictional force with the solid and fluid properties and established the Ergun Equation (Ergun and Orning, 1949; Ergun, 1952):

$$f_r = \alpha \mu V_o + \beta \rho_g V_o^2 \tag{4.38}$$

where α and β are functions of properties of the packing,

$$\alpha = 150 \frac{(1-\phi)^2}{\phi^3 (S_{fa} d_p)^2} \tag{4.39}$$

and

$$\beta = 1.75 \frac{(1-\phi)}{\phi^3 (S_{fa} d_p)} \tag{4.40}$$

where S_{fa} and d_p are a shape factor and a surface area mean diameter of particles, respectively; and μ is gas viscosity.

(4) The rate of momentum accumulation is

$$\frac{\partial M}{\partial t} = \frac{\partial}{\partial t} (\rho_g \frac{V_o}{\phi} \Delta x \phi) \tag{4.41}$$

A substitution if Equations (4.35) - (4.41) into Equation (4.34) results with

$$\frac{\partial}{\partial t}(\rho_g \frac{V_o}{\phi}) = -\frac{\partial P}{\partial x} - \frac{\partial}{\partial x}(\rho_g \frac{V_o^2}{\phi^2}) - \alpha \mu V_o - \beta \rho_g V_o^2 \qquad (4.42)$$

According to numerical estimation (refer to details in appendix II), extreme values of the second and the fourth terms on the right hand side of Equation (4.41) are about 48.8 and 2.79×10^3 ($kg/m^2/s^2$), respectively. They are at least two orders of magnitude smaller than the first and the third terms, which are about 1×10^5 and 7.9×10^6 ($kg/m^2/s^2$), respectively. Thus the second and fourth terms of the equation may be neglected in the computation in the present work without introducing significant errors. Equation (4.41) may be simplified to become

$$\frac{\partial}{\partial t}(\rho_g \frac{V_o}{\phi}) = -\frac{\partial P}{\partial x} - \alpha \mu V_o \qquad (4.43)$$

The viscosity of the gaseous mixture in the above equation can be estimated by the following equation (Rosner, 1986)

$$\mu = \frac{\sum_j M_j^{\frac{1}{2}} y_j \mu_j}{\sum_j M_j^{\frac{1}{2}} y_j} \qquad (4.44)$$

where μ_j and y_j are viscosity and mole fraction of species j, respectively. Value of μ_j are available from the literature (Kaminski, 1993; Touloukian, 1970).

4.6.3 Equation of state

Gas density varies with temperature and pressure. For the ranges of temperature and pressure values observed in the present system, the gases may be considered as incompressible and obey ideal gas law:

$$P = \frac{\rho_g}{M_g} RT \qquad (4.45)$$

In principle, three properties of the gas phase (i.e. density, pressure and flow velocity) can be determined by simultaneously solving three equations: continuity and momentum equations, and the equation of state. However, after recognizing that temperature is another unknown, these equations must be solved simultaneously with the heat transfer Equation (4.12).

4.7 Summary of the mathematical model

A non-isothermal and non-isobaric mathematical model for reactions in iron ore/coal composites has been developed as shown above. It includes: an equation of thermal energy balance (Equation (4.12)), kinetic expressions for heterogeneous reactions (Equations (4.19), (4.21), (4.24), (4.26) and (4.27)), six equations of mass balance for gaseous species (Equation (4.29)), a continuity equation (Equation (4.32)), momentum equations (Equation (4.43)) for gaseous phase, and an equation of state of an ideal gas (Equation (4.45)). There are 19 independent equations to be solved simultaneously by numerical methods to give local values of temperature, pressure, velocity and density of gas flow, nine rates of reactions, and six concentrations of gases as function of x and t. Composition of solids are determined by the values of rates of reaction up to that time in a given location through mass balance of carbon, the three states of iron and the remaining volatile in the char.

In carrying out simultaneous numerical solutions, values of parameters, such as heat capacities, effective thermal conductivity, porosity, viscosity and diffusivity of gases, etc., are provided initially according to experimental condition and updated based on known relations after each iteration. The computational results of these parameters are

discussed later in this chapter.

4.8 Initial and boundary conditions

To solve these equations in the mathematical model, initial and boundary conditions must be specified according to experimental conditions (refer to Chapter Three for details of experimental conditions) for each of these partial differential equations.

4.8.1 Initial conditions

In most of experiments conducted, the ore and coal ratio was 80/20 by weight, and packed in a stainless steel crucible with an initial packing density of 1900 kg/m^3. Initial conditions for the present model are specified according to this initial experimental condition unless a different condition is specified.

Table 4.2. Initial properties of solid materials and the packed bed

Iron ore particles			Coal particles			Packed bed
Number density (m^{-3})	Average diameter (m)	Shape factor	Number density (m^{-3})	Average diameter (m)	Shape factor	Void fraction
1.02E10	3.9E5	1.75	1.61E9	6.9E5	1.37	0.405

The initial number density, average size and shape factor of the ore and the coal particles, and initial void fraction of the packed bed are listed in Table 4.2.

When ore and coal were mixed and packed in the crucible in air at ambient temperature, the initial condition may be expressed as

When $t=0$, $0 \le x \le 0.028$ (m)

$T=298.16$ K

$V_o=0$ m/sec.

$P=1.0133\times10^5$ Pa

$\rho_j=0$ kg/m^3 (j=CO, CO_2, H_2, H_2O, CH_4 and tar)

4.8.2 Boundary conditions

The present one-dimensional reaction system has two boundaries; the bottom and the top face of the packed bed. The bottom face sits on the flat bottom of the crucible; heat is transferred from the crucible to packed bed. The bottom of crucible is the hot face. The top face, through which the gaseous species leave the packing, is a free face.

a. Boundary conditions at the hot face

One thermocouple was embedded at bottom face to monitor local temperature during experimentation. The measured temperature was used in the present model as the temperature

boundary condition at this boundary of the system. The bottom wall is impermeable to mass flux. These boundary conditions may be expressed as:

When x=0, t>0

$T=T_1$ K, which is directly measured on a continuous basis as discussed above;

$V_o=0$ m/s; and,

$\partial\rho_j/\partial x=0$ kg/m^3/m

b. Boundary conditions at the top face

A steel screen was placed at top face of the packing to prevent solids from moving up but allows gas to leave the packing (see Figure 3.1). As the crucible which contained the packing was opened to the atmosphere, the pressure at the top face of the packed bed is atmospheric; therefore,

at x=0.028 (m), t>0

$P=1.0133\times10^5$ Pa; and,

$$\rho_g=\frac{P\overline{M_g}}{RT} \quad ,kg/m3. \tag{4.46}$$

In addition to sensible heat carried away by gas flow, radiation heat lost from the top face to the surroundings may become significant. Heat may be transferred by radiation between the top face and crucible wall and space outside the crucible. As the steel crucible wall was insulated from outside, the temperature difference between the top face and

crucible wall was small, and the radiation heat transfer between these two surfaces is neglected. The opening of the crucible may be treated as a black surface which totally absorbs the heat radiated from the top face. The radiation heat flux at this surface may be expressed as

at x=0.028 (m), t>0

$$\dot{q}_{rad} = -F_{sm}\varepsilon_m\sigma\left(T^4 - T^4_{ambient}\right) \qquad (4.47)$$

where F_{sm} is a view factor for the top face of packed bed and the opening of the crucible. It was calculated according to this configuration to be 0.25 (Geiger, 1973,pp.378). ϵ_m is emissivity of mixture, and may be assumed to be 0.85 according to the above quote reference; while σ is the Stefan-Boltzmann constant (=5.6651×10^{-8} J/s.m^2.k^4).

4.9 Numerical method

The equations in present model have to be solved simultaneously by numerical methods to obtain local values of the various dependent variables as function of x and t. The explicit finite difference method was used to solve these equations, i.e. these differential equations were changed into a finite difference form, which were solved numerically on a 486 IBM compatible computer.

In the numerical solution of velocity fields of gas flow, the "staggered" grid (Patankar, 1980) for the velocity

components was employed, i.e. the velocity field's computational grid points were staggered relative to the main grid point, (where the values of all the variables except the velocity are stored). With this method, the velocity component is computed at the mid-point of the faces of the main grid control volume, thus facilitating the calculation of the convection terms on these surfaces.

The procedure of numerical computation is shown in Figure 4.2. The computation stopped at the sixtieth minute which is the longest reaction time for the experiments conducted.

4.10 Values of kinetic parameters

There are three types of parameters included in this mathematical model, namely; (a) physical and chemical properties of the system related to the apparatus and raw materials which were determined in the laboratory and listed in Table 4.2; (b) physical kinetic parameters, such as 'effective' thermal conductivity, 'effective' diffusivity, viscosity, etc, which were computed from accepted correlations in the literature; and (c) chemical parameters which may be divided into two groups: (i) equilibrium constants which were calculated from thermochemical data in the literature, and (ii) the rate constants which were obtained by curve fitting of data obtained with the furnace temperature at 1200°C. The

evaluation of rate constants are discussed in detail in Chapter 5.

4.10.1 Physical properties of the partially reacted solid mixture

4.10.1.1 Specific heat of the partially reacted mixture

Figure 4.3 shows the calculated values of specific heat of the partially reacted mixture as a function of reaction time, which are calculated based on the specific heat and relative amount of each component in the partially reacted mixture at local temperature (see Appendix I for details). The specific heat of reacting mixture at a given location increases with reaction time first, then decreases after reaching a peak value. The increase is due to the fact that the specific heat of iron, iron oxides and coal increase with temperature. The decrease is due to the conversion of magnetite (Fe_3O_4) to metallic iron (the latter has a lower value of specific heat) and the disappearance of the coal.

4.10.1.2 Specific heat of gaseous mixture

Figure 4.4 shows calculated values of specific heat of gas at different locations within the bed as functions of reaction time. They were calculated based on the specific heat of each gas species and gas composition at local temperature (see Appendix I for details). The appearance of a maximum value is mainly due to a maximum hydrogen content in the gaseous phase (such as in reaction time about 5 minutes at location 1, Figure 5.17). The specific heat of hydrogen is about one order of magnitude higher than that of the other gaseous species in the reacting system (for examples, refer to Table 4.3).

Table 4.3. Specific heat of gaseous species at 700°C

Species	H_2	H_2O	CO	C_2O	CH_4	Tar
C_p, J/kg.K	15,522	2,523	1,196	1,134	4,012	879

4.10.2 Physical kinetic parameters of the reacting mixture

4.10.2.1 Effective thermal conductivity of solid and gaseous mixtures

The computed values of effective thermal conductivity of solid mixture, K_{effm}, as functions of reaction time are shown in Figure 4.5. They are calculated based on properties and

relative amount of each component in the partially reacted mixture at the local temperature (refer to Appendix I for details). The calculated value of effective thermal conductivity is proportional to the content of metallic iron because metallic iron has a much higher value of thermal conductivity than all the other materials in the mixture.

4.10.2.2 Viscosity of gaseous mixture

Figure 4.6 shows the calculated viscosity of the gaseous mixture at different locations as a function of reaction time. The high viscosity at about the third minute of reaction results from high tar content in the gas, as viscosity of tar is about one order of magnitude higher than that of the other species. The increase of viscosity after about the fifth minute is mainly due to the increase of the gas temperature.

4.10.2.3 Diffusivity of gaseous mixture

Figure 4.7 shows the diffusivity of individual species in the gaseous mixture. Diffusivity of a species is calculated from binary diffusivity, gas composition and local temperature (refer to Equation (4.30)). Diffusivity of hydrogen is much higher than that of the other gas species.

4.10.3 Standard free energy changes and heat of chemical reactions

The standard free energy changes of iron oxide reduction and carbon gasification as functions of temperature, used in the present study, are taken from Elliott et al (1960) and Bogdandy and Engell (1971), and are listed in Table 4.4.

Table 4.4. Values of heat and standard free energy change of reactions

Reactions	(2.2)	(2.3)	(2.4)	(2.9)	(2.10)	(2.11)	(2.12)	(2.13)
ΔH°(J/mole)	36,250	-17,305	-3,916	77,404	23,848	37,238	172,464	131,293
ΔG°(J/mole)	297,90-38.07T	-22,802 +24.476T	-9,652 +8.828T	65,772 -70.291T	13,189 -7.740T	26,325 -23.389T	170,707-174.891T	134,724 -142.674T

The heat of a chemical reaction at a higher temperatures may be calculated from the reported heat of the chemical reaction at reference temperature of 298.16 K. The values of heat of iron oxide reduction and carbon gasification at 298.16 K are taken from Bogdandy and Engell (1971) and Ross (1980), and are listed in reactions (2.2) to (2.4) for the reduction of iron oxides by CO, reactions (2.9) to (2.11) for the reduction of iron oxides by H_2, and reactions (2.12) and (2.13) for the carbon gasification by H_2O and CO_2, which are also summarized in Table 4.4.

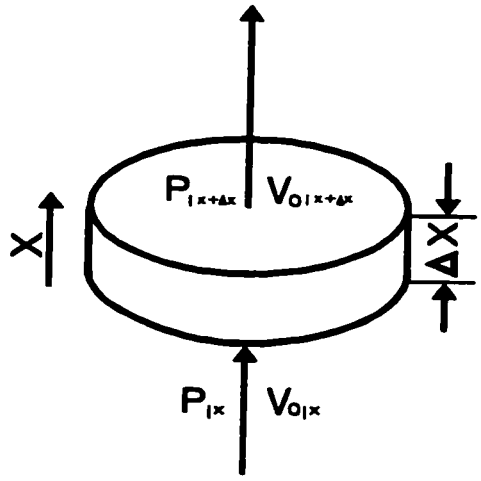

Figure 4.1 Illustration of a control volume

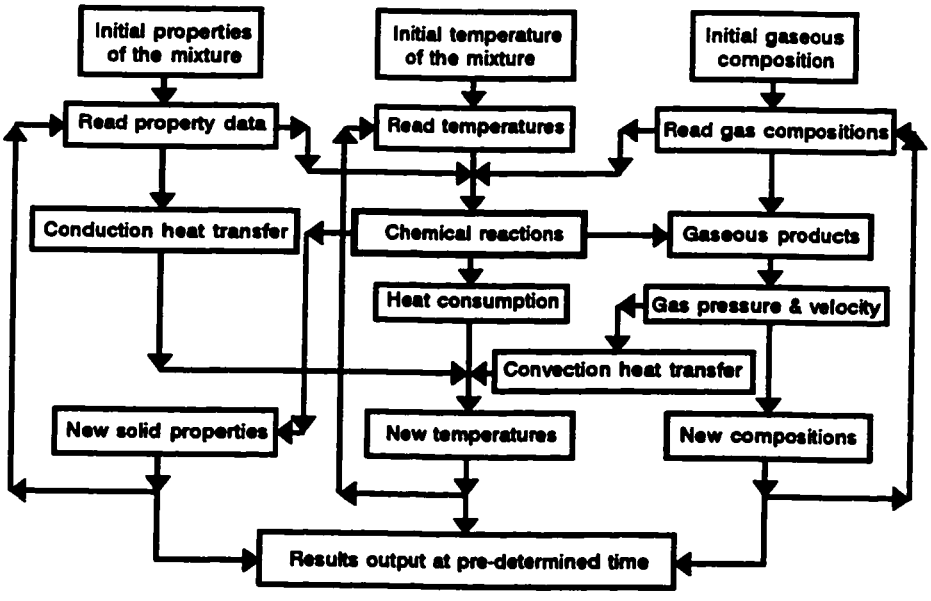

Figure 4.2 Computation procedure of the model

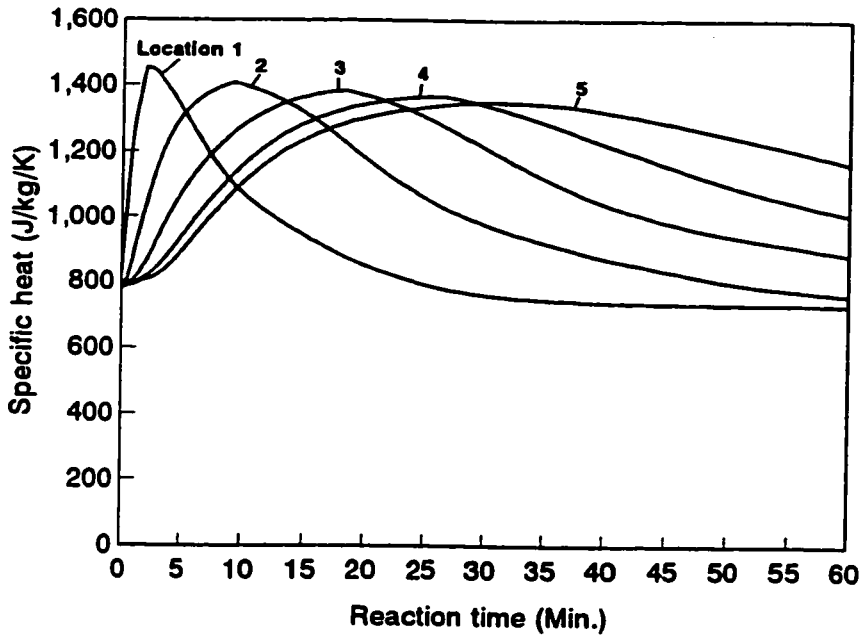

Figure 4.3 Computed specific heat of partial reacted mixture as a function of reaction time, (Ore/coal=80/20, furnace temperature=1200°C)

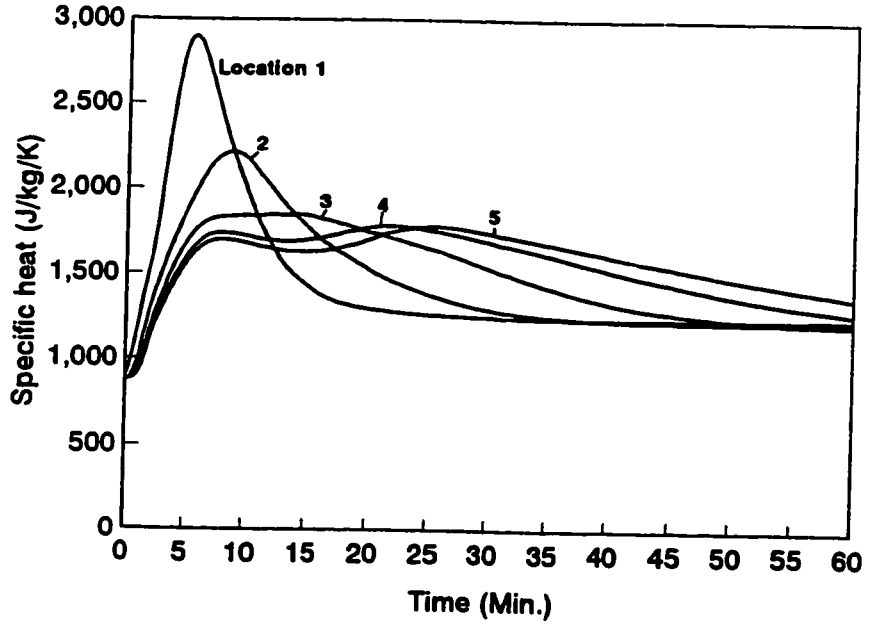

Figure 4.4 Computed specific heat of gas as a function of reaction time (Ore/coal=80/20, furnace temperature=1200°C)

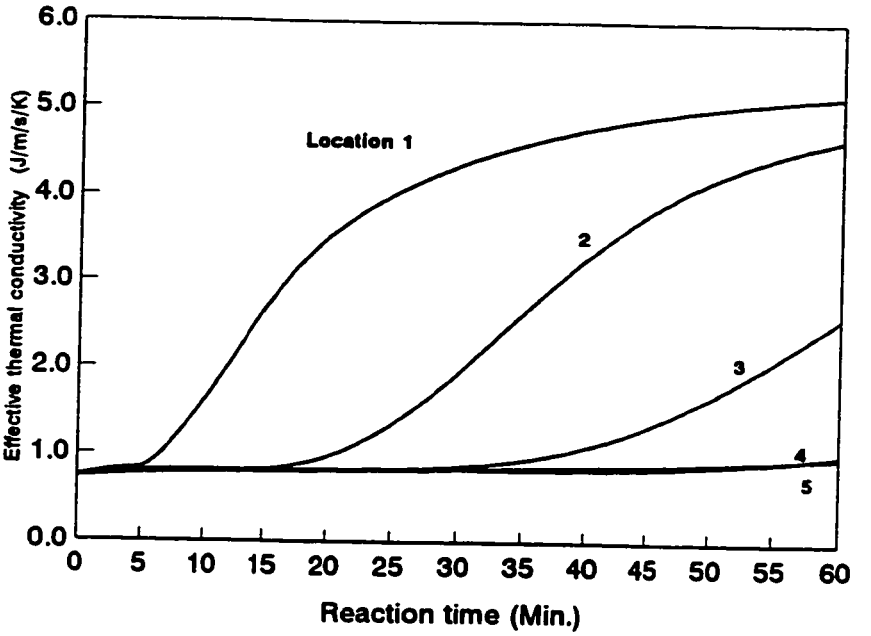

Figure 4.5 Computed effective thermal conductivity of partially reacted mixture as a function of time, (Ore/coal=80/20, furnace temperature =1200°C)

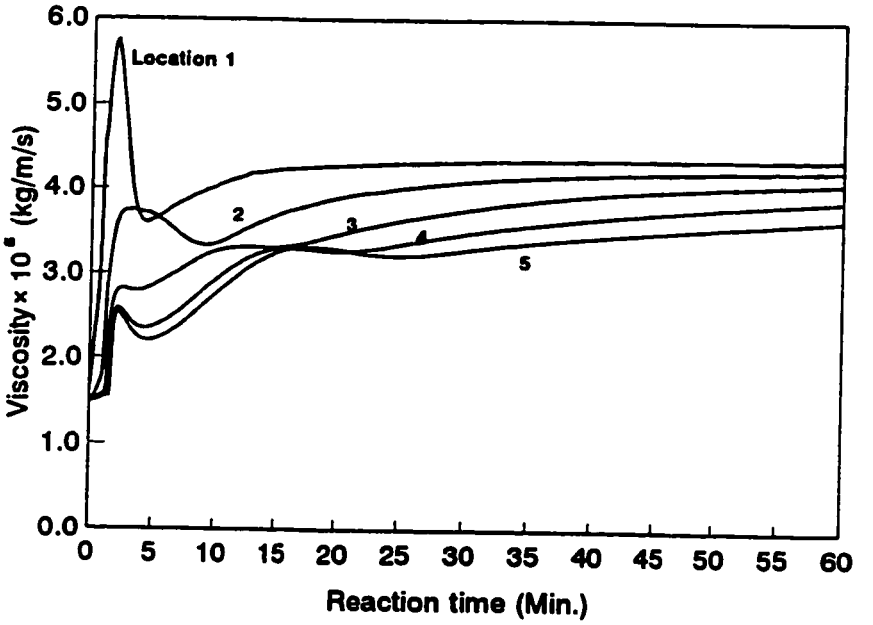

Figure 4.6 Computed gaseous viscosity as a function of reaction time (Ore/coal=80/20, furnace temperature =1200°C)

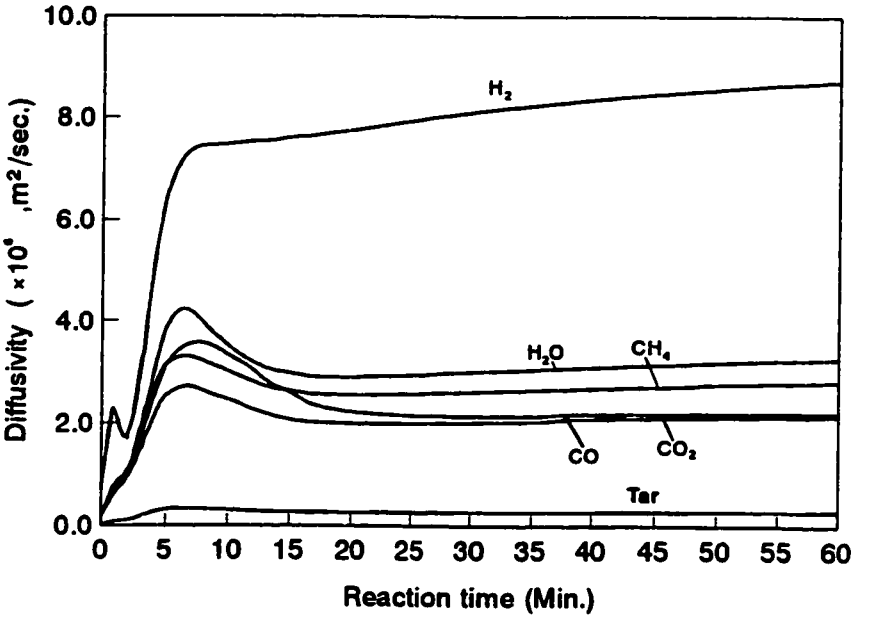

Figure 4.7 Computed diffusivities as a function of reaction time at location 1 (Ore/coal=80/20, furnace temperature = 1200°C)

CHAPTER FIVE: COMPARISON BETWEEN COMPUTATIONAL RESULTS AND EXPERIMENTAL DATA AND MODEL VALIDATION

The equations in the mathematical model developed in Chapter Four were solved by a numerical method to obtain local values of the various dependent variables as functions of time. There are four sets of independent experimental data generated with different experimental conditions, i.e. different furnace temperatures and initial ore/coal ratios (refer to Section 3.1.4). The set of data with the furnace temperature of 1200 °C and the initial ore/coal ratio of 80/20 was used to evaluate the values of rate constants of individual chemical reactions. The remaining three sets of data (i.e. with a furnace temperatures of 1300 °C and an ore/coal ratio of 80/20, and with a furnace temperature of 1300 °C and the ore/coal ratios of 82/18 and 85/15) were used to validate the model.

5.1 The evaluation of rate constants of iron oxide reduction and char gasification

Figures 5.1 to 5.7 and Table 5.1 show the value of rate constants for reduction of magnetite and wustite by CO and H_2, and for gasification of char by CO_2 and H_2O, respectively. The reported values from literatures are also included in the figures. These rate constants were determined by fitting experimental data with model by trial and error at a furnace face temperature of 1200°C and initial ore/coal ratio of 80/20.

Table 5.1. Values of parameters used for calculation of rate constants of reactions

Reactions	(2.2)	(2.3)	(2.4)	(2.9)	(2.10)	(2.11)	(2.12)	(2.13)
k_{i0}	10.7	59.0	16.0	11.0	20.0	6.5	1.87E8	6.0E5
ΔE_i^*(J/mole)	65,689	69,454	73,638	61,505	63,597	68,618	221,752	172,799

The values of rate constants for iron oxide reduction obtained in the present work fall within the ranges of the reported literature values which used different experimental techniques to determinate the interfacial area for the chemical reactions (i.e. by a topochemical calculation of a partially reacted pellet or by B.E.T. method, refer to Figures 5.1 to 5.5). As discussed in Chapter Two (Section 2.3), a topochemical calculation under-estimates the interfacial area

for a gas-solid system, and thus over-estimates the values of the rate constant. On the other hand, the B.E.T. method over-estimates the interfacial area for a chemical reaction, and thus under-estimates the values of the rate constant. It is reasonable to expect the values of rate constants obtained in the present work to fall in between the reported values from literature.

In the absence of data in the literature for the reduction of magnetite to metallic iron by CO, the values of the rate constants evaluated in the present work is included in the Figures 5.5.

The values of rate constant of char gasification evaluated in the present study is close to that reported in the literature with the interfacial area determined by the topochemical calculation of a char particle (refer to Figures 5.6 and 5.7). Similar size ranges of char particles (tens to hundreds micro-meter), and methods in determination of interface area were used.

5.2 Comparison between computational results and experimental data

Computational results with values of parameters discussed in Sections 4.10 and 5.1 are compared with experimental data with furnace temperature controlled at 1200 °C, as reported in

Section 3.2. The results are compared include temperature profiles throughout the reacting mixture and local temperature as a function of reaction time; local solid composition, i.e. metallic iron (Fe^{o}), ferrous iron (Fe^{2+}) ferric iron (Fe^{3+}) and residual carbon; and local gaseous pressures and compositions of exit gas.

5.2.1 Temperature Profiles

Computed local temperatures as functions of reaction time, and temperature profiles across the layer of reacting mixture at 10, 20, 30, 40, 50 and 60 minutes with furnace temperature set at 1200°C are shown in Figures 3.3 and 3.6. The computed temperatures are in good agreement with measured temperatures which are shown as points and connected by dotted lines in the figures, particularly after about 20 minutes of reaction time. Before the twentieth minute, the computed values of temperature at locations away from the hot surface are higher than that measured, especially in locations 3, 4, and 5, which may be seen clearly in Figure 3.3. One of the reasons is due to water vapour from higher temperature regions (such as locations 1 and 2), which condenses and later re-vaporizes at these locations. The present model does not include the heat exchange due to this water vapour condensation and re-vaporization, thus has a higher values of

computed temperatures.

5.2.2 Reduction of iron oxides and degree of reduction

Computed local degrees of metallization and reduction of iron oxide as functions of time are shown in Figures 3.9 and 3.10. The computed profiles for degree of reduction are shown in Figure 3.11.

In Figures 3.9 and 3.10, the computed values for the degree of metallization and reduction of iron oxide in location 1 is higher than that measured, and the opposite is true in locations away from the hot face. That may be due to part of iron oxides reacting with the gangue to form a slag phase, i.e. a solution at high temperatures. It would lower the thermodynamic activity of the iron oxide and reduce its reactivity for reduction. The formation of a slag phase usually occurs at high temperature and in the final stage of reduction, and was observed by many experimentalists (Ross, 1980). The present model does not include the effect of the slag phase formation on the rate of reduction, thus resulting in a disagreement in degrees of metallization and reduction of iron oxide at high temperatures as shown in Figures 3.9 and 3.10.

Computed values of both ferrous iron (Fe^{2+}) and ferric iron (Fe^{3+}) as functions of reaction time are included in

Figures 3.12 and 3.13, which show general agreement with experimental data.

5.2.3 Degree of carbon gasification

Figures 3.14 and 3.15 show the computed and measured values for the degree of carbon gasification as functions of location and reaction time, and the profile for the degree of carbon gasification over the height of the packing when the furnace temperature was set at 1200°C, respectively. The lower computed values versus the measured ones in about 20 minutes at locations 3, 4 and 5 may be due to our inability to instantaneously stop the coal devolatilization at the end of an experiment, even though the crucible containing the reacting ore/coal mixture was quickly removed from furnace and quenched by running water, as described in Chapter Three. It took a certain finite time to cool down the interior locations 3, 4 and 5 (Figure 3.3).

The higher computed value of carbon gasification in location 2 may result from the error of average radius for coal particles in this location. It was assumed that the average radius of char particles increased due to swelling during the heating; this results in a higher rate of carbon gasification. Figure 5.8 shows the computed average radius of coal/char particles. The initial average radius of the coal

particle is 3.45×10^{-5} m. In location 1 and 2, the calculated average radius of the particle is larger than that of its initial respective value at reaction times of about 15 and 30 minutes, due to the swelling of coal. Coal swelling at this location may not be so great or last for so long.

5.2.4 Pressures and gas flow velocity

Figure 3.7 shows computed and measured pressures as functions of location and reaction time when the furnace temperature was set at 1200°C. There is no unique value of pressure measured in the ore/coal reacting system. The measured values are simply the resultant pressure due to the rates of gas generation and removal at this location. The changes in pore structure, such as crack formation, would have a pronounced effect on the rate of removal of gases, i.e. it lowers the pressure build-up. Thus, it is not possible to accurately calculate the pressures by mathematical modelling without detailed structural information of the packing, which is not available. However, the computed pressures have the same pattern as observed in experiments.

The pressure peaks computed in the first 20 minutes are most likely resulting from high rates of gas generation and the lower void fraction of the packing during devolatilization of coal. The computed local rate of gas generation (at

location 1 for example) and the void fraction of packing as a function of reaction time are shown in Figures 5.9 and 5.10. The high values of gas generation at approximately 5 minutes of reaction time at location 1 (Figure 5.9) were from coal devolatilization, and responsible for the high pressure computed in this location. The decrease in void fraction of the packing due to the swelling of coal resulted in the high pressure at this location for about 20 minutes. From the computed results, we assumed that the high pressure observed in the earlier stage of reaction in the mixture is due to changing coal properties.

Computed values of superficial gas flow velocity are shown in Figure 5.11. The maximum superficial velocity is about 0.014 m/s, as anticipated in the modelling.

5.2.5 Gas compositions

Computed gas compositions as functions of reaction time are shown in Figures 5.12 to 5.17. The gases generated at the earlier stage mainly originate from devolatilization of the coal. Water vapour and CO_2 were the first two gases to evolve from the coal (Figures 5.12 and 5.13), followed by CH_4 and tar (Figure 5.14 and 5.15), then CO and H_2.

The concentration of CH_4 and tar decreased quickly after a concentration peak was reached (Figure 5.14 and 5.15). This

may be due to the fact that they were generated only by coal devolatilization. The H_2O and H_2 (Figures 5.12 and 5.17), although initially generated by the coal devolatilization, may react with carbon or iron oxide before they leave the reacting system. As in Figure 5.12, the first concentration peak of H_2O at about the second minute of reaction (at location 1 for example) is due to its generation by devolatilization. The concentration then became lower as the other gaseous species were evolved. When H_2 was generated by devolatilization at about the fifth minute (Figure 5.17), the reduction of ore by H_2 started, and the H_2O generated by the reduction resulted in the second concentration peak of H_2O at about the sixth minute.

The concentration of CO, however, kept increasing after the fifth minute (Figure 5.16) during the course of reaction. It is due to the fact that the CO was not only generated by devolatilization (in the first five minutes), but also by gasification of char (after the fifth minute).

Figure 5.18 shows the computed and measured CO, CO_2, H_2 and CH_4 in exit gas as a function of reaction time. The higher values of computed H_2 and lower values of computed CO than that measured may due to the uncertainty in modelling of gaseous product of coal devolatilization.

5.3 Validation of the model

The mathematical model developed in the present work has been applied to the other three sets of independent experiments varying in furnace temperatures and ore/coal ratios. One set of experiments was carried out with a furnace temperature at 1300°C and an ore/coal ratio of 80/20, and two sets of experiments were carried out with a furnace temperature at 1200 °C but with ore/coal ratios of 82/18 and 85/15, respectively. Other than the change in temperature or ore/coal ratio, all other experimental conditions in these three sets of experiments were the same as reported in Section 3.2.

At higher furnace temperatures, experimental difficulties in controlling the initial conditions, such as introducing a cold object to a hot chamber, arose, particularly in determining time zero and in effectively stopping the chemical reactions at the end of the experiment. On the other hand, higher furnace temperatures are favoured by industry in process development. Therefore, two experiments were conducted for the chemical analysis of solid compositions with reaction times of 30 and 60 minutes, and another two for measurements of mixture temperatures and gaseous pressures up to 60 minutes of reaction time. The results of experiments and computations at this experimental condition are compared in Figures 3.18 to

3.24.

In experiments with ore/coal ratio of 82/18 and 85/15, three experiments were conducted for each ore/coal ratio with reaction times of 60 minutes, i.e. each for temperature measurement, pressure measurement and chemical analysis of solid composition were performed. The results of experiments and computations at these conditions are shown in Figures 3.26 to 3.33.

General agreement exists between the computed and measured temperatures, the degree of reduction and the degree of carbon gasification as functions of reaction time and location (refer to Figure 3.18 to 3.33). These data appear to be comparable with the first set of data reviewed in Section 5.2. These results illustrate that this mathematical model is capable of representing the behaviour observed in this system.

5.4 Summary

The general agreement between the computed and measured temperature, the degree of reduction and the degree of carbon gasification, gaseous pressure and composition of exit gas, as functions of reaction time and location, illustrate that this mathematical model is capable of representing the temperature and composition change observed in this system.

The cause of higher values of computed temperature at the cold end, during the first 20 minutes (Figures 3.3 and 3.7), is likely due to water vapour condensation and subsequent vaporization, which is not evaluated in the present model.

The higher values of computed metallic iron content at a location near the hot face may be due to a fast rise in temperature which causes a portion of the iron oxide to form a slag phase with gangue before it can be reduced.

The lower values of computed carbon gasification, at lower temperature locations at about 20 minutes, may be due to experimental errors. Specifically, it may be due to the inability to instantaneously stop the devolatilization of coal at the end of an experiments.

Further improvement in modelling may be made by including changes mentioned above; however, additional efforts are not justified for the present work.

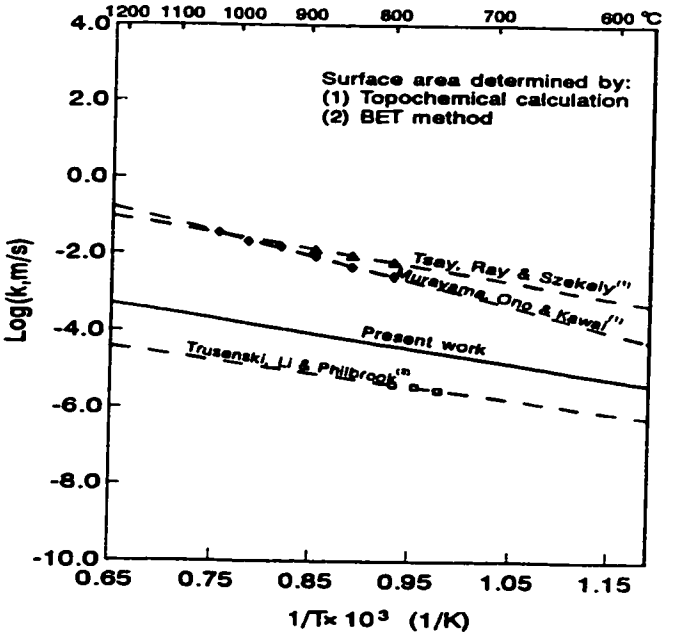

Figure 5.1 Plot of rate constants against the reciprocal temperature for reduction of Fe_3O_4 to FeO by CO

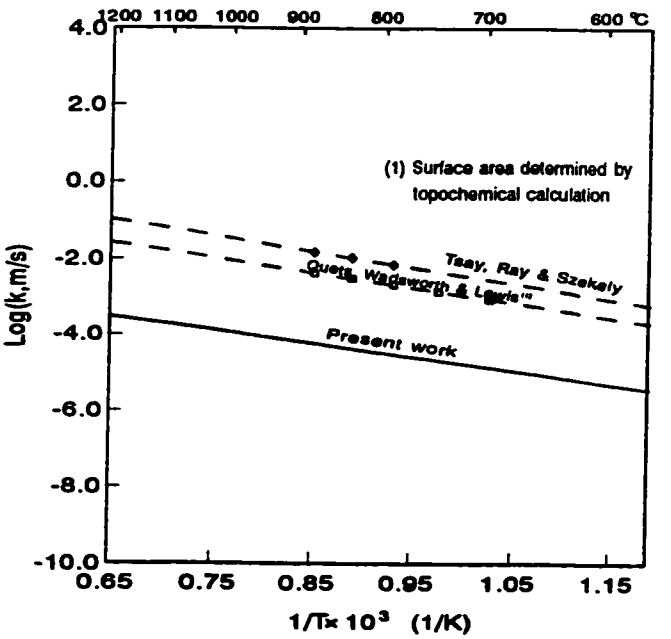

Figure 5.2 Plot of rate constants against the reciprocal temperature for reduction of Fe_3O_4 to FeO by H_2

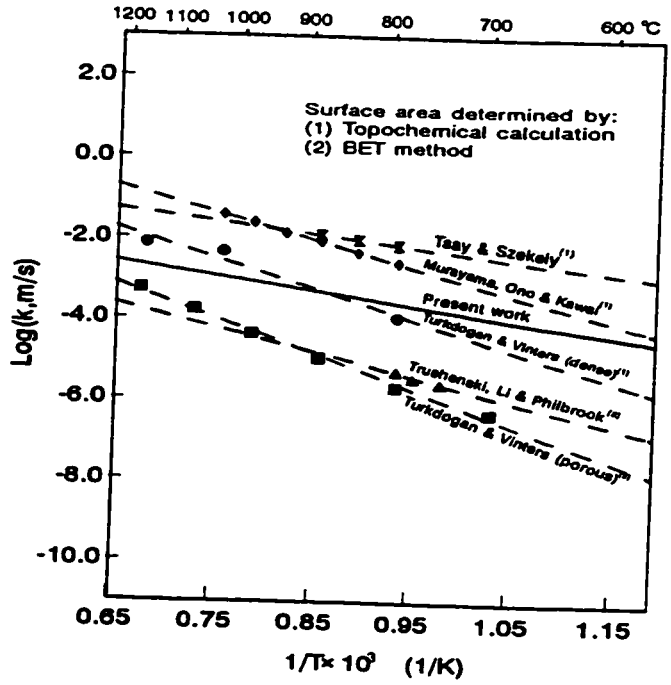

Figure 5.3 Plot of rate constants against the reciprocal temperature for reduction of FeO by CO

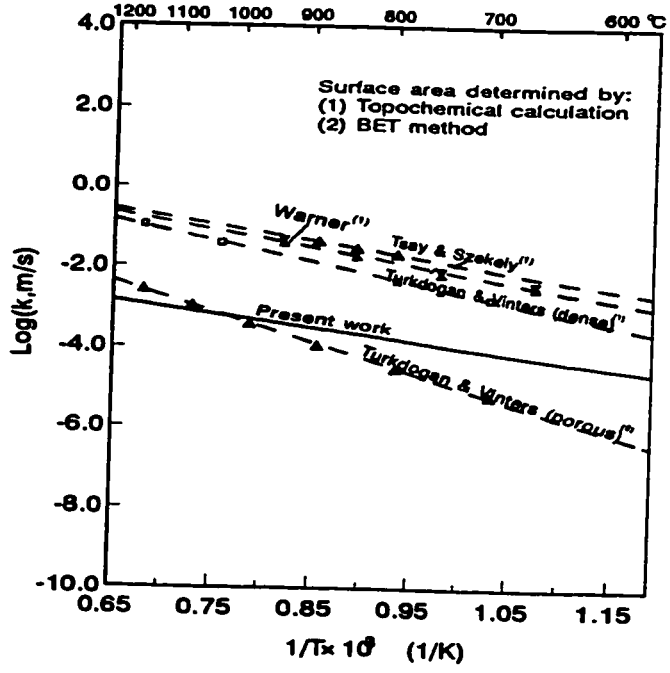

Figure 5.4 Plot of rate constants against the reciprocal temperature for reduction of FeO by H_2

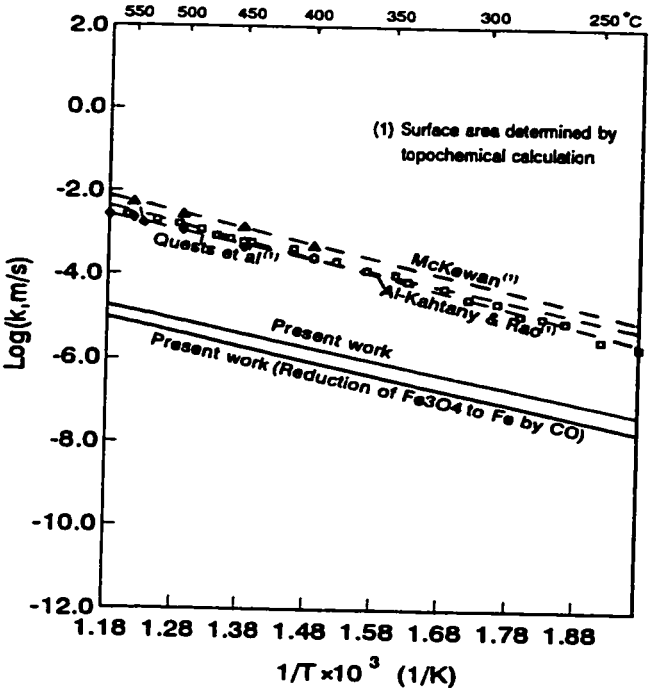

Figure 5.5 Plot of rate constants against the reciprocal temperature for reduction of Fe_3O_4 to Fe by H_2

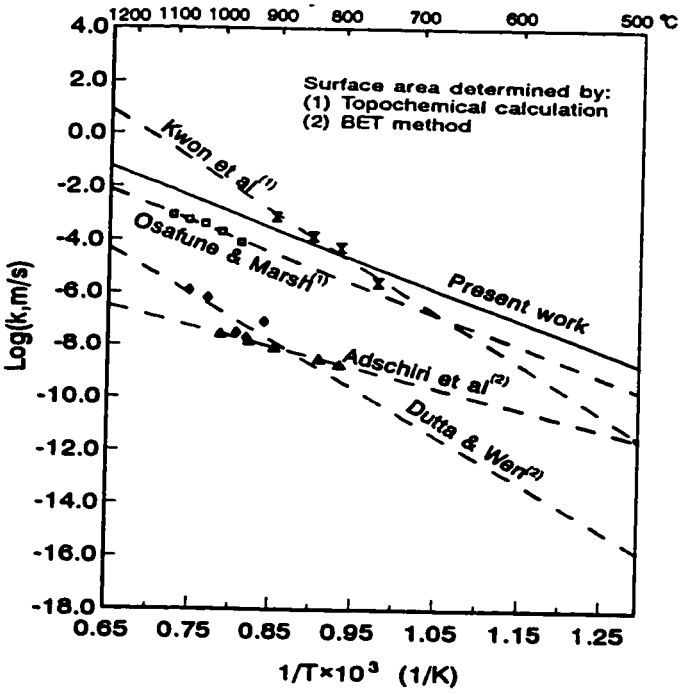

Figure 5.6 Plot of rate constants against the reciprocal temperature for char gasification by CO_2

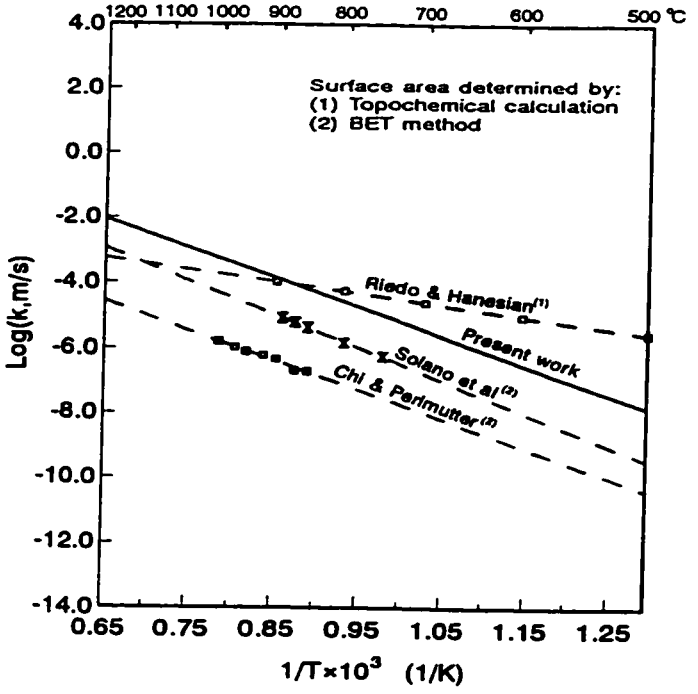

Figure 5.7 Plot of rate constants against the reciprocal temperature for char gasification by H_2O

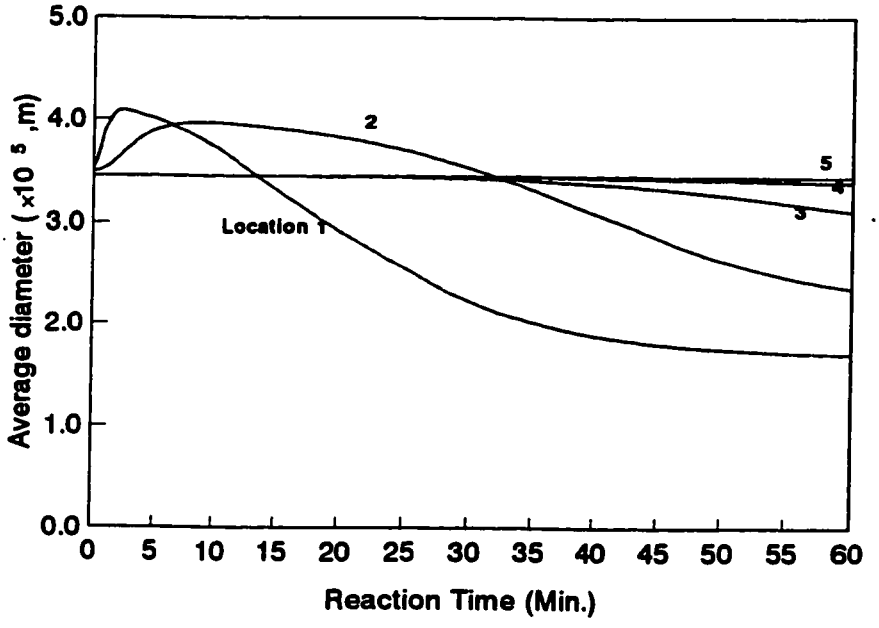

Figure 5.8 Computed local average radius of coal particles as a function of reaction time (Ore/coal=80/20, furnace temperature=1200°C)

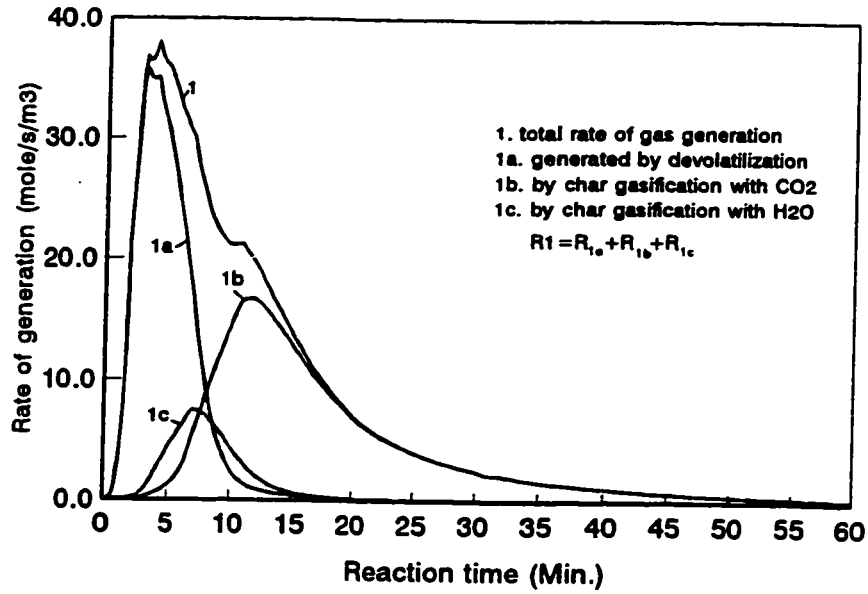

Figure 5.9 Computed local rate of gas generation by devolatilization of coal and gasification of char at location 1 (Ore/coal=80/20, furnace temperature=1200°C)

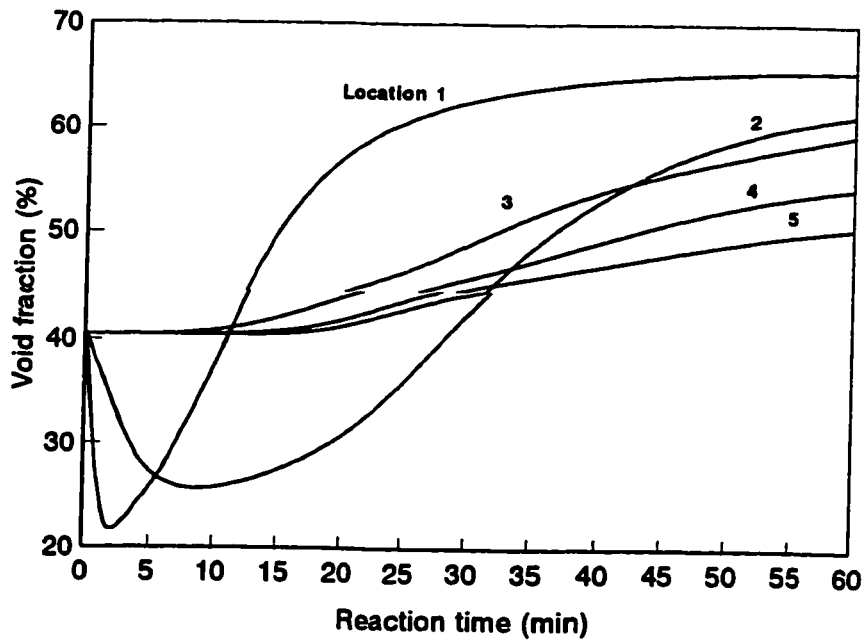

Figure 5.10 Computed local void fraction of the packing as a function of reaction time (Ore/coal=80/20, furnace temperature=1200°C)

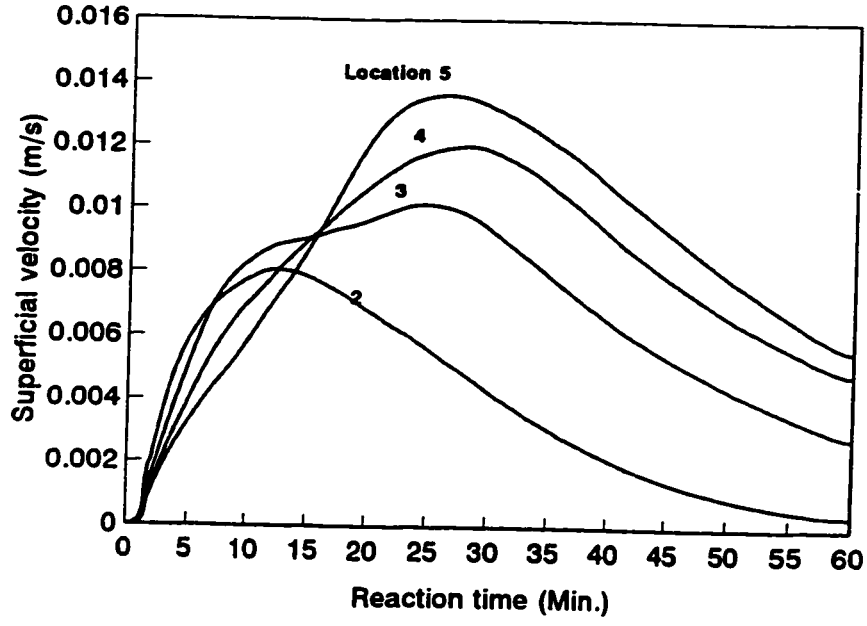

Figure 5.11 Computed local superficial velocity as a function of reaction time (Ore/coal=80/20, furnace temperature=1200°C)

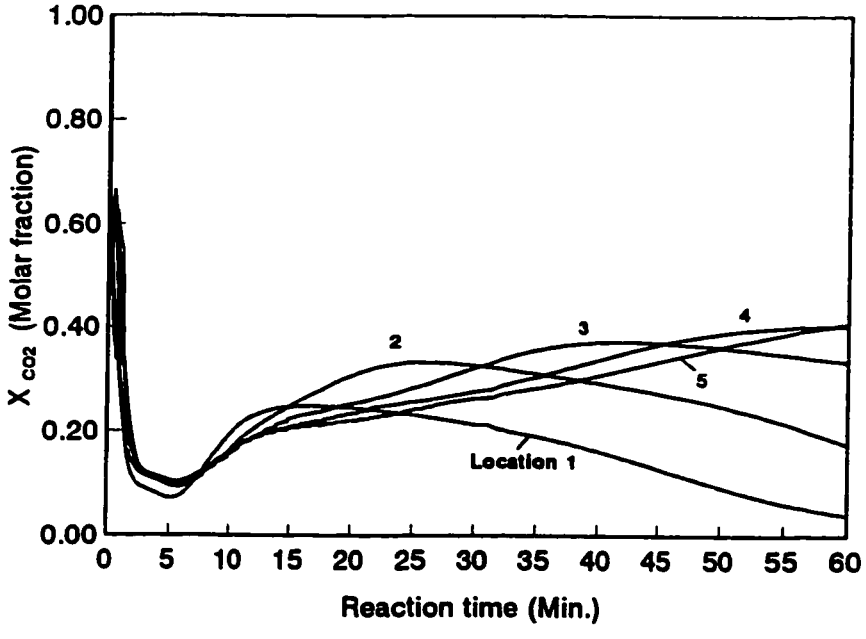

Figure 5.12 Computed molar fraction of CO_2 in local void space as a function of function time, (Ore/coal=80/20, furnace temperature=1200°C)

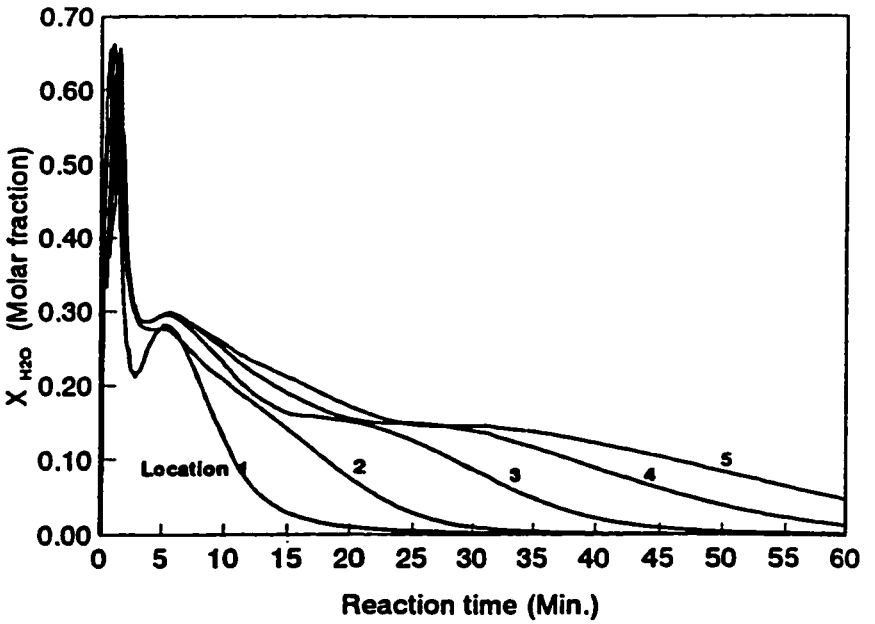

Figure 5.13 Computed molar fraction of H_2O in local void space as a function of reaction time, (Ore/coal=80/20, furnace temperature=1200°C)

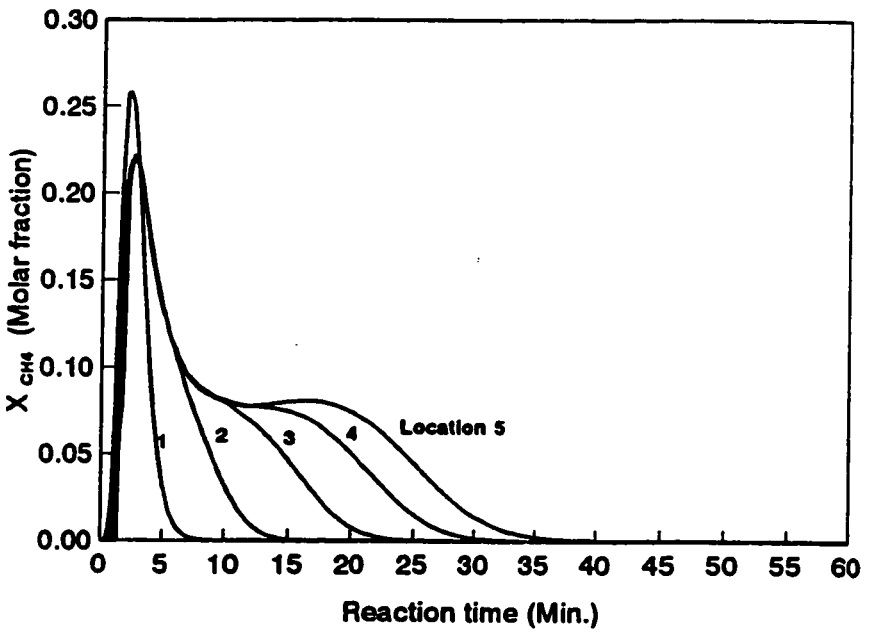

Figure 5.14 Computed molar fraction of CH_4 in local void space as a function of reaction time, (Ore/coal=80/20, furnace temperature=1200°C)

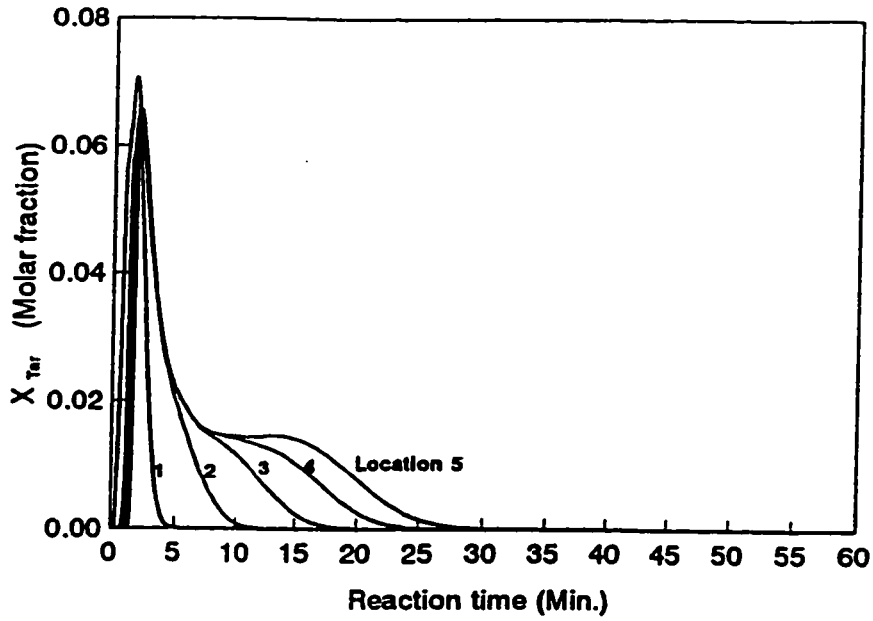

Figure 5.15 Computed molar fraction of Tar in local void space as a function of reaction time, (Ore/coal=80/20, furnace temperature=1200°C)

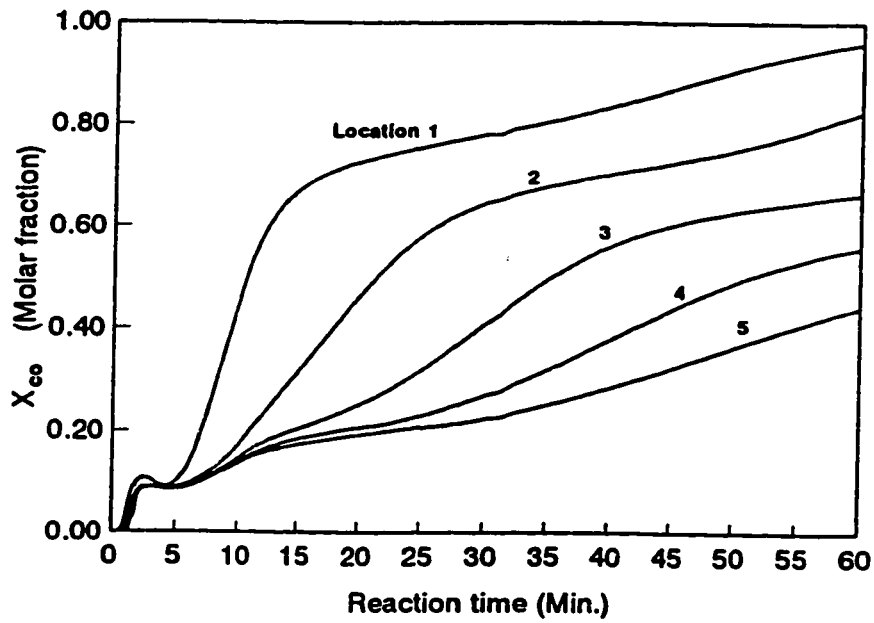

Figure 5.16 Computed molar fraction of CO in local void space as a function of reaction time, (Ore/coal=80/20, furnace temperature=1200°C)

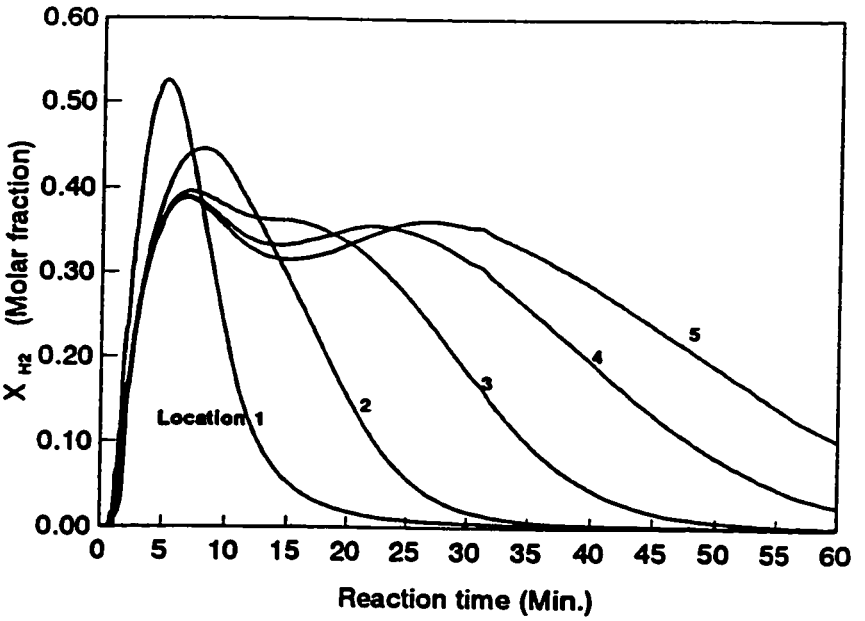

Figure 5.17 Computed molar fraction of H_2 in local void space as a function of function time, (Ore/coal=80/20, furnace temperature=1200°C)

CHAPTER SIX: RATE CONTROLLING KINETIC STEPS

The kinetics of reduction of iron ore concentrate by pulverized coal in this ore/coal composite is complex. The reduction involves simultaneous heat transfer, mass transfer and heterogeneous chemical reactions (gas/solid reactions). In this chapter, the individual rate steps involved in the reaction are discussed with the use of the mathematical model developed in the present work to assess the possible rate controlling step to the overall reaction. Values of certain physical parameters, such as furnace temperature, coal type, mixture packing density and ore/coal ratio, are varied to assess their effects on the rate of overall reaction. Implications of the present work in the development of new iron ore reduction processes are discussed.

In the following discussion, the computational results for the case of an ore/coal ratio of 80/20 and a furnace temperature of 1200°C, i.e. Figures 3.3, 3.10 and 3.14, are used as references for comparison. Values of parameters used in the mathematical model are systematically varied for comparison of the results with the references.

6.1 The establishment of rate-controlling step or steps

The possible rate controlling steps to the overall kinetics in this heterogeneous system may be: (a) one or more heat transfer steps between the solid particles and/or between solids and gaseous phase; (b) one or more mass transfer steps within the gaseous phase, and/or between solids and gaseous phases; (c) chemical reactions at interfaces; (d) a general case, likely a combination of (a), (b) and (c). In this section, the contribution of individual step of heat transfer, mass transfer, and rate of interfacial reactions are compared, and the possible rate controlling steps to the overall reaction (iron ore reduction by coal) are illustrated.

6.1.1 Endothermic reaction and heat transfer

Most chemical reactions in the iron ore/coal mixtures are endothermic and temperature sensitive. The exceptions are the reduction of magnetite under 570°C and reduction of wustite by CO. Heat must be supply continuously to the mixture in order to sustain these reactions. This section discusses how the heat is transferred to and consumed in the reacting system.

6.1.1.1 Heat consumption by endothermic reactions

When the iron ore/coal mixture at ambient temperature is placed in the furnace at a set temperature (1200°C), heat transfer from furnace to the mixture starts. The heat initially transferred to the mixture is essentially consumed to raise the temperature physically. As the temperature in the mixture increases, chemical reactions take place at certain locations. Most of reactions in the system are endothermic, especially, coal devolatilization and carbon gasification by CO_2 and H_2O. A portion of heat transferred to the interior of the system is consumed by these reactions chemically. The relative amounts of these physical and chemical heat requirements depend on the local situation, such as temperature, composition of solid and gaseous materials, and the nature of active endothermic reactions. Figure 6.1 shows the computed total heat consumed for both physical and chemical requirements at different locations as a function of reaction time. Figures 6.2 and 6.3 show the computed amount and percentage of net heat consumed by all chemical reactions and by carbon gasification (by both CO_2 and H_2O). At locations 1 and 2, about 58% of the heat input is consumed by endothermic reactions, mainly by carbon gasifications (about 54% of heat input). Only about 42% of heat is used for raising the temperature of solids. As a result of intensive heat

consumption by carbon gasifications at these locations, heat transfer to locations beyond this zone (i.e. locations 4 and 5), is limited. Therefore, the temperature rise and the rate of reactions at these locations are very low (see Figures 3.3 and 3.6).

The effect of heat consumption by carbon gasification on the rate of heat transfer and iron oxide reduction may be assessed by computing a hypothetical case, i.e. the heats of reaction of carbon gasification are assumed to be zero without any other changes in the model. The computed local temperatures, the degrees of iron ore reduction and the degrees of carbon gasification at different locations as functions of reaction time are shown in Figures 6.4, 6.5 and 6.6. The computed results shown in Figures 3.3, 3.10 and 3.14 are also included for comparison. Without the consumption of heat by carbon gasification, higher temperatures within the reacting system were reached (Figure 6.4). The rate of iron ore reduction and carbon gasification were also significantly increased. The computational results show that carbon gasification (by CO_2 and H_2O) has a very strong effect on the temperature increase and rate of reactions in the interior of the reacting system. This effect would be more pronounced with an increase of the reactor size.

6.1.1.2 Heat transfer by conduction

Heat transfer in this reacting system may proceed by conduction, convection and radiation mechanisms. The relative importance of these three mechanisms of heat transfer to different locations depends on the local temperature and properties of solid and gaseous phases. Due to the small size of the solid particle (about 4.5×10^{-5} m in diameter), and the relevant temperature range, the radiation heat transfer has been numerically estimated to be at least two orders of magnitude smaller than conduction heat transfer (refer to Appendix I). Thus conductive and convective heat transfer are the mechanisms for comparison.

Figures 6.7 and 6.8 show computed heat fluxes (total flux, $-K_{effm}\partial T/\partial x + \rho_g C_{pg} V_o T_g$, and conductive heat flux, $-K_{effm}\partial T/\partial x$) and conductive heat flux as percentage of the total. Heat is transferred essentially by conduction at a location near the hot face (Figure 6.8). The percentage of conductive flux decreases at locations far away from the hot face where conductivity of solids are low and gas flow is high during coal devolatilization.

The effect of convective heat transfer on both the temperature increase of the reacting mixture and the rate of overall reaction can be evaluated by the removal of convective term in the heat transfer equation (Eq. 4.12). Figures 6.9,

6.10 and 6.11 show the computed temperatures and degree of iron ore reduction at different locations as functions of reaction time when the convective term is taken from the equation. Computed results in Figures 3.3, 3.10 and 3.11 are also included for comparison. Thermal convection has a very limited effect on the temperature of the system, and thus the rate of overall reaction. This is due to the fact that the amount of gas generated and the flow rate of gas are limited, which, in turn, limits the convective heat transfer.

6.1.1.3 Effect of effective thermal conductivity on heat transfer and the overall rate of reaction

Figures 6.12, 6.13 and 6.14 show the computed temperature, the degree of iron ore reduction and the degree of carbon gasification, respectively, as a function of reaction time when the value of effective thermal conductivity of reacting mixture is increased arbitrarily by 50% in the model. With higher effective conductivity of the mixture, the temperature within the system and the rate of reactions are significantly increased. This is due to the increase in the effective thermal conductivity of reacting mixture, which increases heat flux in the system, and subsequently increases the rate of the chemical reactions. Furthermore, earlier metallization will increase thermal conductivity of reacted

mixture due to the higher content of metallic iron. By these compounded positive effects, the increase in the value of the effective conductivity of the initial mixture significantly accelerates the rate of the overall reaction.

These results (Figures 6.12 to 6.14) further confirm that conduction is the dominant mechanism of heat transfer in this iron ore/coal reacting system.

An increase in the effective conductivity of the initial mixture can be achieved by different methods, such as recycling metallic fines or increasing the density of packing.

6.1.2 Convective mass transfer

Mass transfer though porous media in this reacting system includes diffusion and convection. CO will be used as an example in the following discussion of these two mass transfer mechanisms.

Figures 6.15 and 6.16 show computed CO transfer fluxes (total flux, $-\phi/\tau D_{eff co}\partial\rho_{co}/\partial x + \rho_{co}V_o$, and convective CO flux $\rho_{co}V_o$) and convective CO flux as percentage of the total.

CO is transferred essentially by convection at most of locations except location 1 (Figure 6.16). At location 1, the portion of CO transfer by convection decreases as the rate of gas generation decreases at a time near the completion of coal devolatilization (near 4-th minute) and char gasification

(near 15-th minute (Figure 5.9)).

The contribution of diffusion to the total mass transfer in the gaseous phase can be evaluated by the removal of diffusion terms in the mass balance equations (Eq. 4.29). Figures 6.17 and 6.18 show the computed values of the degrees of iron ore reduction and carbon gasification when the diffusion terms in the mass balance equations were removed. Gaseous diffusion has a very minor effect in determining the rate of reactions.

6.1.3 Rate of chemical reactions

Chemical reactions in the system include devolatilization of coal, reduction of iron oxides and gasification of carbon. Devolatilization of coal takes place at a lower temperature and proceeds at a much faster rate than the other reactions, and is unlikely to be the rate limiting step. Thus, the reduction of iron oxides and the gasification of char are the reactions that are compared here. As these two kinds of reactions are coupled through reacting gases, the one with the slower specific rate of reaction would exercise more control on the rates of these reactions. Sensitivity of this coupled reacting system with respect to the rate of the individual reactions were tested by varying the value of specific rate of each reaction.

Figures 6.19 and 6.20 show the computed degree of iron ore reduction and degree of carbon gasification when values of specific rate of every iron oxide reduction (reactions 4.13 to 4.15) were doubled. This can be realized by using more porous or smaller sized ore particles. Figures 6.21 and 6.22 show the computed degrees of iron reduction and carbon gasification when the values of the specific rate of carbon gasification were doubled, i.e. with more reactive or smaller sized carbon.

An increase in the rate constants of iron oxide reduction has a minor effect on the rate of overall reactions. On the other hand, with more reactive carbon, the overall reaction could be accelerated.

An increase in the specific rate of oxide reduction tends to increase rate of reduction in the system. However, as the reduction of iron ore and gasification of carbon are coupled through their gaseous products, this increase in the rate of reduction requires an increase of reductant supply, i.e. an increase of the rate of CO/H_2 generation by carbon gasification. When an increase of the rate of reductant generation is not available due to the slow rate of carbon gasification, the potential of higher rates of reduction is not realized, as shown in Figures 6.19 and 6.20.

An increase in the specific rate of carbon gasification, on the other hand, increases the rate of reductant supply. At locations where the reductant can be consumed rapidly by

reduction reactions, this leads to higher rates of reduction. The increased rate of reduction reactions, in turn, increases the rate of generation of CO_2 and H_2O for carbon gasification. With these compounded positive effects, the rates of both carbon gasification and iron oxide reduction were significantly increased, as shown in Figures 6.21 and 6.22.

With the results shown in Figures 6.19 to 6.22, one may conclude that the gasification of carbon is the slowest reaction among the reactions in this reacting system.

6.1.4 Rate controlling steps to overall reaction

After similar identification of the most critical kinetic step in each category as discussed above, the rate controlling step of the overall reaction in this iron ore/coal reacting system is likely to be one of (a) for heat transfer it is conduction; (b) for mass transfer it is convection in gaseous phase; and (c) for chemical reactions it is gasification of carbon. The kinetics of the whole system is determined by a combination of the rate of each of these three steps. The distance for gaseous reactant (such as CO_2) to move away from the site of its creation (an iron ore particle) to the site of its elimination (a char particle) may be of the order of tens of microns in the higher temperature regions, where chemical reactions are more active. These distances are comparable to

the mean free path of the gases. This leads to the belief that mass transfer of gases is very unlikely to be important in comparison with the other two. Thus, heat transfer and the carbon gasification may play a relatively more dominant role.

The carbon gasification has a high value of activation energy, and thus rate of the reaction is strong temperature dependent. As shown in Figures 3.6 and 3.15. The temperature at reaction site is adjusted between the rate of supply of heat by conduction and the rate of consumption by the gasification reaction. The larger the value of rate constant of gasification reaction the more dominant the rate-limiting role of heat conduction. The rate of the overall reaction is more sensitive to the value of effective thermal conductivity (Figures 6.13 and 6.14), furnace temperature (Figures 3.19 and 3.20), than that of rate constant of carbon gasification (Figures 6.21 and 6.22). The persistence of temperature gradients in the reacting system results from the low value of effective thermal conductivity of the mixture on one hand, and the strongly endothermic reaction of carbon gasification on the other. In view of the fact that one can not change the heat of reaction of carbon gasification, attention should be focused on the value of effective thermal conductivity, the distance of the heat transfer, and temperature of the heat source.

6.2 Effect of certain physical parameters on overall rate of reaction

For industrial applications of iron ore/coal reaction systems, physical parameters, such as furnace temperature, coal type, mixture packing density, ore/coal ratio, and size of the system are of great concern. The values of these parameters were varied to assess their individual effects on the rate of the overall reaction.

6.2.1 Effect of higher furnace temperature

Figures 6.23, 6.24 and 6.25 show computed results with furnace temperature kept at 1300°C (experimental data points were shown in Figures 3.18, 3.19 and 3.23). The results with furnace temperature at 1200 °C (from Figures 3.3, 3.10 and 3.14) are also included for comparison. A higher furnace temperature increased the rate of heat transfer to the system, and resulted in faster rise in temperature and increased the rate of iron ore reduction.

6.2.2 Effect of coal type

The coal used in the experiments in the present work is high-volatility bituminous coal. In commercial production,

coke breeze or coal char may be used as a reductant. To compare the effect of volatile matter on the rate of overall reaction, char was used as a reductant in the model for calculation. Initial ore/char ratio was set to be 83.7/16.3 by Wt%, which is the same oxygen/carbon ratio as in the case of the ore/coal (80/20) system.

Figures 6.26 and 6.27 show computed degrees of iron ore reduction and carbon gasification when char is used as the reductant. Results with the use of coal are also included for comparison. Up to the time when approximately 80% of the reduction is completed, the rate of iron ore reduction is faster when using coal as the reductant (Figure 6.26). It is due to coal devolatilization at lower temperatures (about 500°C) which releases gaseous reductant (CO and H_2) to start reduction at these temperatures. In the case of using char, less gaseous reductant was generated until it reached a higher temperature (about 750°C), where gasification of char becomes significant (Figure 6.27). The results in Figures 6.26 and 6.27 show that coal as the source of reductant leads to a higher rate of iron ore reduction compared to char or coke, but coal has a lower efficiency of reduction.

6.2.3 Effect of ore/coal ratio

Figures 6.28 and 6.29 show the computed degree of

reduction and carbon gasification when the initial mixture was packed at ore/coal ratios of 75/25, 80/20 and 85/15, respectively, with other conditions unchanged. With a lower ore/coal ratio, a higher degree of reduction is reached at the same location and reaction time (Figure 6.28), which is due to more reductant being available for reductions. However, too low of an ore/coal ratio (such as at 75/25) introduces an excess amount of coal in the system, and results in both a higher residual carbon content in the reacted mixture (Figure 6.29) and a poor energy efficiency. An inadequate supply of coal (i.e. ore/coal = 85/15) leads to incomplete reaction. An ore/coal ratio of about 80/20 appears to be optimum for both rate of reaction and energy efficiency.

6.2.4 Effect of initial packing density

Figures 6.30 and 6.31 show computed temperatures and degrees of reduction as a function of time with packing densities of 1900 and 2300 kg/m^3, respectively, with all other conditions unchanged. An increase in packing density increases the effective thermal conductivity of the porous solid. However, it increases heat consumption per unit volume of the mixture. In Figure 6.30, the temperature rise is slower at locations far from hot surface where the increase in the heat requirement outweighs the increase in effective thermal

conductivity. As the result, the degree of reduction is lower at most locations, except location 1, for the higher packing density (Figure 6.31). This calculated result suggests that for smaller sized composites, such as a sphere of 0.007 m radius or smaller, the benefit of higher density is significant for the increase of productivity.

6.2.5 Effect of pre-reduction of ore

Magnetite concentrates are used in the present study. Pre-reduction of magnetite to wustite can be facilitated with a gas of lower reducing potential and at lower temperature, such as exit gas from current reacting system. Potentially, the exit gas from the reacting system at a temperature of about 500 to 600°C may be used for pre-reduction.

Figures 6.32 and 6.33 show the effect of pre-reduction of magnetite on local temperatures and degrees of reduction. Pre-reduced magnetite to wustite, which accounts for 25% removal of oxygen in the initial iron oxide, results in an earlier formation of metallic iron, which increases the effective thermal conductivity of the reacting mixture. This promotes heat conduction and a faster increase in the mixture temperature (Figure 6.32). The higher temperature at all locations, in turn, increases the rate of the overall reaction.

6.2.6 Effect of configuration and size of composite

The present work is designed with one-dimensional cylindrical geometry for its simplicity in modelling. However, it is the worst form for heat transfer based on surface/volume ratio. The best configuration is a spherical pellet. The present model was used to calculate the overall rate of reduction for a pellet of different sizes, in a furnace kept at different temperatures under an inert atmosphere. The results are shown in Figures 6.34 and 6.35. For a large sized pellet (0.014 m in diameter), an eighty percent reduction may be reached within 10 minutes of the charging of the pellet at ambient temperature into a chamber kept at 1200°C.

6.2.7 Direct heating from above

Reduction processes with the use of carbon-containing agglomerates in a rotary hearth furnace have heat sources above the bed with radiation as the dominant heat transfer mechanism. In the present work, heat is supplied by conduction through the conductive bottom plate. For comparison, heat fluxes at various locations and times in the one dimensional system of the present work are shown in Figure 6.7. It is clear that for a given location, the heat flux increases with the increase of metallization of iron ore for higher effective

thermal conductivity, and decreases in the later stage due to slower rates of heat consumption by the endothermic reactions. Radiation heat fluxes from the refractory surface (and indirectly from a flame) to the surface of an ore/coal mixture of an assumed temperature are given in Figure 6.36. In those cases where the hot gas, which is the source of heat, is oxidizing with respect to sponge iron (such as in the FASTMET Process), the re-oxidation of iron in the later stage of process will become critical, not the rate of heat supply.

6.3 Summary

The validated mathematical model has been used to study the kinetics and mechanisms of reactions in ore/coal composites. The results show that conduction heat transfer is the dominant rate limiting step to the overall reaction in the reacting system. This is due to the fact the low effective thermal conductivities of the mixture, and the highly endothermic reactions of carbon gasification. An increase in heat flux may be achieved by increasing the temperature of the heat source and/or by increasing the effective thermal conductivity by various means. For practical applications, the shape and size of agglomerates (briquettes or pellets) and the mechanism of external heat transfer (by radiation or convection) to the agglomerate are the most important factors in the process design.

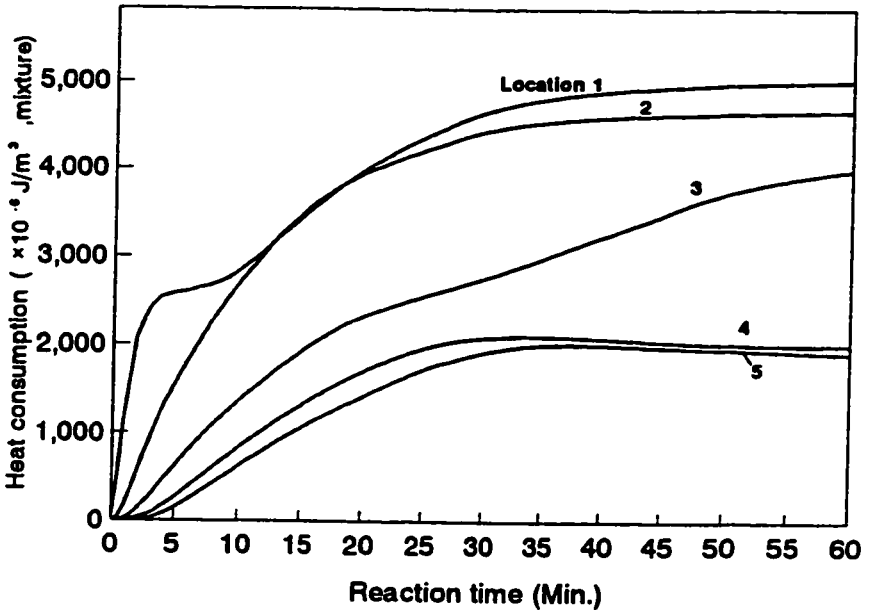

Figure 6.1 Computed total accumulated heat consumption as a function of reaction time (Ore/coal=80/20, furnace temperature=1200°C)

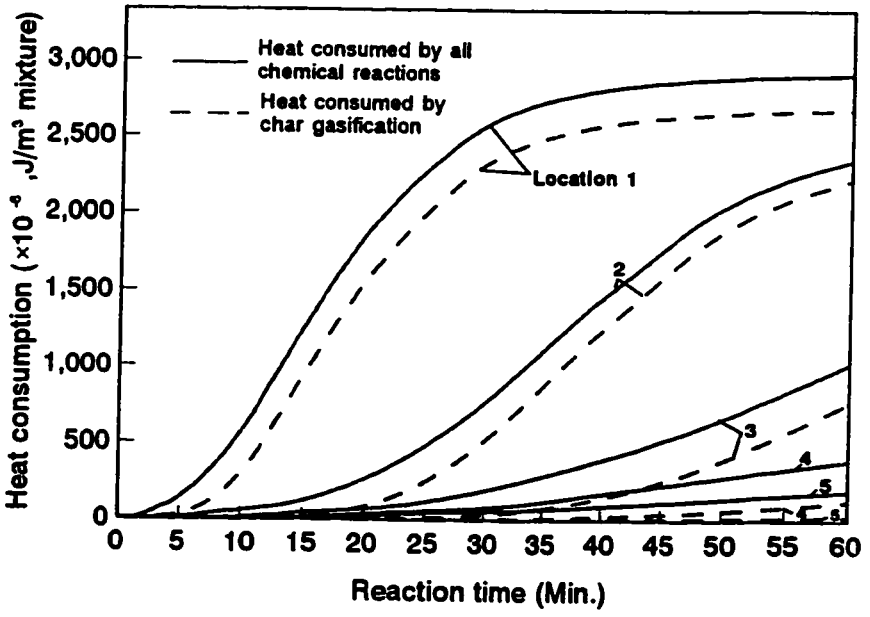

Figure 6.2 Computed accumulated heat consumption by chemical reactions as a function of reaction time, (Ore/coal=80/20, furnace temperature =1200°C)

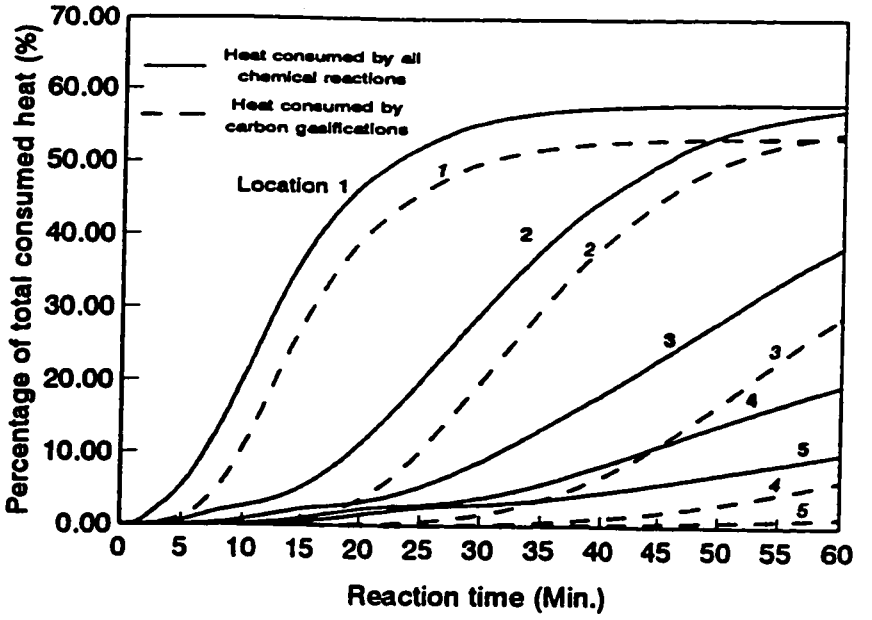

Figure 6.3 Percentage of heat consumed chemically as a function of reaction time (Ore/coal=80/20, furnace temperature=1200°C)

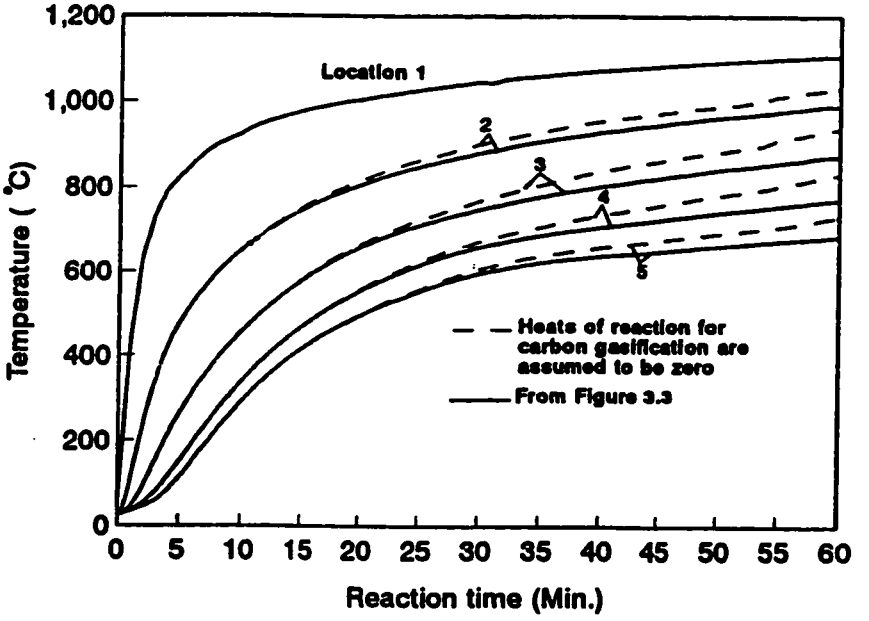

Figure 6.4 Effect of heat of reactions on computed local temperature (Ore/coal=80/20, furnace temperature =1200°C)

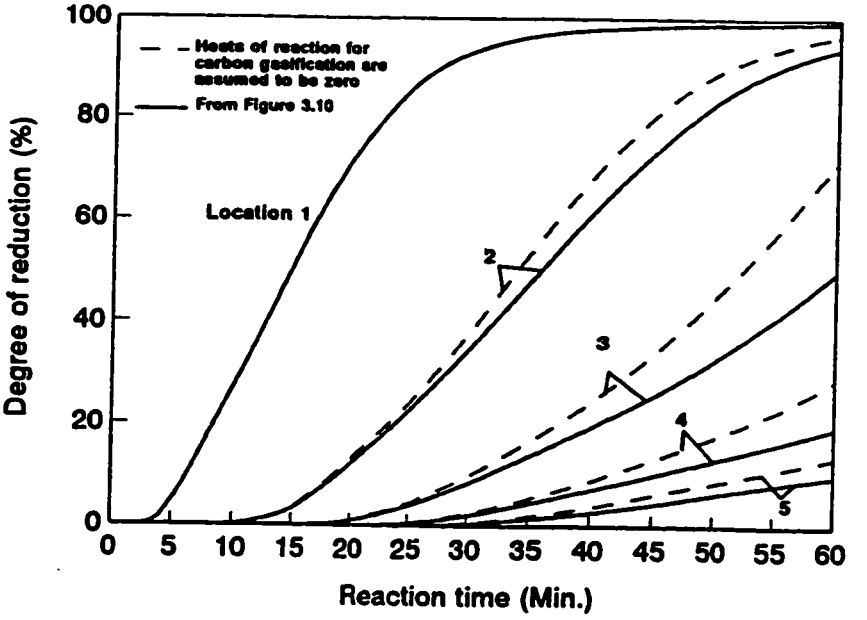

Figure 6.5 Effect of heat of reactions on computed degree of reduction (Ore/coal=80/20, furnace temperature =1200°C)

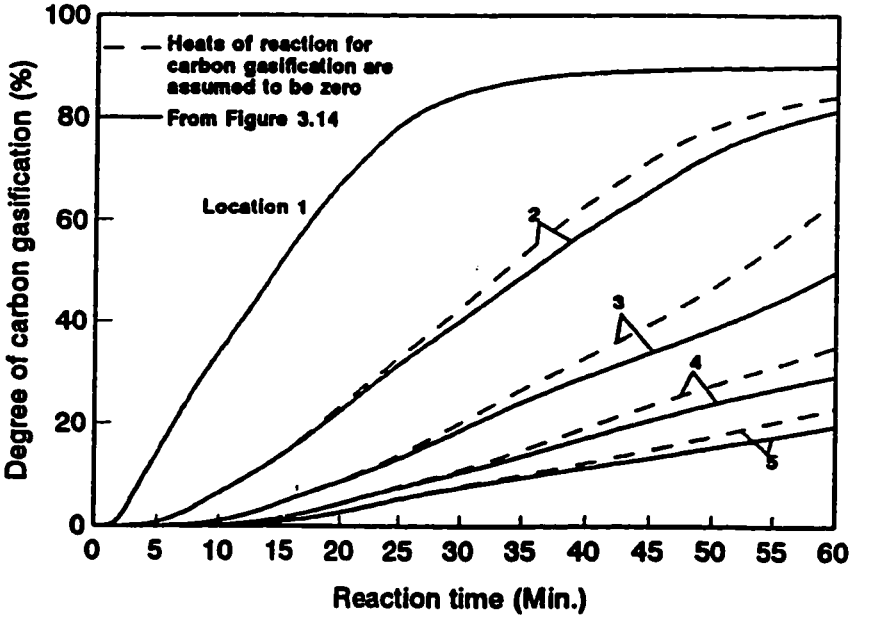

Figure 6.6 Effect of heat of reactions on computed degree of carbon gasification (Ore/coal= 80/20, furnace temperature = 1200°C)

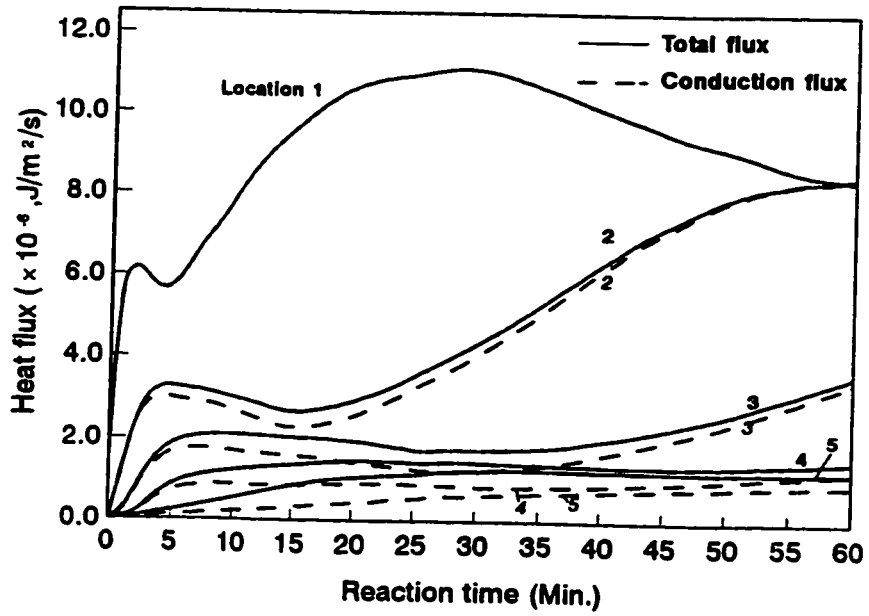

Figure 6.7 Computed head flux as function of reaction time (Ore/coal=80/20, furnace temperature=1200°C)

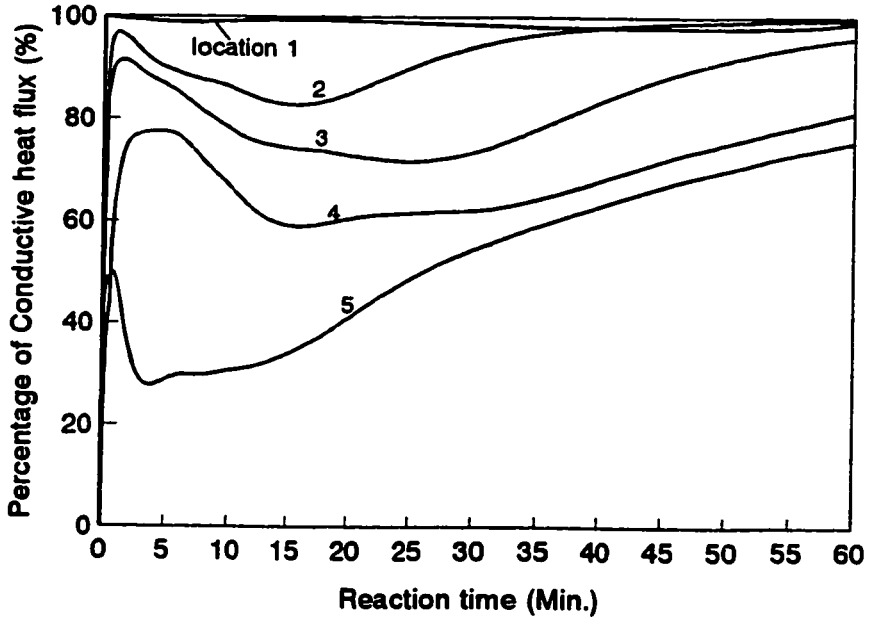

Figure 6.8 Computed percentage of heat flux transferred by conduction (Ore/coal=80/20, furnace temperature =1200°C)

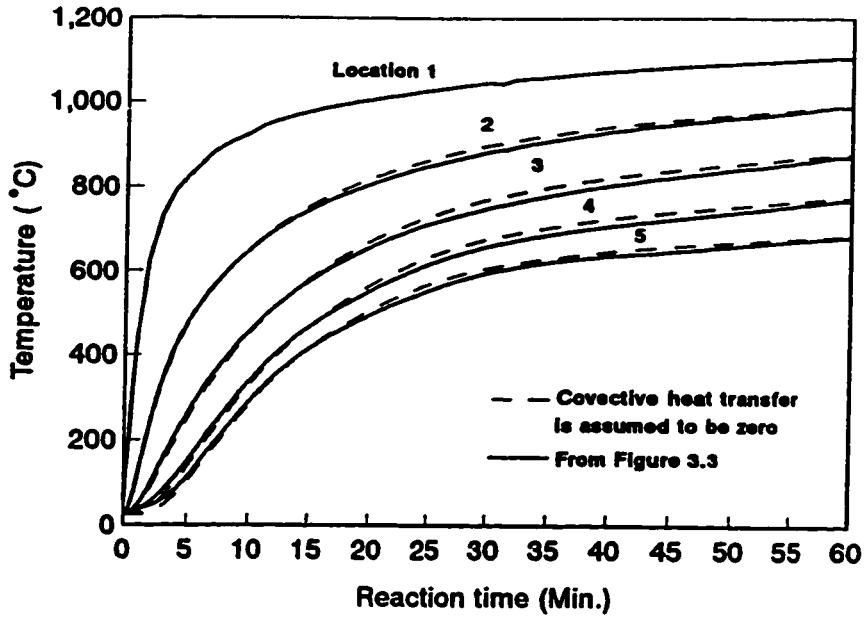

Figure 6.9 Effect of convective heat transfer on computed temperature (Ore/coal=80/20, furnace temperature =1200°)

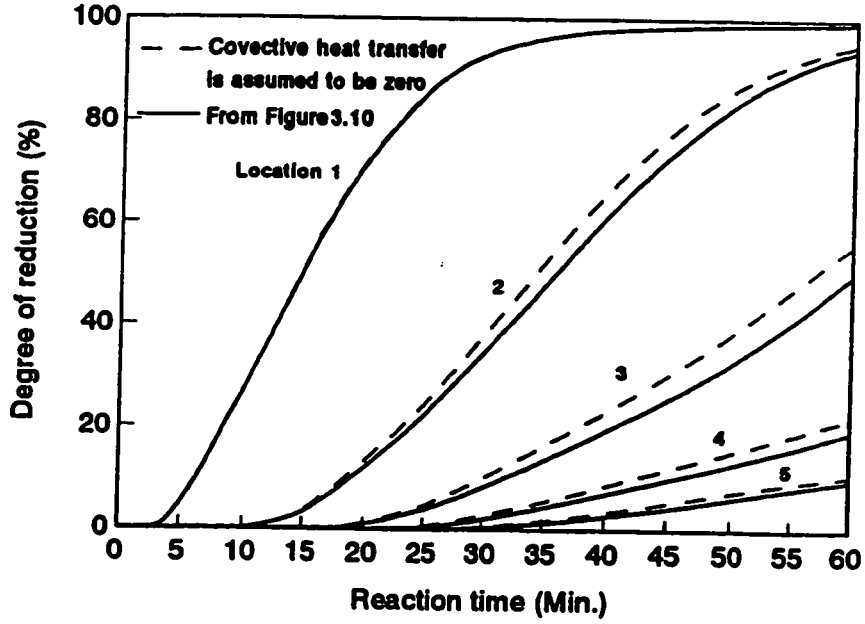

Figure 6.10 Effect of convective heat transfer on computed degree of reduction (Ore/coal=80/20, furnace temperature =1200°C)

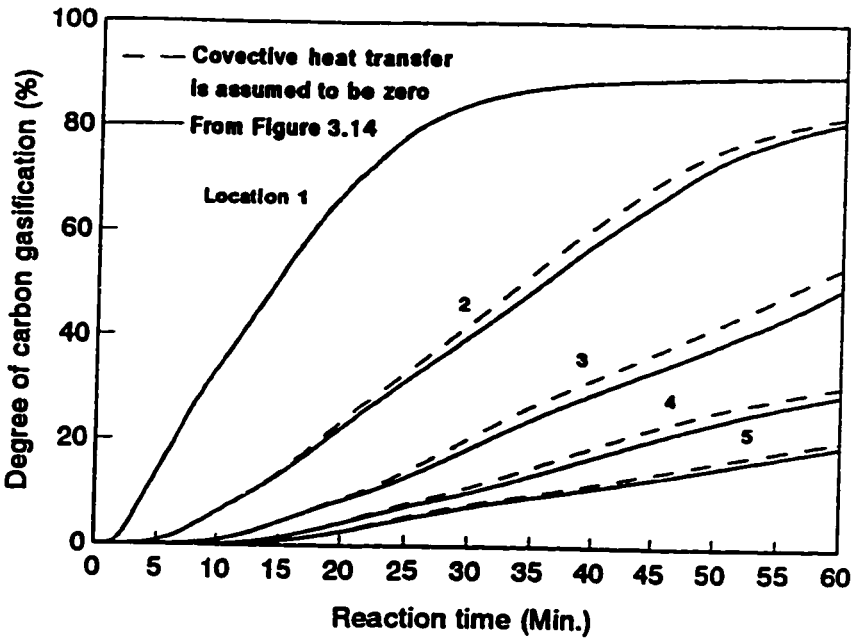

Figure 6.11 Effect of convective heat transfer on computed degree of carbon gasification (Ore/coal=80/20, furnace temperature=1200°C)

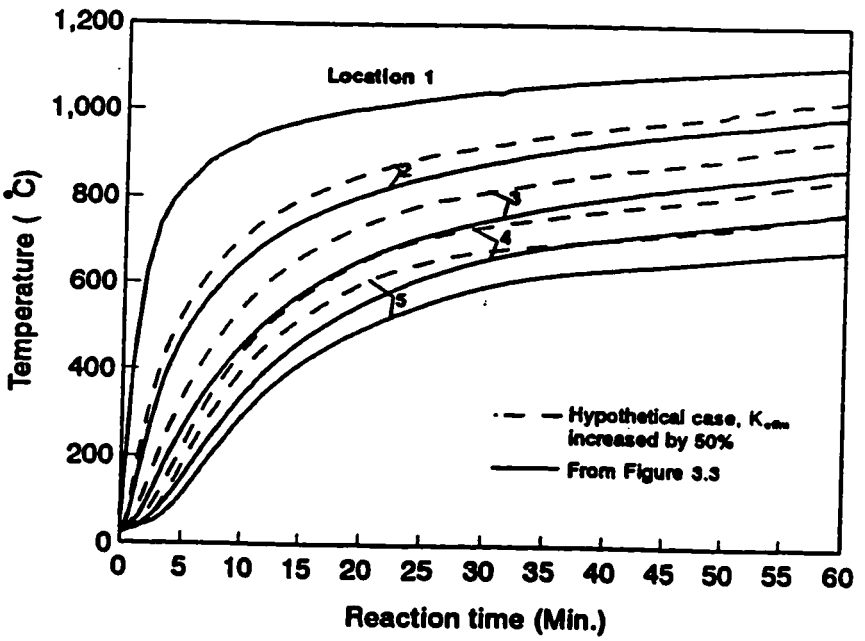

Figure 6.12 Effect of value of effective thermal conductivity on computed temperature (Ore/coal=80/20, furnace temperature=1200°)

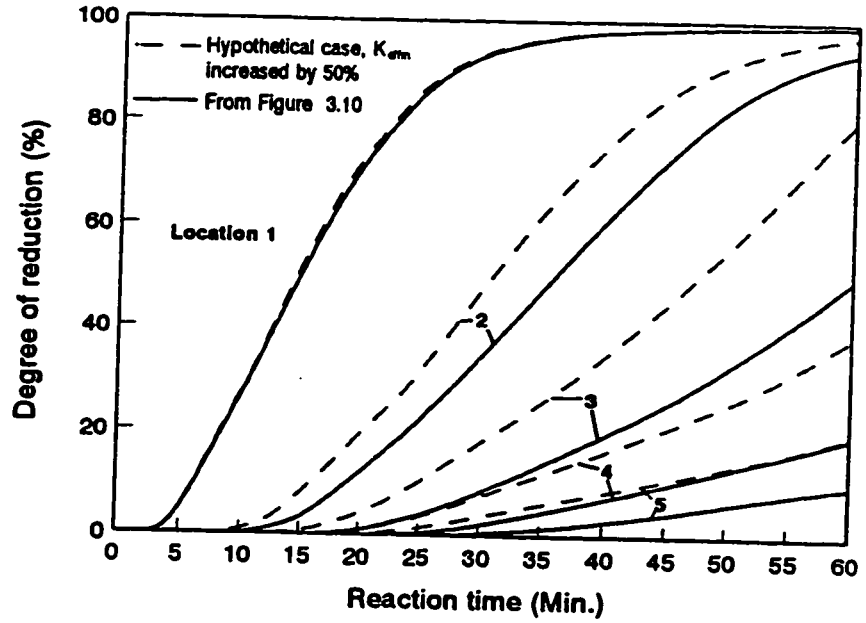

Figure 6.13 Effect of value of effective thermal conductivity on computed degree of reduction, (Ore/coal=80/20, furnace temperature=1200°)

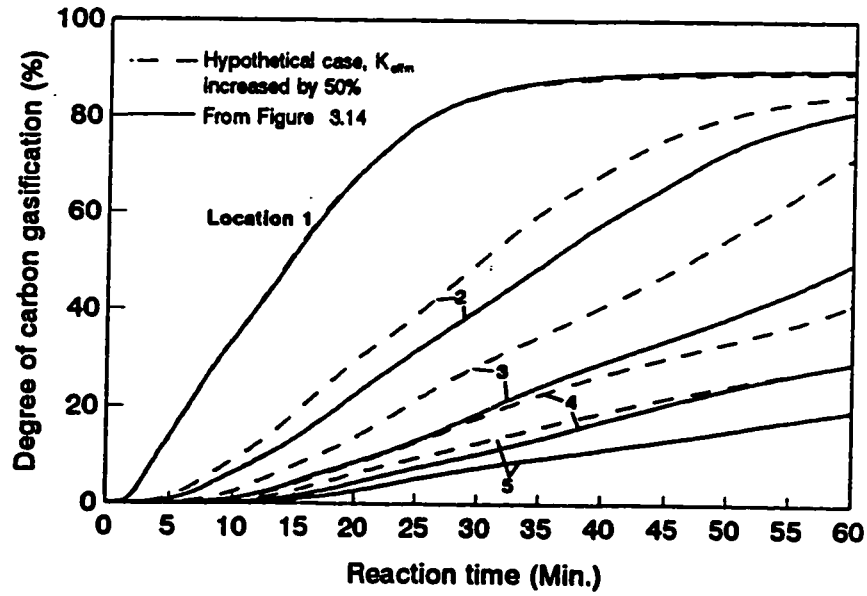

Figure 6.14 Effect of value of effective thermal conductivity on computed degree of carbon gasification, (Ore/coal=80/20, furnace temperature=1200°)

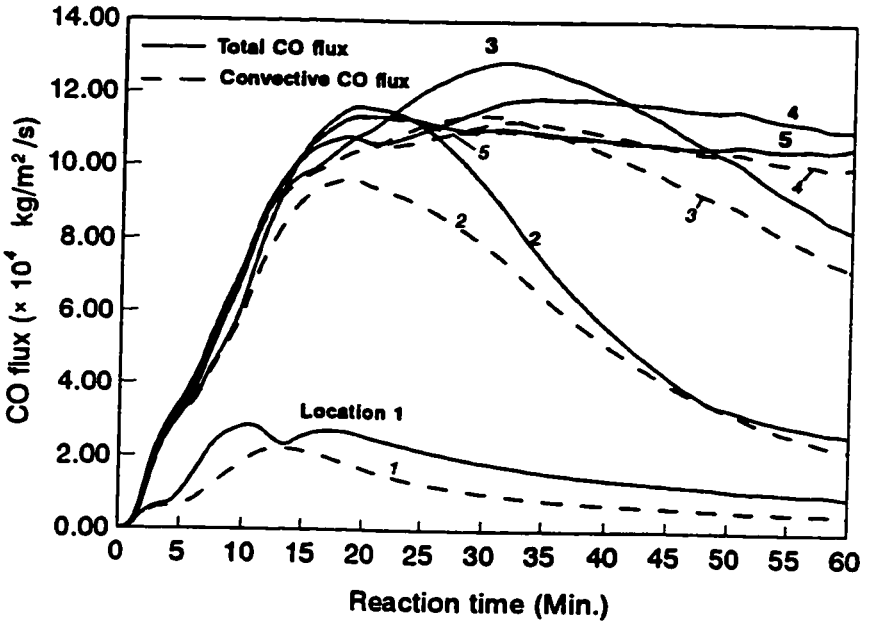

Figure 6.15 Computed CO flux as a function of reaction time (Ore/coal=80/20, furnace temperature=1200°)

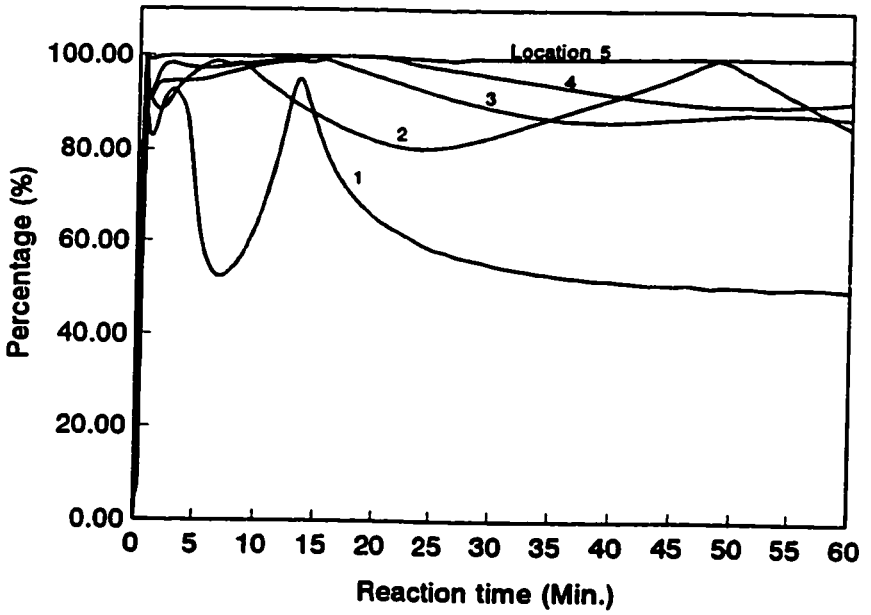

Figure 6.16 Computed percentage of CO flux by convection (Ore/coal=80/20, furnace temperature=1200°)

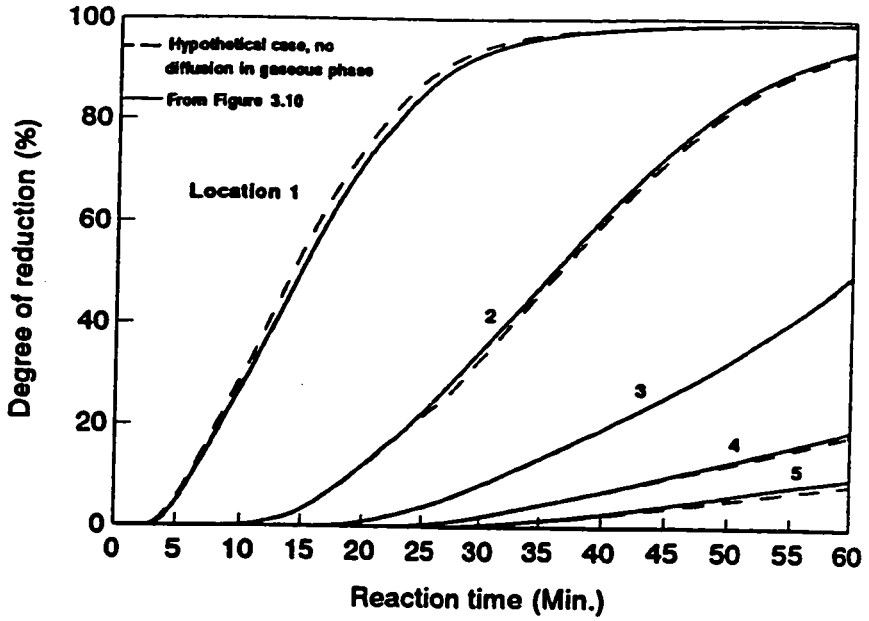

Figure 6.17 Effect of gas diffusion on computed degree of reduction (Ore/coal=80/20, furnace temperature =1200°)

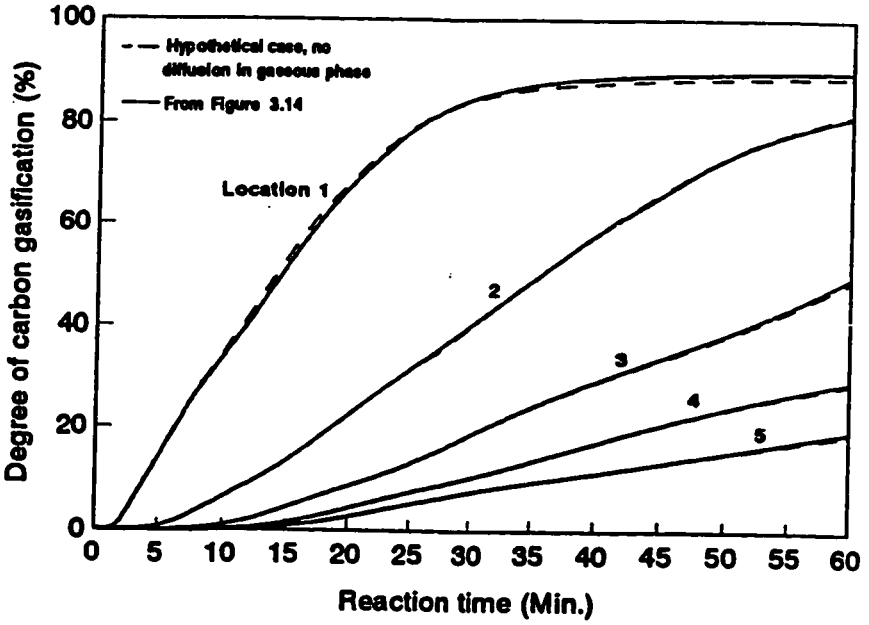

Figure 6.18 Effect of gas diffusion on computed degree of carbon gasification (Ore/coal=80/20, furnace temperature = 1200°)

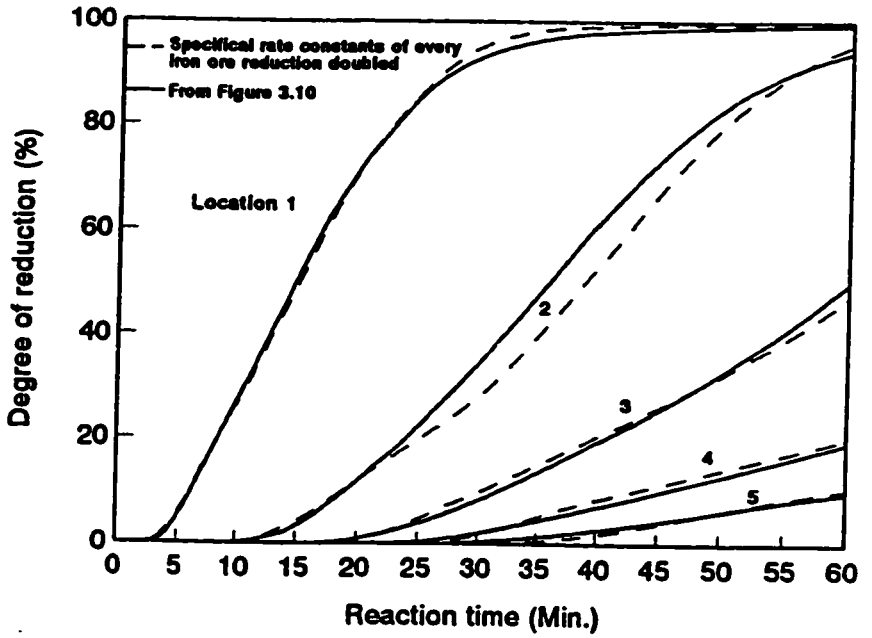

Figure 6.19 Effect of specific rate of iron ore reduction on computed degree of reduction, (Ore/coal=80/20, furnace temperature = 1200°)

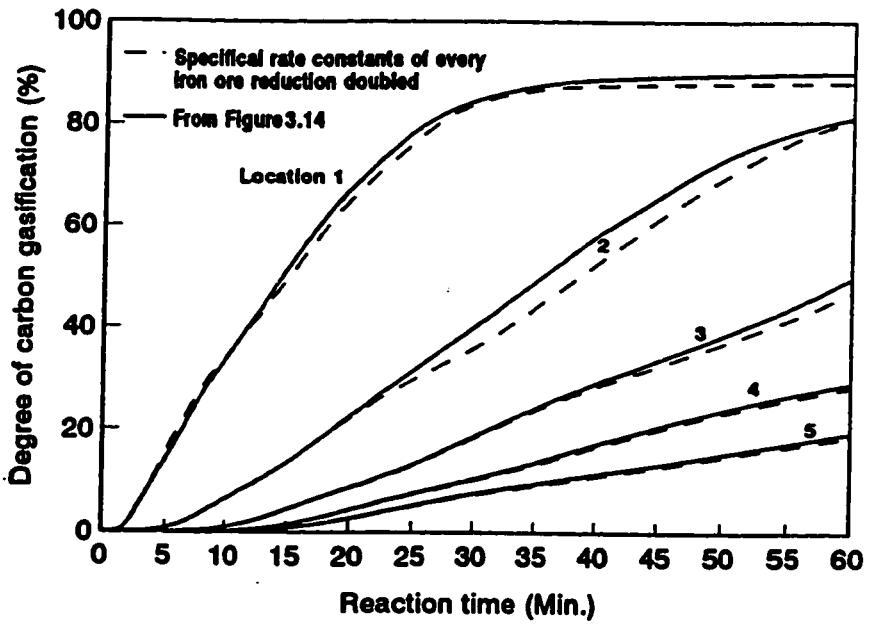

Figure 6.20 Effect of specific rate of iron ore reduction on computed degree of carbon gasification, (Ore/coal=80/20, furnace temperature=1200°)

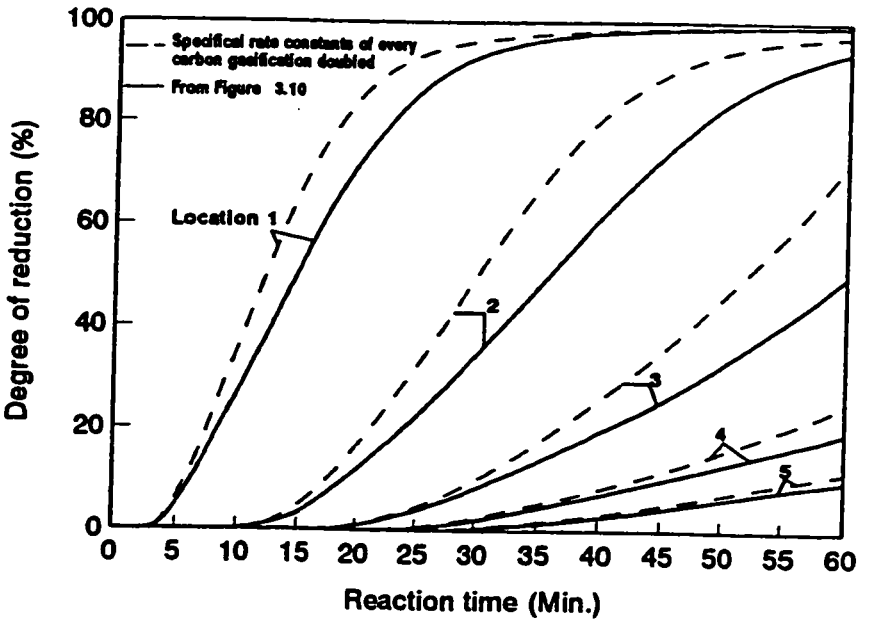

Figure 6.21 Effect of specific rate of carbon gasification on computed degree of reduction, (Ore/coal=80/20, furnace temperature=1200°)

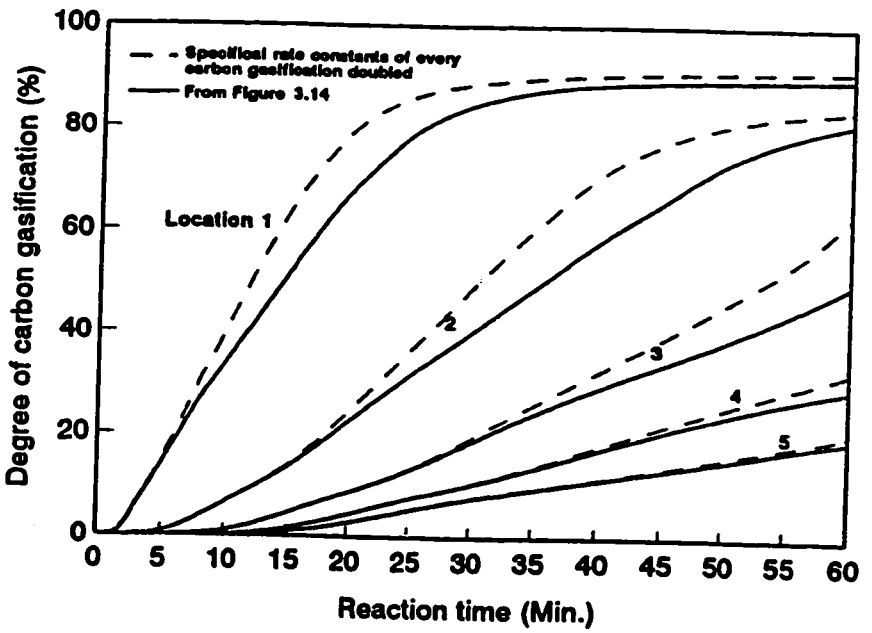

Figure 6.22 Effect of specific rate of carbon gasification on computed degree of carbon gasification, (Ore/coal=80/20, furnace temperature=1200°)

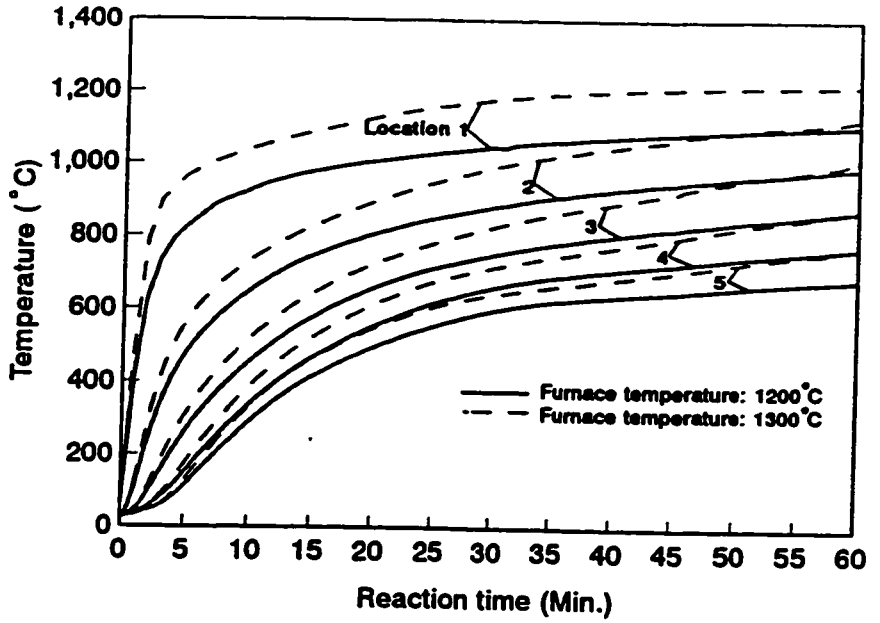

Figure 6.23 Effect of furnace temperature on computed local temperature (Ore/coal=80/20, two furnace temperatures)

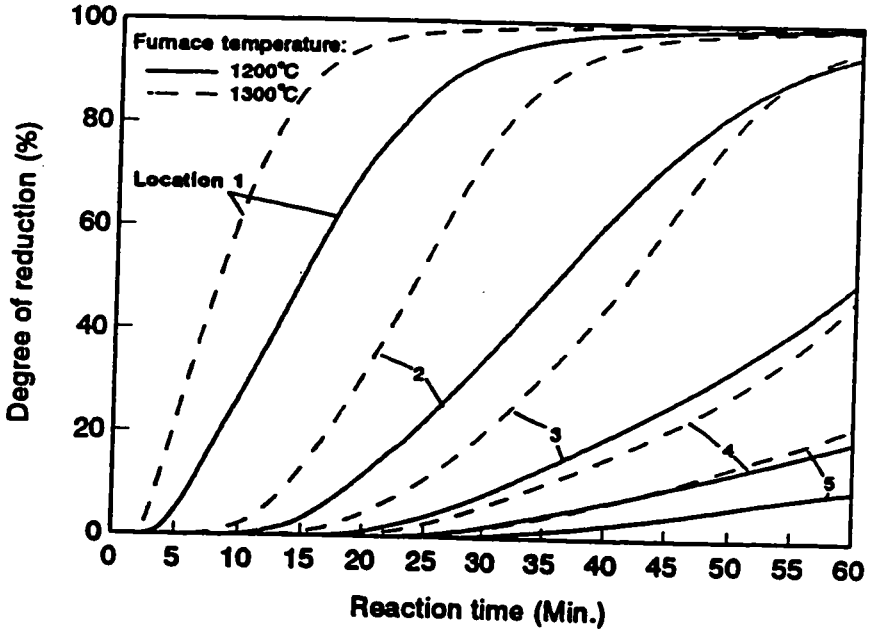

Figure 6.24 Effect of furnace temperature on computed degree of iron ore reduction (Ore/coal=80/20, two furnace temperatures)

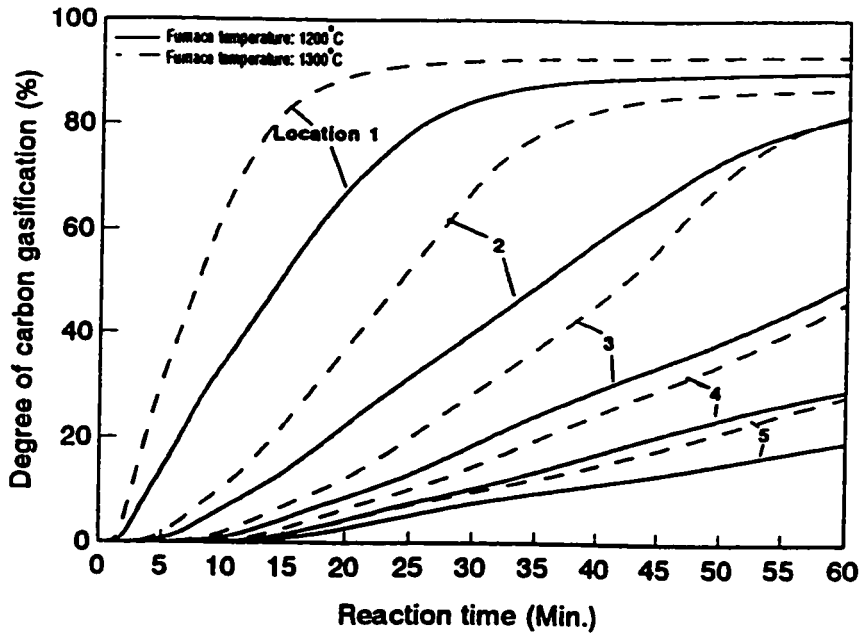

Figure 6.25 Effect of furnace temperature on computed degree of carbon gasification (Ore/coal=80/20, two furnace temperatures)

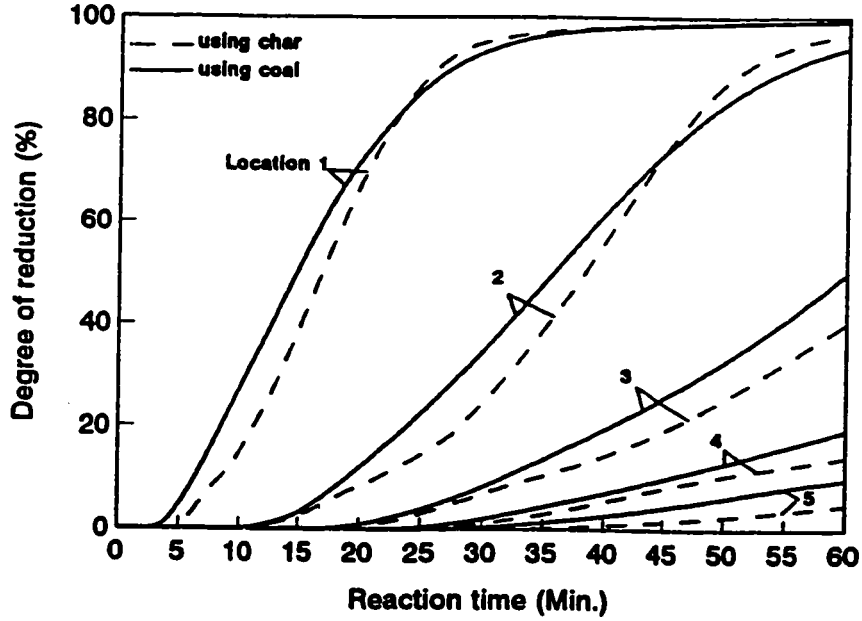

Figure 6.26 Effect of coal type on computed degree of iron ore reduction (Ore/char=83.7/16.3, furnace temperatures= 1200°)

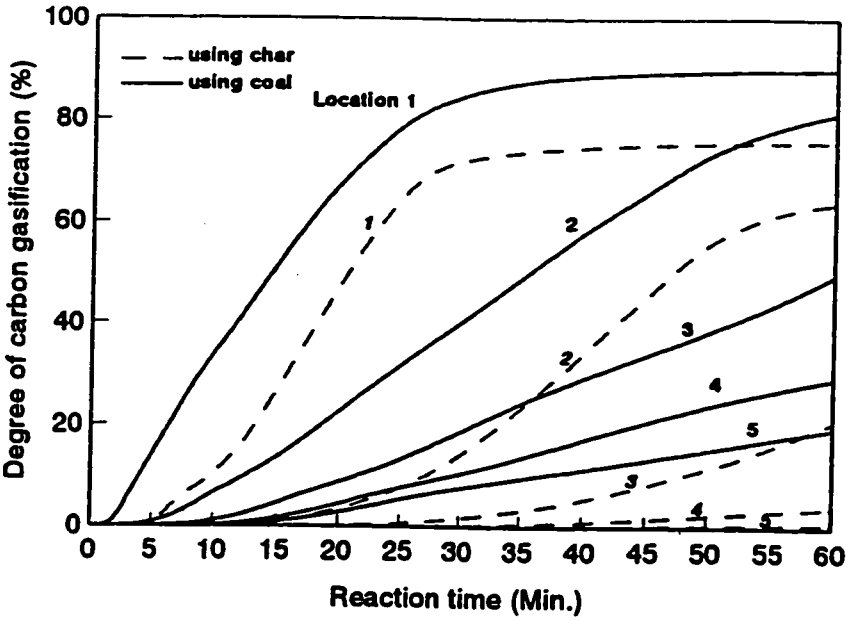

Figure 6.27 Effect of coal type on computed degree of carbon gasification (Ore/char=83.7/16.3, furnace temperatures= 1200°)

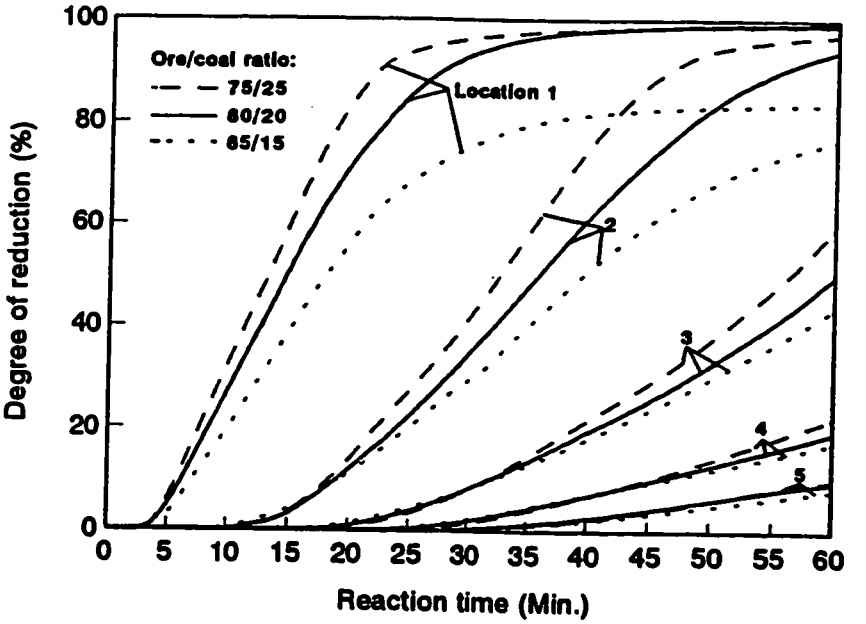

Figure 6.28 Effect of ore/coal ratio on computed degree of iron ore reduction (Different ore/coal ratio, furnace temperatures=1200°)

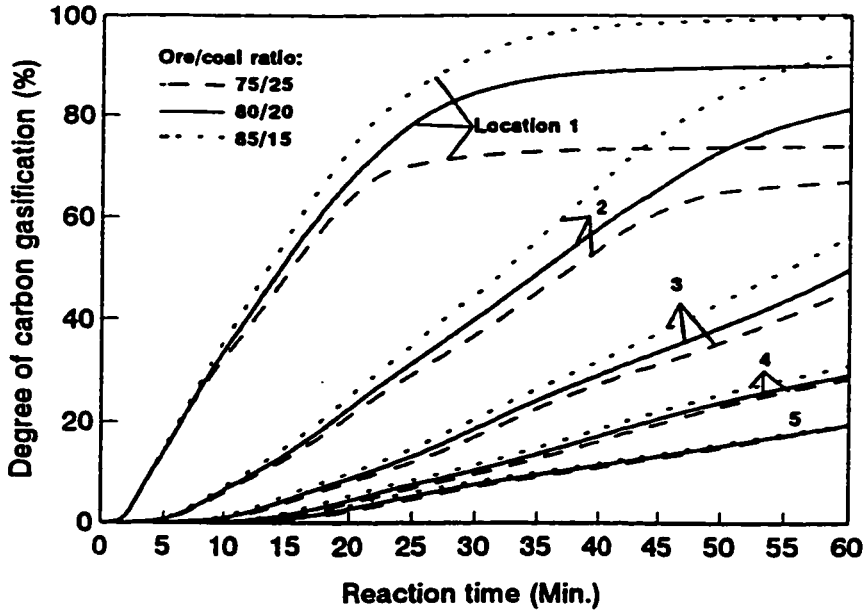

Figure 6.29 Effect of ore/coal ratio on computed degree of carbon gasification (Different ore/coal ratio, furnace temperatures=1200°)

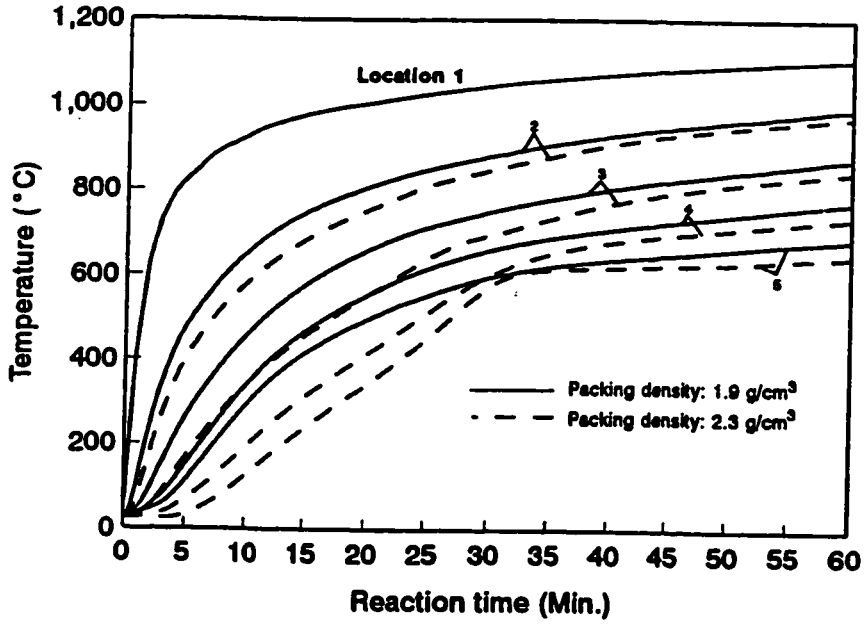

Figure 6.30 Effect of packing density on computed local temperature (Ore/coal=80/20, furnace temperatures =1200°)

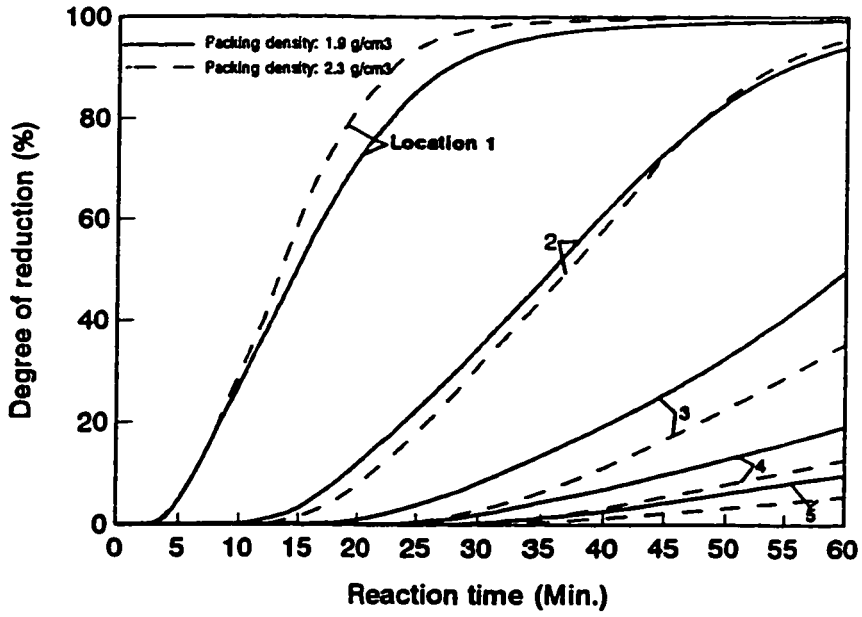

Figure 6.31 Effect of packing density on computed degree of iron ore reduction (Ore/coal=80/20, furnace temperatures = 1200°)

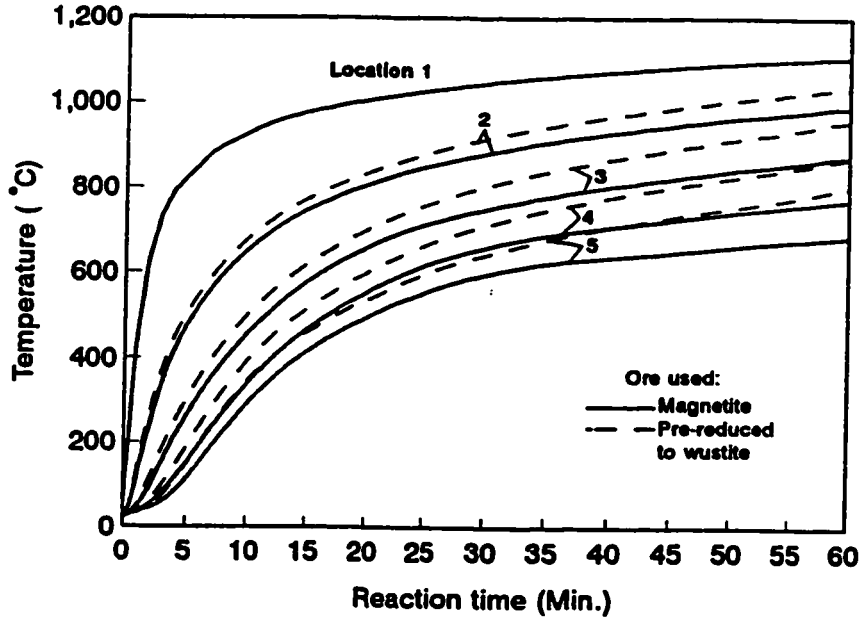

Figure 6.32 Effect of pre-reduction on computed local temperature (Furnace temperatures=1200°)

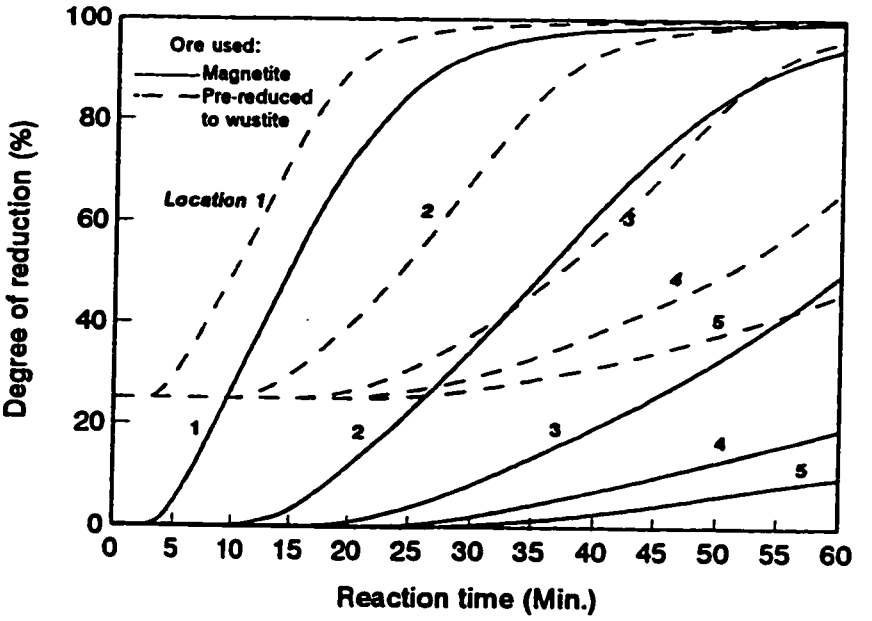

Figure 6.33 Effect of pre-reduction on computed degree of iron ore reduction (Furnace temperatures=1200°)

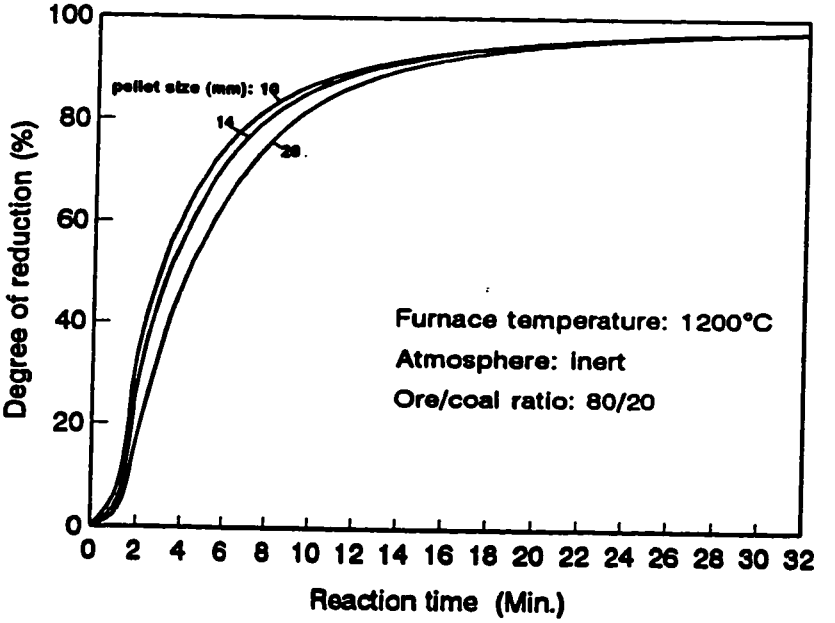

Figure 6.34 Computed degree of reduction of individual pellet for different pellet size

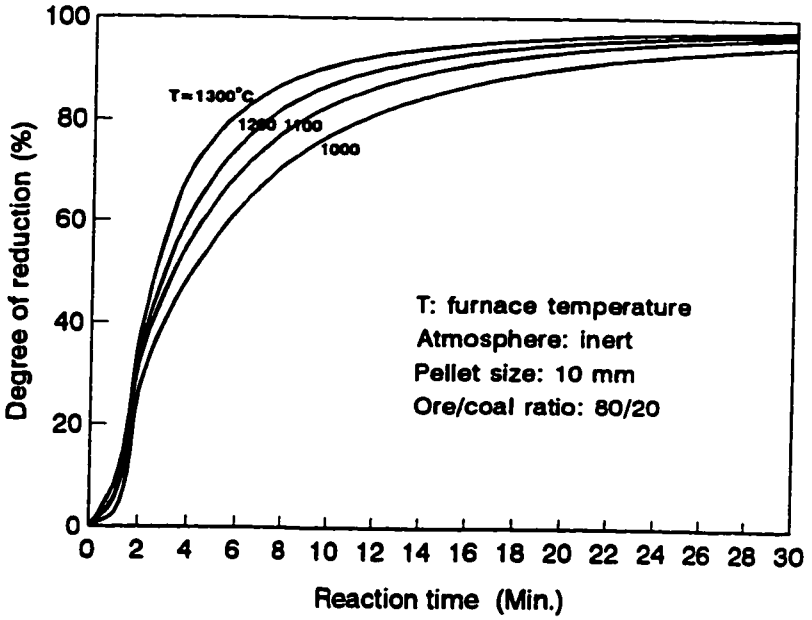

Figure 6.35 Effect on furnace temperature on computed degree of reduction of individual pellet

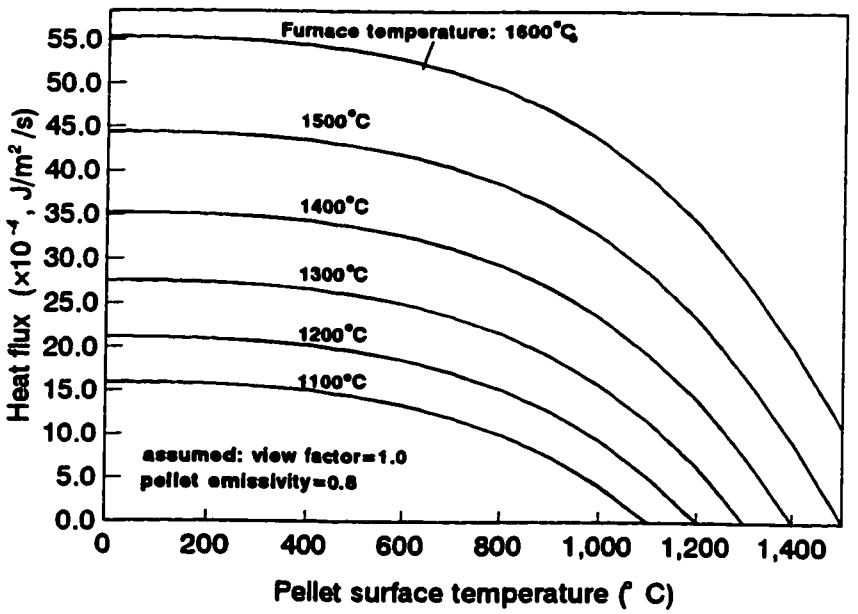

Figure 6.36 Computed radiation heat flux from furnace to pellet as a function of pellet surface temperature

CHAPTER SEVEN: CONCLUSIONS

Carefully designed experiments have been conducted to study the kinetics and mechanisms of iron ore reduction in ore/coal composites. Experimental data obtained as functions of time and furnace temperature include in-situ measurements of temperature and pressure, profiles of chemical compositions across partially reacted iron ore/coal mixture, and chemical compositions of exit gas.

A non-isothermal and non-isobaric mathematical model has been developed for the study of the mechanisms of this system, and validated by comparison with experimental data. Based on the experimental measurement and theoretical study of the present work, the following conclusions have been reached:

(1) Heat transfer across the product layer and within the mixture of solid reactants has been found to be the dominant rate limiting steps to the overall rate of reaction. It is due to the low effective thermal conductivities of the porous media, and highly endothermic reaction of carbon gasification.

(2) Among the heat transfer mechanisms, conduction is dominant.

(3) Convection due to gas flow within this porous system has been found to be the dominant mass transfer mechanism in

comparison with diffusion. The gases are generated by chemical reactions and the flow is driven by pressure gradient in the system.

(4) The reduction of iron ore and gasification of carbon in the system are coupled through reacting gases, and the gasification is the slowest reaction.

(5) The extent of the pressure build-up in the early stage depends on the rate of gas generation by the decomposition of coal and the resistance to gas flow in the porous medium.

(6) As heat conduction is the rate limiting step to the overall reaction, any efforts that could increase the rate of heat conduction would increase the rate of the overall reaction. Such an increase in the heat conduction rate could be facilitated through an increase in the furnace temperature, an increase in effective thermal conductivity by recycling metallic fines, an increase in packing density and a decrease in the size of the composite.

(7) A smaller size of coal and more reactive char would increase the rate of the overall reaction. However, the change of size of ore particle has only a minor effect on the rate of the overall reaction under the conditions studied in the present work.

(8) In comparison with the coke and char results, coal results in a higher rate of overall reaction due to early

release of reductants (CO and H_2) by coal devolatilization.

(9) Pre-reduction of the magnetite concentrate to wustite would significantly increase the rate of processing due to an earlier formation of iron, resulting in a faster heat transfer.

(10) The present work is designed in an one-dimensional cylindrical geometry for simplicity in modelling. However, it is the worst form for heat transfer based on surface/volume ratio. For practical applications, preparing ore/coal mixtures in the form of pellet will be beneficial in heat transfer, and subsequently in the overall reaction.

(11) The size of the pellet and the mechanism of external heat transfer to the pellets are the most important factors in any process design, such as in the case of FASTMET Process.

(12) In the case where a hot gas is the source of heat and this gas is oxidizing with respect to sponge iron, the re-oxidation of iron in the latter part of process will become critical, not the rate of heat supply.

FUTURE WORK

(1) Experiments may be designed and carried out to study the effect of both direct heating and an oxidative atmosphere on the rate of the overall reaction in the ore/coal pellet. Mathematical modelling may also be upgraded to reflect the new experimental design.

(2) The methodology and mathematical model in the present work may be applied to other carbothermic processes, such as the sintering of iron ore, direct reduction processes such as FASTMET, and coking processes.

NOTATION:

a_{Fe}	activity of Fe
a_{FeO}	activity of FeO
a_s	specific surface area, m^2/kg
A_z	reaction surface area in the reaction zone, m^2
C_{CO}	concentration of CO, $mole/m^3$
C_{CO_2}	concentration of CO_2, $mole/m^3$
C^b_{CO}	concentration of CO at the bulk gas phase, $mole/m^3$
C^b_{CO2}	concentration of CO_2 at the bulk gas phase, $mole/m^3$
C^o_{CO}	concentration of CO at exterior surface of the particle, $mole/m^3$
C^o_{CO2}	concentration of CO_2 at exterior surface of the particle, $mole/m^3$
C_{H_2}	concentration of H_2, $mole/m^3$
C_{H_2O}	concentration of H_2O, $mole/m^3$
C_{Pm}	specific heat of the solid mixture, J/kg/K
C_{Pg}	specific heat of the gas, J/kg/K
D_{effCO}	effective diffusivity for CO, m^2/s
D_{effCO2}	Effective diffusivity for CO_2, m^2/s
D_{effj}	Effective diffusivity of species j in the gaseous phase, m^2/s

D_{effj}	Effective diffusivity of species j in the gaseous phase, m^2/s
d_p	average diameter of the particle, m
ΔE_i^*	'activation energy' of reaction i, J/mole
f_{mi}	volume fraction of component i in the control volume
f_r	frictional force acting on gas by packed bed, N/m^3
F_{sm}	view factor for top face of the packed bed and the mouth of crucible
ΔG^o	standard free energy change of the reaction
h_{CO}	mass-transfer coefficient for CO, m/s
h_{CO2}	mass-transfer coefficient for CO_2, m/s
h_j	mass-transfer coefficient for gaseous species j, m/s
H	enthalpy, J/m^3
ΔH_i	heat of chemical reaction i, J/mole
k_i	rate constant for reaction i
k_{i0}	pre-exponential constant in rate constant for reaction i
K_E	equilibrium constant for reaction
K_{Ei}	equilibrium constant for reaction i
K_{effm}	effective thermal conductivity of the mixture, W/m/K
K_{effmc}	portion of effective thermal conductivity of the mixture by conduction, W/m/K

K_{effmr} portion of effective thermal conductivity of the mixture by radiation, W/m/K

L height of packed bed, m

M_j molecular weight of the gaseous species j, kg/mole

M_m mean molecular weight of the gaseous mixture, kg/mole

n_i number of particles of solid reactant for reaction i in the mixture, m^{-3}

$\dot{n}^D_{CO}$ molar flow of CO by diffusion across the product layer, mole/s

$\dot{n}^D_{CO2}$ molar flow of CO_2 by diffusion across the product layer, mole/s

$\dot{n}^m_{CO}$ molar flow of CO from bulk gas phase to the exterior surface of the pellet, mole/s

$\dot{n}^m_{CO2}$ molar flow of CO_2 from exterior surface of the pellet to the bulk gas phase, mole/s

$\dot{N}_{ij}$ net rate of gaseous species j consumed/generated by chemical reaction i, mole/s/m^3

P pressure, Pa

P_{CO} partial pressure of CO

P_{CO2} partial pressure of CO_2

q heat flux, J/m^2/s

r radius, m

$\bar{r}_i$ average radius of particle for reaction i, m

$\dot{R}_i$	rate of chemical reaction i, mole/m^3/s
$\dot{R}_o$	rate of oxygen removal by the interfacial reaction, mole/sec
R	gas constant, 8.314 J/mole/k
S_f	shape factor of particles
t	time, s.
T	temperature, K
V_a	average velocity of gas flow in the interstices of the packed bed, m/s
V_o	superficial gas velocity ($V_a\phi$), m/s
W_o	weight of oxygen in iron oxide, mole
W_{vi}	un-evolved portion of volatile component i, kg/kg-coal
x	distance, m
Y_j	mole fraction of species j in the gaseous phase, %
ρ	density of a solid reactant, kg/m^3
ρ_o	oxygen density in a solid reactant, mole/m^3
φ	reacted fraction of iron oxide
ρ_m	density of mixture, kg/m^3
ρ_g	density of gas, kg/m^3
ρ_j	density of gaseous species j, kg/m^3
ϕ	void fraction of the packed bed
φ_i	reacted fraction of iron oxide i
μ	viscosity of fluid, Pa·s

τ	tortuosity factor
ϵ	emissivity
σ	Stefan-Boltzmann constant, 5.147×10^{-10} W/m^2.k^4

REFERENCES:

Akiyama, T., Ohta, H., Takahashi, R., Waseda, Y. and Yagi, J. (1992), ISIJ International, Vol. 32, pp.829.

Atinson, B. and Merrick, D. (1983), Fuel, Vol. 62, pp.553.

Aukust, E. (1992), Proceedings of the Savard/lee International Symposium of Bath Smelting, The Mineral, Metals & Materials Society, pp. 591.

Bandyopadhyay, D., Chakraborti, N. and Ghosh, A. (1993), Steel Research Vol. 64, No. 7, pp. 340

Bear, J. (1972), Dynamics of Fluids in Porous Media, Dover Publications, Inc., New York, pp.648.

Biswas, A.K. (1981), Principles of Blast Furnace Ironmaking, Cootha Publishing House, Brishane, Australia.

Bodsworth, C. (1963), Physical Chemistry of Iron and Steel Manufacture, Lonmans, London.

Bogdandy, L.V. and Engell, H.-J. (1971), The Reduction of Iron Ores, Springer-Verlay, New York

Bryk, C. and Lu, W-K. (1986), Ironmaking and Steelmaking, Vol. 13, No. 2, pp. 70.

Dancy, T.E. (1991), 1991 Ironmaking Conference Proceedings, Iron and Steel Society of AIME, Warrendale. PA, pp. 611

Darken, L.S. and Gurry, R.W. (1945), Jour. Amer. chem. Soc., Vol. 57, pp. 1389.

Delport, H.M.W. (1992), Ironmaking and Steelmaking, Vol. 19, No. 3, pp.183.

Edstrom, J.O. (1953), Journal of the Iron and Steel Institute, Nov. pp.289.

El-geassy, A.A. and Nasr, M.I. (1990), ISIJ International, Vol. 30, No. 6, pp. 417.

Elliott, J.F. and Gleiser, M. (1960), Thermochemistry for Steelmaking, Vol. 1, Addison-Wesley Publishing Co. Inc., Reading, Mass.

Elsenheimer, G. et al (1994), Iron and Steelmaker, Vol. 21, No. 8, pp. 27.

Ergun, S. and Orning, A. A. (1949), Industrial and Engineering Chemistry, Vol. 41, pp.1179.

Ergun, S. (1952), Chemical Engineering Progress. Vol. 48, pp.89.

Fruehan, R.J. (1977), Metallurgical Transaction B, Vol. 8B, pp. 279.

Fukushima, T. (1994), An Intensive Course: Blast Furnace Ironmaking, Ed. by W-K. Lu, McMaster University, Canada, pp.20-1

Gabor, J. D. and Botterill, J. S. M. (1985), in Handbook of Heat Transfer Applications, 2nd Ed. Chapter 6, Ed. by Rohsenow, W. M., Hartnett, J. P. and Ganic, E. N., McGraw-Hill Book Co., New York, pp.6-16

Gavalas, G. R. (1982), Coal Pyrolysis, Elsevier Scientific Publishing, New York, pp.49.

Geerdes, M. (1994), An Intensive Course: Blast Furnace Ironmaking, Ed. by W-K. Lu, McMaster University, Canada, pp.13-16.

Geiger, G. H. and Poirier, D. R. (1973), Transport Phenomena in Metallurgy, Addison-Wesley Publishing Company, Menlo Park, California, pp.469.

Geiger, G. H. and Stephens, F. A. (1993), 1993 Ironmaking Conference Proceedings, Iron and Steel Society of AIME, Warrendale. PA, pp. 333,

Ghosh, P.C. and Tiwari, S.N. (1970), Journal of The Iron and Steel Institute, pp. 255

Haque, R, Ray, H.S. and Mukjerjee, A. (1992), Ironmaking and Steelmaking, Vol. 19, No. 2, pp. 127.

Haque, R, Ray, H.S. and Mukjerjee, A. (1992), Metallurgical Transactions B, Vol. 24B, pp. 511.

Hbika, A, Dupre, B. Gleitzer, C. and Marliere, E. (1990), Steel Research, Vol. 61, No. 9, pp. 401

Hoffman, G. and Myers, J. (1996), 1996 Ironmaking Conference Proceedings, Iron and Steel Society of AIME, Warrendale, PA, pp. 241

Ibaraki, T. et al (1995), Iron and Steelmaker, Vol. 22, No. 3, pp. 83.

ISS,(1996), (Iron and Steel Society), Iron and Steelmaker, Vol. 23, No. 3, pp. 6.

Johnson, J. L. (1981), in Chemistry of coal utilization, Second Supplementary, Ed. by Elliott, M. A, John Wiley and Sons, Inc., New York, pp. 1491.

Kaminski, A. (1993), Heat Transfer and Fluid Flow Date Book, Section 410.2, General Electric, pp.57.

Kawasaki, E. Sanscrainte, J. and Walsh, T.J. (1962), A.I.Ch.E. Journal, Vol. 8, pp. 48.

Kirov, N. Y. (1965), BCURA Monthly Bull., Vol. 29, pp.33.

Lepinski, J.A. (1993), 1993 Ironmaking Conference Proceedings, Iron and Steel Society of AIME, Warrendale. PA, pp. 349.

Loison, R.,Peytacy, A., Boyer, A. F and Grillot, R. (1963), in Chemistry of Coal Utilization, Supplementary Volume, Ed. by Lowry, H. H., John Wiley & sons, Inc., New York, pp.187.

Lu, W-K. (1963), Trans. Met. Soc. AIME, Vol. 227, pp. 203.

Lu, W-K., Bryk, C. and Gou, H.Y. (1986), 1986 Process Technology Proceedings, Vol. 6, Iron and Steel Society of AIME, Warrendale. PA, pp. 1065.

McAloon, T.T. (1994), Iron & Steelmaker, Vol. 21, No. 2, pp.37.

McKewan, W.M. (1958), Trans. AIME, Vol. 212, pp. 791.

McKewan, W.M. (1960), Trans. Met. Soc. AIME, Vol. 218, pp. 2.

McKewan, W.M. (1961), Trans. Met. Soc. AIME, Vol. 221, pp.140.

McKewan, W.M. (1965), Steelmaking: The Chipman Conference, Ed. by Elliott, J.F., The M.I.T. Press, Cambridge, Mass., pp. 141.

Merrick, D. (1983), Fuel, Vol.62, pp. 540.

Murayama, T., Ono, Y. and Kawai, Y. (1978), Transactions ISIJ, vol. 18, pp.579.

Nabi, G. and Lu, W-K. (1968), Tran. Met. Soc. AIME, Vol. 242, pp. 2471.

Nelko, S.M. (1994), Iron and Steelmaker, Vol. 21, No. 8, pp.8.

Otsuka, K. and Kunii, D. (1969), Journal of Chemical Engineering of Japan, Vol. 2, No. 1, pp. 46

Patankar, S.V. (1980), Numerical Heat Transfer and Fluid Flow, McGraw-Hill, New York.

Pisila, E. A. (1994), An Intensive Course: Blast Furnace Ironmaking, Ed. by W-K. Lu, McMaster University, Canada, pp.19-1.

Quets, J.M., Wadsworth, M.E. and Lewis, J.R. (1960), Trans. Met. Soc. AIME, Vol. 218, pp. 545.

Ranada, M.G. (1994), An Intensive Course: Blast Furnace Ironmaking, Ed. by W-K. Lu, McMaster University, Canada, Vol. 2, pp.9-41.

Rao, Y.K. (1971), Metallurgical Transactions, Vol. 2, pp.1439.

Ritt, A. (1996), New Steel, No. 10, pp.68.

Rosner, D. E. (1986), Transport Processes in Chemically Reacting Flow Systems, Butterworths Publishers, Boston, pp.109-120

Ross, H. (1980) Direct Reduction Iron, Ed. by Stephenson, R.L., The Iron and Steel Society of AIME, Warrendale, PA, pp. 9.

Schlosberg, R. H. (ed) (1985), Chemistry of coal conversion, Plenum Press, New York, pp.74.

Seaton, C.E., Foster, J.S. and Velasco, J. (1983), Transactions ISIJ, Vol. 23, pp. 490.

Sherwood, T. K., Pigford, R. L. and Wilke, C. R. (1975), Mass Transfer, McGraw-Hill Book Company, New York, pp.19.

Smith, N.D. and McKewan, W.M. (1962), Blast-Furnace, Coke Oven and Raw Materials Proceedings, Vol. 21, pp.3

Smith, R.B. and Corbett, M.J. (1988), 1988 Process Technology Conference Proceedings, Vol.7, Iron and Steel Society of AIME, Warrendale. PA, pp.147.

Smithells, C. J. (1967), Metals Reference Book, 4-th Ed., Vol. 1, Plenum Press. New York, pp.257.

Solomon, P. R. and Colket, M. B. (1979), 17th Symposium (int.) on Combustion, The Combustion Institute, Pittsburgh, pp.131.

Spitzer, R.H., Manning, F.S. and Philbrook, W.O. (1966), Trans. Met. Soc. AIME, Vol. 236, pp. 726

Srinivasan, N.S. and Lahiri, A.K. (1977), Metallurgical Transactions B, Vol. 8B, pp. 175.

Steffen, R. (1989), Steel Research, Vol. 60, No. 3+4, pp. 96.

Stephenson, R.L. (1980) Editor, Direct Reduced Iron, Iron and Steel Society of AIME, Warrendale, PA, pp. 64.

Strassburger, J.H. (1969), (Ed.) Blast furnace Theory and Practice, Gordon and Breach, New York

Szekely, J. and Evans, J. W. (1976), Gas-Solid Reactions, Academic Press, New York, pp.65.

The Metal Society, London (1979), Direct Reduction of Iron Ore, a bibliographical survey, The Chameleon Press Limited, London

Themelis, N.J. and Gauvin, W.H. (1963), Trans. Met. Soc. AIME, Vol. 227, pp. 290.

Touloukian, Y. S. (1970), Thermophysical Properties of Matter, IFI/Plenun, New York, Vol. 3, pp.220; Vol. 6, pp.245; Vol. 11, pp.189.

Towhidi, N. and Szekely, J. (1981), Ironmaking & Steelmaking, vol. 8, No. 6, pp. 237.

Trushenski, S.P., Li, K. and Phibrook, W.O. (1974), Metallurgical Transactions, Vol. 5, pp 1149.

Tsay, Q.T., Ray, W.H. and Szekely, J. (1976), AIChE Journal, Vol. 22, No.6, pp. 1064.

Turkdogan, E.T. and Vinters, J.V. (1972), Metallurgical Transactions, Vol. 3, pp. 1560.

Unger, G. R. and Suuberg, E. M. (1984), Fuel, Vol. 63, pp.606

Wingrove, G, Cusack, B.L. and Hardie, G.H. (1994), Paper present at Ironmaking 2000, The 18-th Advanced Technology Symposium, Myrtle Beach, SC, USA.

Appendix I: Estimation of effective thermal conductivity and thermal capacity of the mixture

A.I.1 The effective thermal conductivity of the mixture, K_{effm}

The effective thermal conductivity of the mixture, K_{effm}, includes heat conduction through the solid and gaseous phases, and radiation across interstices. It may be expressed as (Gabor and Botterill, 1985)

$$K_{effm} = K_{effmc} + K_{effmr} \qquad (A.1)$$

where K_{effmc} and K_{effmr} are the portions of effective thermal conductivity by conduction and radiation in the mixture, respectively, and are evaluated as follows.

A.I.1.1 The effective thermal conductivity of solid and gaseous phases, K_{effmc}

In a multiple phase system, the effective thermal conductivity is a function of temperature, properties of each phase (i.e. size, shape and conductivity), and relative amounts of, and interactions between, each phase. It may be

expressed as follows (Bear, 1972):

$$K_{effmc} = \frac{1}{2}\left(\sum_i f_{mi}K_{mi} + \frac{1}{\sum_i \frac{f_{mi}}{K_{mi}}}\right) \qquad (A.2)$$

where i is index for components in the mixture (i=Fe, FeO, Fe_3O_4, coal and gas), and f_{mi} and K_{mi} are the volume fraction and thermal conductivity of component i in the control volume, respectively. The temperature dependence of K_{mi} for iron and its oxides can be obtained from experimental results of Akiyama et al (Akiyama, Ohta, Takahashi, Waseda and Yagi, 1992). The thermal conductivity of coal may be estimated from following equation, which was derived by Atinson and Merrick (Atinson and Merrick, 1983) specifically for coking coals during their thermal decomposition

$$K_{mcoal} = \left(\frac{\rho_{mcoal}}{25.32}\right)^{3.5} \times T^{\frac{1}{2}} \qquad (A.3)$$

Finally, the thermal conductivity of gas mixtures is usually estimated by the following equation (Rosner, 1986)

$$K_{gas} = \frac{\sum_j y_j K_{gj} M_j^{\frac{1}{3}}}{\sum_j y_j M_j^{\frac{1}{3}}} \qquad (A.4)$$

where y_j is the mole fraction of component j (j=CO, CO_2, H_2, H_2O, CH_4 and tar) with a molecular weight M_j and a thermal conductivity K_{gj}. Values for K_{gj} are obtained from references (Kaminski, 1993; Touloukian, 1970).

A.I.1.2 The equivalent conductivity of radiation heat transfer, K_{effmr}

In this reacting system, the equivalent conductivity of radiation heat transfer, K_{effmr}, is a function of temperature, properties of the solid component (size and emissivity of particles) and the void fraction of packing. It may be calculated from the following equation (Geiger and Poirier, 1973)

$$K_{effmr} = \frac{1-\phi}{(1/K_s) + (1/K_r^0)} + \phi K_r^0 \qquad \text{(A.5)}$$

where

$$K_r^0 = 0.229 e D_p \left(\frac{T^3}{10^8}\right) \qquad \text{(A.6)}$$

In order to appreciate the relative importance of each term in Equation (A.1), a typical case is analyzed as an example. At a temperature of 1150 °C a specific reacted mixture composition (listed in Table A.1), and a particle size diameter of 4.5×10^{-5} m (mean diameter of initial mixture), K_r^0 is equal to 2.97×10^{-2} W/m/K when emissivity is assumed to be

1.0. The thermal conductivity of sponge iron or solid metallic iron may be chosen to be 24.27 W/m/K according to experiments by Akiyame et al (1992). The void fraction of the mixture is chosen to be 0.683. From Equations (A.5) and (A.6) and the values chosen above, K_{effmr} and K_r^o would be essentially equal. On the other hand, K_{effmc} may be calculated from Equation (A.2) (with solid properties listed in Table A.1 and values of thermal conductivity from Akiyama's at this temperature), to be about 31.38 W/m/K. Therefore K_{effmr} is estimated to be three orders of magnitude smaller than K_{effmc}.

Table A.1. Composition of reacted mixture when local temperature reacted about 1423 K

components	Fe	FeO	Fe_3O_4	Char	void
measured volume fraction (%)	0.246	0.067	0.004	0.048	0.635

In the present work, the reaction temperature is below 1150 °C and emissivity is less than 1.0; therefore, in Equation (A.1), K_{effmr} may be neglected without introducing significant error in computation.

A.I.2 Effective specific heat for the mixture C_{Pm} and C_{pg}

the effective specific heat of a mixture of gases depends on temperature and composition. It is usually calculated from the specific heat of each pure component by the method of

weighted average. Thus, the effective specific heat of the mixture at certain temperatures in the present reacting system may be calculated based on the following equation

$$C_{pm} = \frac{1}{\rho_m} \sum_i f_{mi} \rho_{mi} C_{pmi} \qquad \text{(A.7)}$$

where C_{pmi} is specific heat of component i in the control volume.

The temperature dependence of the specific heat for iron and iron oxides are chosen from references (Smithells, 1967). "Specific heat of a coal" is usually estimated by empirical equations due to the fact that the compositions of coals are very complex. Kirov (1965) and Merrick (1983) proposed a model for the estimated specific heat of coal. In this model, coal is regarded as simple mixture of coke, volatile matter and ash. Correlations for the variation in the specific heats of these components with temperature are proposed, and (by assuming additivity) the specific heat of coal during decomposition may be expressed as

$$C_{pmcoal} = f_{cf}C_{pcf} + f_{cv}C_{pcv} + f_{ca}C_{pca} \qquad \text{(A.8)}$$

where f_{cf}, f_{cv} and f_{ca} are mass fractions of fixed carbon, volatile matter and ash in the coal, respectively; C_{pcf}, C_{pcv} and C_{pca} are specific heat of fixed carbon, volatile matter and ash in the coal, respectively. Their correlation with temperature may be expressed as

$$C_{pcf} = -912.11 + 15.928T - 7.355\times10^{-3}T^2 \qquad \text{(A.9)}$$

$$C_{pcv} = 4920.38 + 13.171T \qquad \text{(A.10)}$$

$$C_{pca} = 2485.30 + 2.452T \qquad \text{(A.11)}$$

The specific heat of the pure gaseous component C_{pgj} is taken from the references (Kaminski, 1993; Touloukian, 1970).

Appendix II. The estimation of values of Reynolds Number and some terms in momentum equation

A.II.1 Reynolds number

In the flow of a fluid through a packed bed, the pressure losses are caused by kinetic and viscous energy losses as described in two separate terms in the Ergun equation. The relative importance of these two types of losses is determined by properties of the packing and the fluid, and velocity of fluid flow. It is correlated as a function of Reynolds number with particle size as the characteristic distance. At a low flow rate of fluid (i.e. low Reynolds number (<10)), the viscous loss dominates the pressure loss, and the kinetic loss may be neglected. At a high flow rate (i.e. high Reynolds number), the kinetic energy loss is dominant. In order to determine the relative importance of these two types of losses in the present reaction system, the Reynolds number is estimated based on the conditions used both in the experiments and in numerical solution of the mathematical model.

The Reynolds number in a porous medium packed with spherical particles is defined as follows (Geiger and Poirier,

1973).

$$R_e = \frac{\rho_g V_o d_p}{\mu(1-\phi)} \qquad (A.12)$$

In the present reaction system, gases are generated by chemical reactions only. The maximum superficial velocity is estimated to be less than 0.10 m/s. The average diameter of the particle (pulverized coal and iron ore concentrate) is measured to be about 4.5×10^{-5} m, and the void fraction of the packed bed is 0.405. The density and viscosity of gas are functions of temperature, pressure and gaseous composition. Over a temperature range from 300 to 1400 K, gaseous viscosities vary from 1.5×10^{-5} to 3.8×10^{-5} (Pa·s). As most of the reaction takes place at temperatures higher than 600 K, an average viscosity of 2.0×10^{-5} Pa·s and average density of 0.8 kg/m^3 may be used to estimate a maximum Reynolds number of 0.303:

$$R_e = \frac{0.8\times0.1\times4.5\times10^{-5}}{2.0\times10^{-5}\times(1-0.405)} = 0.303 \qquad (A.13)$$

As the Reynolds number is less than 1, the kinetic energy loss is much less important in comparison with viscous loss in this reaction system, and the kinetic term in the Ergun equation may be neglected.

A.II.2 The contribution of each term on the right-hand-side of Equation (4.42) to the momentum change

In order to determine the importance of each term in right-hand-side of Equation (4.42) to the momentum change in the control volume, the value of these terms is estimated numerically based on the conditions used in experiments and in numerical solutions of the mathematical model.

In the numerical solution, the value of Δx (mesh size) is chosen to be 0.001 m, which is used in the estimation. The same values of gas and solid properties as in the estimation of Reynolds number are also used here.

a The pressure gradient

As only a very small pressure difference (about 100 Pa) exits over a distance of 0.001 m, the value of the pressure gradient term may be estimated as:

$$\frac{\partial P}{\partial x} = \frac{100}{0.001} = 100{,}000 \quad (kg/m^2/s^2) \qquad \text{(A.14)}$$

b Term $\frac{\partial}{\partial x}(\rho_g \frac{V_o^2}{\phi^2})$

The maximum value of $\rho V_o^2/\phi^2$ may be estimated from the maximum gas flow velocity and minimum void fraction to be $0.8\times0.01/0.405^2=0.0488$. The maximum gradient would be

$$\frac{1}{\Delta X}\left[(\rho_g \frac{V_o^2}{\phi^2})_{max}-0\right]=48.8 \quad (kg/m^2/s^2) \qquad (A.15)$$

c Term $\alpha\mu V_o = 150\frac{(1-\phi)^2}{\phi^3 (S_{fa}D_p)^2}\mu V_o$

This term may be estimated as follows with the assumption that the particle shape factor is unity:

$$\alpha\mu U=150\times\frac{(1-0.405)^2\times2.0\times10^{-5}}{0.405^3\times(4.5\times10^{-5})^2}\times0.1=7.9\times10^6 \quad (kg/m^2/s^2) \qquad (A.16)$$

d Term $\beta\rho_g V_o^2 = 1.75\frac{(1-\phi)}{\phi^3 (S_{fa}D_p)}\rho_g V_o^2$

The maximum value of this term may be estimated as

$$\beta\rho_g V_o^2 = 1.75\times\frac{(1-0.405)}{0.405^3\times4.5\times10^{-5}}\times0.8\times0.1^2=2.79\times10^3 \quad (kg/m^2/s^2) \qquad (A.17)$$

By comparison, the pressure gradient is three and two orders of magnitude larger than the gradient of kinetic energy and the kinetic terms, respectively. The viscous term is four and three orders of magnitude larger than the gradient of kinetic energy and the kinetic terms, respectively. For

numerical computation, Equation (4.42) may be simplified as follows without introducing significant error in computation.

$$\frac{\partial}{\partial t}\left(\rho_g \frac{V_o}{\phi}\right) = -\frac{\partial P}{\partial x} - \alpha \mu V_o \qquad \text{(A.18)}$$

IMAGE EVALUATION TEST TARGET (QA-3)

150mm

6"

APPLIED IMAGE . Inc
1653 East Main Street
Rochester, NY 14609 USA
Phone: 716/482-0300
Fax: 716/288-5989